2013-04-26

Mimicking the Mechanical Behavior of Advancing Disc Degeneration Through Needle Injections

Jeremy S. Alsup
Brigham Young University - Provo

Mimicking the Mechanical Behavior of Advancing Disc Degeneration Through Needle Injections

Jeremy S. Alsup

A thesis submitted to the faculty of
Brigham Young University
in partial fulfillment of the requirements for the degree of

Master of Science

Anton E. Bowden, Chair
Steven K. Charles
Larry L. Howell

Department of Mechanical Engineering

Brigham Young University

April 2013

ABSTRACT

Mimicking the Mechanical Behavior of Advancing Disc Degeneration
Through Needle Injections

Jeremy S. Alsup
Department of Mechanical Engineering, BYU
Master of Science

Objective - To investigate the effects of injected protease solution on the mechanical advancement of disc degeneration, and to establish test protocol for future pre-clinical validation of spinal arthroplasty devices. The hypothesis that injection of a protease into a cadaveric lumbar disc will mimic advanced degeneration mechanics was the subject of this study.

Summary of Background Information - Spinal disc degeneration is a universal condition that progresses in adults due to aging, disease, or injury. Stages of disc degeneration have been categorized in cadaver specimens, with each degeneration level exhibiting characteristic changes in flexibility parameters. Spinal disc tissue can be compromised through introduction of proteolytic enzymes into the collagenous fibers of the annulus fibrosus.

Methods - 18 motion segments from 8 human lumbar spines were subjected to flexibility testing. Each specimen was either injected with 600 μL of trypsin solution in the annulus fibrosus, 600 μL of phosphate-buffed saline, or a fluid-less needle-stick. Motion testing followed with rotations applied in all three major spinal motions. Test sections were transected mid-disc after testing to characterize initial degeneration severity, and acquired motion data was analyzed to show flexibility traits over time.

Results - Trypsin, saline, and control injections all caused changes in motion from pre-injection baselines. Saline injections were slightly more effective at mimicking the mechanics of higher grades of degeneration with more fidelity than trypsin injections. All motion parameters were altered by the study treatments, with hysteresis and neutral zone parameters experiencing changes similar to that seen in natural degeneration with greater fidelity. Lateral Bending motion showed the greatest magnitude response to injections, with Flexion-Extension tests showing the smallest change.

Discussion - Unexpectedly, fluid-less control injections caused changes to hysteresis and neutral zone parameters, suggesting an alteration to viscoelastic properties due to simple needle puncture. Fluid injections (Trypsin and Saline) caused an immediate transient post-injection change to biomechanics that dissipated over time, except in Axial Rotation. Saline injections provided the highest fidelity in mimicking the motion of more advanced stages of degeneration.

Keywords: spinal motion, disc degeneration, intervertebral disc mechanics, protease injection

ACKNOWLEDGMENTS

I first wish to thank Dr. Anton Bowden for the immeasurable amount of time and help he has provided in making this research a success. Without him, none of this would have happened. I also want to recognize the contributions of the National Science Foundation for providing the research funding that supported this work (CMMI-0952758). Any opinions, findings, and conclusions or recommendations expressed in this material are those of the author(s) and do not necessarily reflect the views of the National Science Foundation.

I wish to also recognize the efforts and help of Dr. Dennis Eggett and Shannon Zirbel in this project. I want to thank Dean Stolworthy for all his aid in running the MASSUCE, running several SAS calculations, and guiding my ideas in the best direction. I am grateful for the many hours Amy Fullwood, Kara Boatwright, and David Williams invested into this project, whether it was data analysis or test days. I especially want to thank my parents, John and Heidi Alsup, for their wonderful support, love, and encouragement throughout my graduate career. I also wish to thank my lovely wife Corinne for her faithful support, help, and encouragement to do my best. Finally, I wish to thank my Father in Heaven from which all I possess and am have come.

TABLE OF CONTENTS

LIST OF TABLES

LIST OF FIGURES

LIST OF ACRONYMS

AF	Annulus Fibrosus
ANOVA	Analysis of Variance
AR	Axial Rotation
CABC	Chondroitinase ABC
DIP	Dual Inflection Point
FE	Flexion-Extension
FSU	Functional Spinal Unit
H	Hysteresis
HA	Hysteresis Area
HA/ROM	Normalized Hysteresis Area
IVD	Intervertebral Disc
K	Stiffness
LB	Lateral Bending
LBP	Low-Back Pain
MASSUCE	Multi-Axial Spine Simulator Under a Controlled Environment
MMP	Matrix Metalloproteinase
MRI	Magnetic Resonance Imaging
MW	Molecular Weight
NP	Nucleus Pulposis
NZ	Neutral Zone
NZ/ROM	Normalized Neutral Zone
PBS	Phosphate Buffered Solution
ROM	Range of Motion
TIMP	Tissue Inhibitor of Metalloproteinases
TDR	Total Disc Replacement
TG	Thompson Grade

1. INTRODUCTION

1.1 Problem Statement

Low-back pain afflicts millions of people every year, but current treatments do not fully alleviate pain. New spinal technologies aimed at replacing degraded intervertebral discs show promise for greater pain reduction and restoration of healthy motion, but need validation before they become more mainstream. Unfortunately, current pre-clinical testing methodologies are inadequate in addressing the changing environment in the human spine due to advancing disc degeneration.

1.2 Chapter Layouts

This thesis explores the effects of simulating the advancement of degeneration on human cadaveric lumbar intervertebral discs. The thesis is broken up into four major sections, as detailed below.

Chapter Two gives a detailed introduction to this research and its motivations. A problem statement is presented, and is then followed by an exploration of the relevant passive anatomy of the spine, a detailed literature review on intervertebral disc degeneration, and a review of current pre-clinical and laboratory models for simulating disc degeneration. The chapter also includes information regarding the function and history of protease enzyme use in the spine, as well as a discussion of previous research that set the stage for the work in this thesis. Finally, a proposed solution to the problem statement is given.

Chapter Three details the specific mechanical changes associated with intervertebral disc degeneration. The data presented in this chapter extends previous work recently published by Zirbel et al. [1] using the same testing apparatus and protocol.

In Chapter Four, needle injection technique, experimental set-up, and data collection and analysis are reported. Statistical results and comparisons to previous research are then discussed, and conclusions on the findings are given.

Chapter Five details all findings, methodologies, and other important information that was not discussed in the peer-reviewed journal article. This includes observations from injection techniques, the application of a follower load, diffusivity of the different injected solutions, and other lessons learned.

Finally, Chapter Six summarizes important discoveries and the direction of future work related to this thesis.

2. BACKGROUND

2.1 Low-Back Pain

Low-back pain (LBP) is a potentially debilitating ailment that afflicts millions of Americans annually. An estimated 75% to 85% of Americans experience it sometime during their lifetime [2]. It is the second most common cause for doctor visits in the U.S., costing Americans approximately 50 billion dollars annually [3]. This amount does not include the cost to companies for lost time from work, the amount spent on chiropractic visits, or any other non-traditional remedies.

The exact cause of LBP is uncertain. Several factors have been linked to LBP, but the magnitude of pain they create is unknown [4]. Such causes include degeneration of the intervertebral disc (IVD), degradation of spinal ligaments, osteoarthritis in the zygopophesial joints (synovial joints that connect two spinal bones), and inflammation of spinal tendons and muscles. Disc degeneration may be the major cause of LBP, and is the focus of extensive research for alleviating pain. Though noninvasive treatments are available [5–7], severe instances of chronic LBP may call for surgical intervention.

2.2 Anatomy

2.2.1 Spinal Sections

In order to address the concerns with current spinal surgeries and the devices they may implant, the anatomy and physiology (or form and function) of the spine must be understood. The spine is the foundation for all upper body activity. It contains 33 vertebrae, which are divided into five sections. The top seven vertebrae are classified as cervical, and are located in the neck. Beneath the cervical section are twelve thoracic vertebrae, which provide the foundation for the rib cage. Below the thoracic vertebrae is the lumbar section, which is comprised of five larger bones that make up the lower back. The sacrum attaches the hips to the bottom of the lumbar spine, and

is comprised of five fused sacral vertebrae. The final section of the spine, the coccyx, is also known as the tailbone and is comprised of four fused bones.

Each section of the spine has distinctly-shaped vertebrae and differs in its relative curvature. The thoracic, sacral, and coccygeal portions have a kyphotic curvature, or curvature that rounds out of the body. The cervical and lumbar sections have a lordotic curvature, or curvature that rounds into the body (See Figure 2.1). The vertebrae in the lumbar section are the largest in the spine, which allows for greater support of upper body weight. The thoracic section has vertebrae with special attachment points on their sides, providing connection sites for the ribs. Some vertebrae, like those in the cervical region, allow for an extensive range of motion, while the thoracic section is much more restrictive.

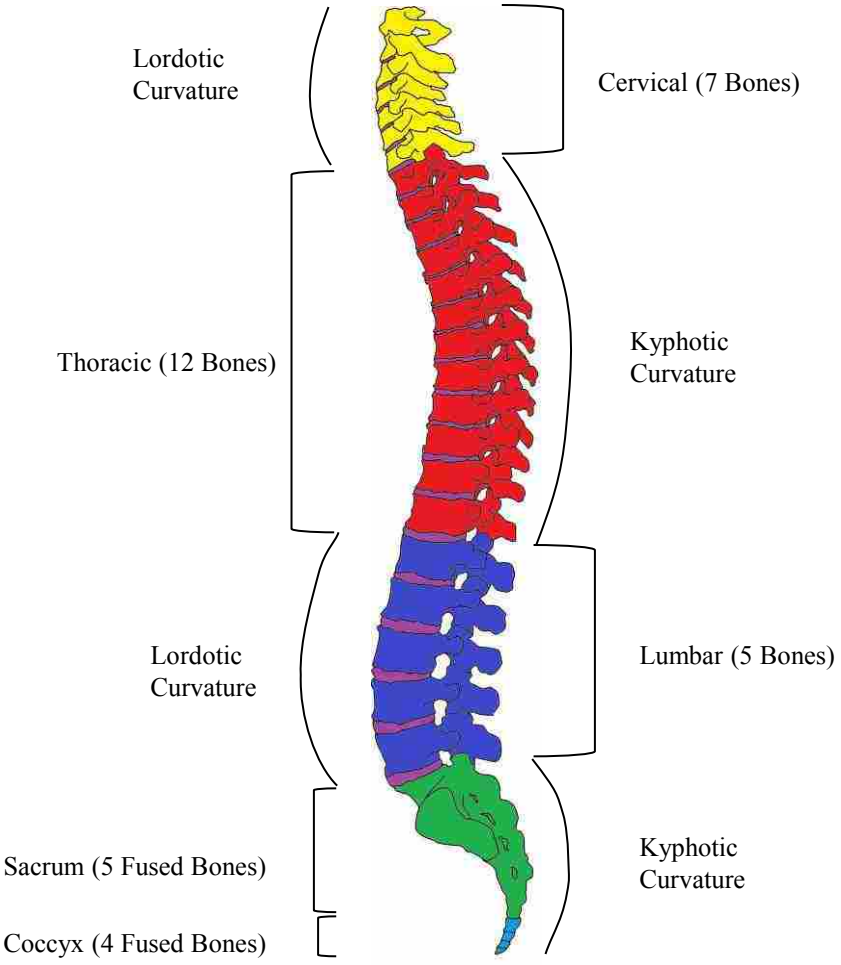

Figure 2.1: Anatomy of the Human Spine (adapted from [8])

2.2.2 Vertebrae and Intervertebral Discs

Nearly every vertebra is made up of the following core components: vertebral body (large cylindrical core of each vertebrae), two transverse processes (bony protrusions that exit out the sides of the vertebrae), and a spinous process (a large bony protrusion out the posterior aspect of the vertebra to which most musculature attaches). Vertebrae also have superior and inferior articular processes (flat surfaces near the back of the vertebral body which interact with adjacent vertebrae via articular synovial joints). The posterior elements of the vertebra are attached to the vertebral body via the pedicles and lamina, which surround and protect the posterior of the spinal cord (See Figure 2.2). For more on Anatomical Directions, see Figure A.1.

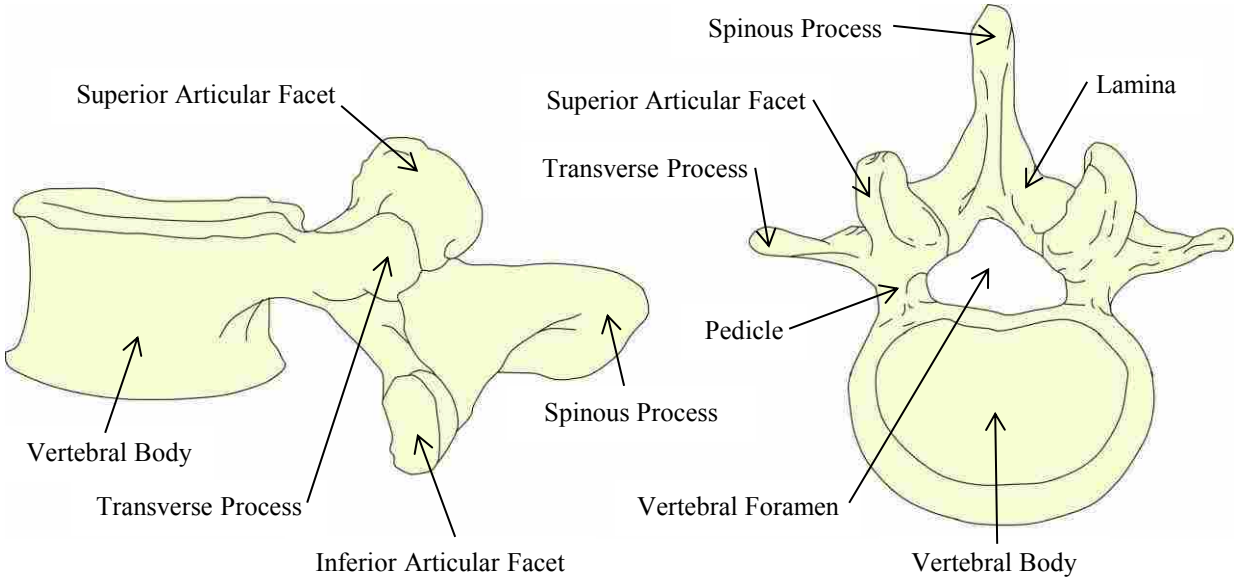

Figure 2.2: Side and Top Views of Lumbar Vertebra Anatomical Landmarks (adapted from [9])

In between each set of vertebrae is the IVD, which is comprised of three main regions (See Figure 2.3). The inner-most section of the disc is called the Nucleus Pulposis (NP), and is characterized as a loose gel-like substance with greater water content than the rest of the disc. Enveloping the NP is the Annulus Fibrosus (AF), which is made up of several concentric layers of fibrocartilage (called lamellae) that alternate at an angle of $\pm 30^{\circ}$ from the horizontal position. This composite structure acts like a pressure vessel, with the AF experiencing tension forces in

containing the higher-pressurized NP (See Figure 2.4) [10]. The AF makes up the largest volume of the disc. On the most superior and inferior faces of each intervertebral disc are the endplates, where the disc is attached to the adjacent vertebral bodies. Nutrients from vascularized bone reach the disc through the endplates. Since there is an absence of vascularization into the inner disc from exterior blood vessels, the endplate provides the majority of needed nutrition to the disc [11].

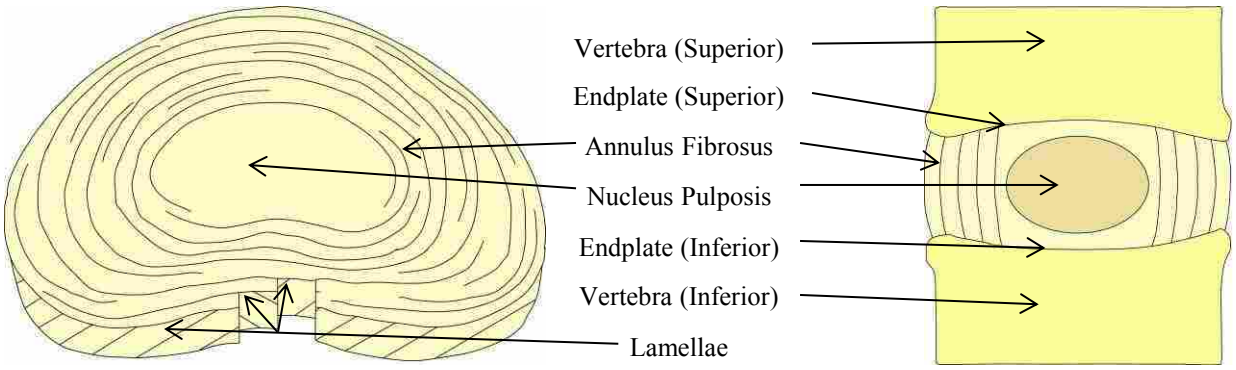

Figure 2.3: Top and Side Cutaway Views of the Intervertebral Disc (adapted from [12, 13])

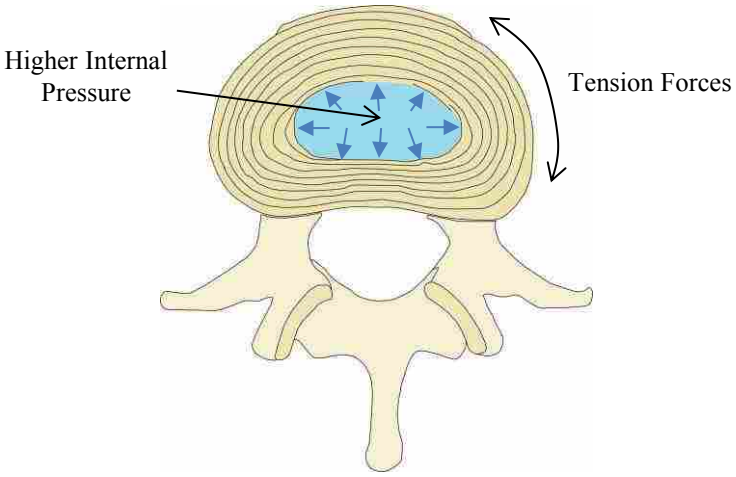

Figure 2.4: Annulus Fibrosus and Nucleus Pulposis Pressures

A motion segment consists of two vertebrae and the disc in between them, and is called a functional spinal unit (FSU). Each FSU contains three joints (the IVD and two zygopophesial joints at the superior/inferior articular facet interface) and five ligaments. Ligaments act as taut sheets

that prohibit excessive relative movement of vertebrae, thus preventing possible shear damage to nerves and other spinal tissues. These ligaments' placement on an FSU is shown in Figure 2.5.

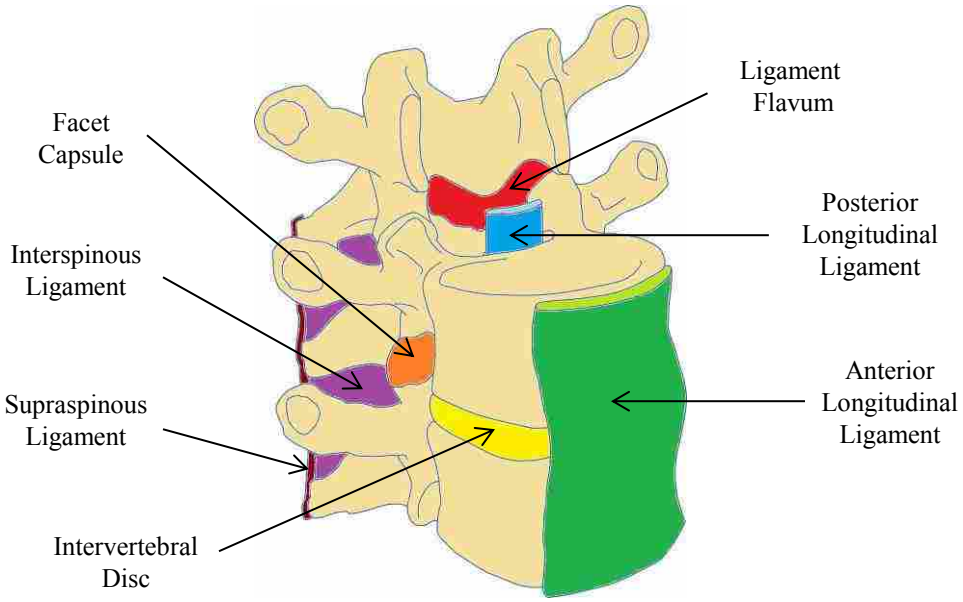

Figure 2.5: Spinal Ligaments (adapted from [14])

2.2.3 Spinal Motion

Motion segments allow the spine to bend in three general directions: axial rotation (AR), flexion-extension (FE), and lateral bending (LB) (See Figure A.2). In every day motion, movements are often coupled (e.g., slight axial rotation during lateral bending). Generally, uncoupled bending movements are utilized when investigating spinal motion.

Seven major motion parameters are considered when describing FSU movement (See Figure 2.6). Range of Motion (ROM) is the maximum distance an FSU rotates when an applied torque of a specified magnitude is applied. This measure is derived by taking the difference between the maximum and minimum rotations. Stiffness (K) determines an FSU's resistance to motion. It is the average of the maximum slopes of the upper and lower curves, which are found in the neutral zone. The Neutral Zone (NZ) is a range where a small change in torque causes a large motion. This is where the majority of daily motion for people takes place. It is calculated by taking the maximum distance between the upper and lower curves at the same applied torque. Normalized Neutral Zone

(NZ/ROM) is a ratio of the neutral zone to ROM, and is done by dividing NZ by ROM. This ratio has been postulated to be a key indicator of spine health, with a large NZ/ROM ratio signifying greater joint laxity [15]. Hysteresis Area (HA) is the area between the upper and lower curves, and is calculated by taking the difference of each curve's integral. This area represents elastic energy lost to friction within the fibers and matrix of the disc [16]. Normalized Hysteresis (HA/ROM) is simply the quotient of HA and ROM. This shows the amount of elastic energy lost in relation to the amount of total movement. The final parameter, Hysteresis (H), is the maximum distance between the upper and lower curves (measured at the same rotation point, or horizontally, in contrast to the same torque point for NZ, or vertically). This is a measurement of the viscoelasticity of the FSU. (Note: Since NZ/ROM and HA/ROM are ratios, they are not shown on the figure below.)

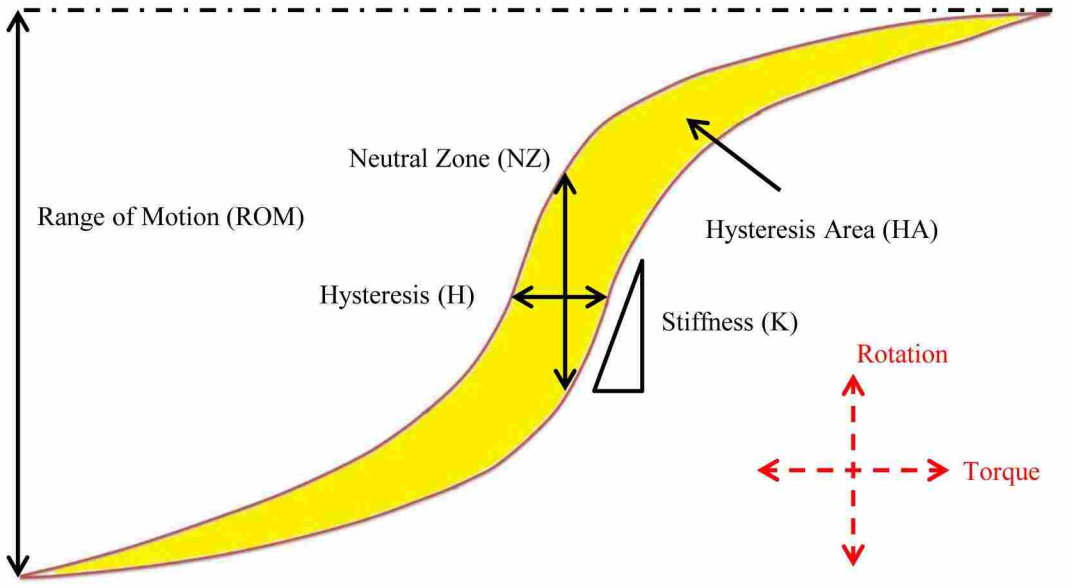

Figure 2.6: Spinal Motion Parameters

2.2.4 Tissue Material Properties

Biological soft tissues exhibit a material response to strain called "viscoelasticity", where both viscous and elastic effects are manifested under an applied deformation. The elastic affect is shown in a material returning back to its original shape almost instantaneously once the stress is removed, and the viscous effect is shown in the greater time-dependency in the strain [17].

Creep, stress relaxation, and hysteresis are more common in these tissues than in normal engineering materials (i.e., metals, ceramics, plastics, etc.). Hysteresis is defined as the lagging of an effect behind its cause. In the case of spinal testing, this is demonstrated through observing that the torque-rotation behavior during loading follows a different path than that observed during unloading.

2.3 Disc Degeneration

2.3.1 Causes and Symptoms

The degeneration of the IVD is a natural occurring phenomenon that all people experience during the aging process [10, 18]. Injury and disease can accelerate the degeneration process [19, 20]. However, causation of disc degeneration is not fully understood at this time. Certain environmental influences, such as frequency and intensity of weight loading [21, 22] and smoking habits [23] have an impact on degeneration. The magnitude of their degenerative role, however, is uncertain. Hereditary factors may also play a significant role in causing degeneration [24, 25]. Although the actual definition of disc degeneration is still under debate [10], it is known that biochemical and cellular changes both contribute to the degradation of disc mechanics, and the body's response to altered mechanics accelerate disc failure.

2.3.2 Biochemical Changes

The NP consists of proteoglycans (mostly aggrecan) and water loosely bound by collagen type II and elastin fibers, while normal AF tissue consists mostly of collagen type I fibers with some proteoglycan content. During aging, an increase in collagen fiber content occurs, corresponding with a decrease in proteoglycan count. The boundary between the AF and NP becomes less distinct, due to NP water content loss and replacement of NP collagen type I fibers with AF type II collagen fibers [10].

Proteoglycans are a family of proteins that have larger carbohydrates attached to their core. They attract water molecules, and since the NP has a much higher dry weight ratio of proteoglycans than the AF (50% compared to $<$10%), the NP acts more incompressible than the AF [18]. As

aging progresses, proteoglycan molecules fragment, leaving them less capable in retaining water. This loss of water retention ability causes the NP to shrink and reduce its hydrostatic pressure. The AF is also negatively affected by proteoglycan breakdown, and exhibits water loss and increased stiffness as a result. As the NP loses hydrostatic pressure, AF tissues support a greater percentage of applied compressive loads. Fissures, radial tears, and delamination of lamellae boundaries frequently follow. Such changes in disc structure also make bulging and herniations (exit of NP material through a fissure in the outer AF) more likely (See Figure 2.7). AF fibers also show greater cross-linking, which reduces potential disc healing by preserving damaged tissue.

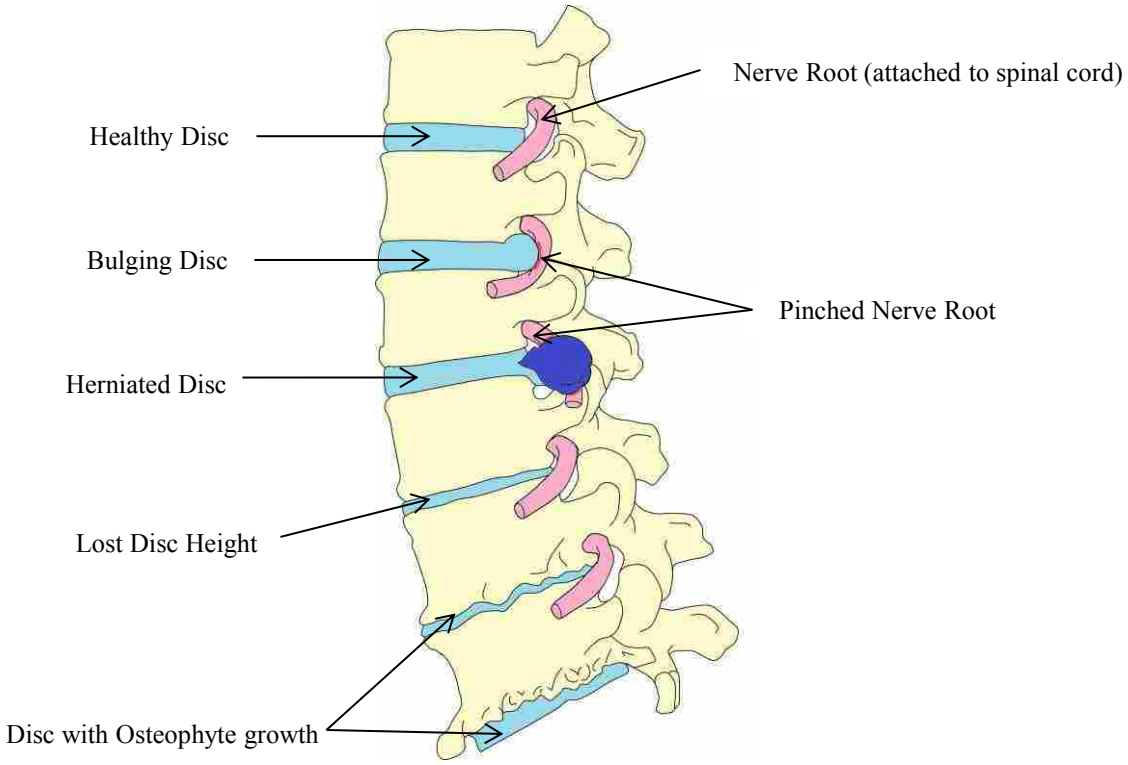

Figure 2.7: Common Forms of Disc Degeneration (adapted from [26])

2.3.3 Cellular Changes

In the embryonic development of most vertebrates, the notochord (a flexible rod) provides a foundation for growth of the spine. During later development stages, the notochord becomes the NP, and notochordal cells eventually become replaced with chondrocyte-like cells (chondrocytes

produce articular cartilage tissue) [27]. NP cells are rounded in shape, whereas AF cells are thin and aligned with collagen fibrils. In humans, cells take up very little disc volume (less than 1%), yet provide a pivotal role in synthesizing proteoglycans, collagen fibers, proteases and protease inhibitors [28]. One key indicator of disc degeneration is an imbalance of molecular synthesis and breakdown of old disc tissue.

During aging, cell density in the disc decreases, with large populations of NP cells disappearing. The white, glossy appearance of healthy NP tissue is eventually replaced with a brownish-yellow look, which is caused by a combination of decreased hydration and accumulation of non-enzymatic glycosylation byproducts (i.e., the cross-linking of glucose and collagen fibers).

2.3.4 Mechanical Failure

As the cellular and chemical composition of the disc changes, the disc experiences decreased hydration, increased stiffness, loss of hydrostatic pressure, fissures in the AF and delamination of lamellae. Herniations of NP tissue, bulging of outer AF layers, and an increased load placement on the AF frequently result. Over time, failed AF tissue causes compressive loads to be resisted by the bony architecture surrounding the nerve roots (commonly called the "neural arch" which is comprised of the lamina, pedicles, and the posterior processes). This is the most likely cause of osteoarthritis in the articular facet joints, as well as the formation of osteophytes (or abnormal exterior bone growths) on the vertebral bodies. The endplate is also vulnerable to NP material expanding into micro-cracks that accumulate over time. A shrinking of disc height may occur, thereby decreasing disc volume. The AF may eventually collapse into the NP. All these alterations may be likened to a car tire slowly going flat [10].

Such changes in disc mechanics cause the disc to attempt healing itself. An increased presence of nerve cells and vascularization in the inner disc accompanies advanced disc degeneration. An increase in cellular synthesis of collagen type II fibers in advanced aging suggests such an attempt at healing [29]. However, the reduction of NP pressure inhibits successful cell synthesis, thus minimizing the effect of any increase in NP cell production [30]. Once mechanical degradation occurs, cellular attempts at repairing disc tissue damage prove futile.

2.4 Surgical Treatments

2.4.1 Spinal Fusion and Arthroplasty

Several current surgical procedures attempt to alleviate pain by removal of damaged or deteriorated disc tissue. The most common spine surgery is discectomy, where a defective portion of the disc is removed [31]. This is typically performed in response to a disc herniation. When extensive degeneration in the disc exists, the current surgical "gold standard" is spinal fusion, where the entire disc is removed and the two adjacent vertebrae are fused via bone graft, rods and screws (See Figure 2.8). This procedure attempts to alleviate pain by permanently replacing a flexible joint segment with solid bone [32]. Even though this surgery is considered successful for treatment of chronic LBP, it has a low rate of satisfaction. A recent study showed that only 53% of patients who undergo this procedure are happy with the results after 2 years, and many need adjacent vertebrae in their spine fused shortly after their first fusion [33].

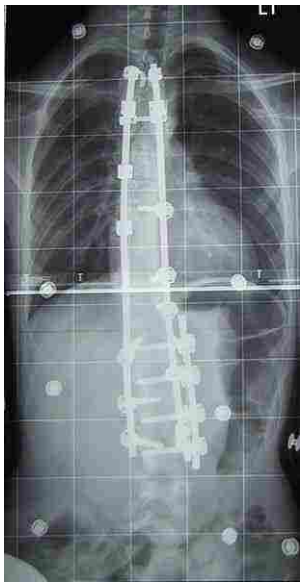

Figure 2.8: X-Ray View of Thoracic Fusion [34]

Since 2004, an alternative to spinal fusion has been available on the medical market in the U.S. Total Disc Replacements (TDR) are a form of arthroplasty that attempt to mimic the natural motion of the disc joint and that may prove to be better than spinal fusions (see Figure 2.9).

Theoretically, the change in spine biomechanics for a disc replacement is much less severe than that seen in a spinal fusion [35]. As with any prosthesis, however, decades of testing may be required to validate its long-term effectiveness. For example, the health of adjacent disc levels (or index levels) may be compromised over time due to TDR mechanics. Also, TDRs may only be effective when replacing discs up to a certain level of degeneration. Such information is paramount to improving TDR designs, as well as necessary to making TDR implantation more acceptable in the medical community [36].

Charité ProDisc FlexBAC

Figure 2.9: Total Disc Replacements

2.4.2 Device Testing and Validation

TDRs undergo several rigorous test phases before entering clinical trials. Biocompatibility testing of device materials with the body is first performed, with emphasis not only on intact device materials, but also on the loose particles created over time by wear. TDRs also undergo mechanical tests to measure strength and deformation in static and dynamic environments [37]. Generally, wear rate tests on the polymers that provide TDR motion are also performed.

Once mechanical testing of the TDR demonstrates its isolated capabilities, its effect in the spine must be shown. The protocol generally applied in investigating the biomechanical effect of a TDR is implantation of the device in a whole cadaveric spine. Ideally, performance of a spine with a TDR matches that of a healthy intact spine [38]. Measurements of intervertebral space, ROM, K, and NZ can be taken for the replacement level, with changes in adjacent level parameters such as intradiscal pressure and spinal alignment also taken [37]. For example, Cakir et al. showed that

TDR implants increased lordosis at their level after 15 months while maintaining the same total lordosis of the lumbar spine [39]. This makes lordosis curvature in adjacent levels decrease, and shows potential long-term change in the motion characteristics at other disc levels.

Currently, long-term impacts can be estimated only through finite element modeling of the spine-device composition. Results of finite element experiments are generally compared to previously published literature values for validation. One such study showed that single FSU ROM increased with a Charité TDR in comparison with a healthy disc, and that stresses in the adjacent vertebral bodies and articular facets increased after device implantation [40]. In multilevel simulations with a TDR installed, ROM, AF stresses, and facet contact pressures generally increase at implant level [41–43]. Chen et al. also showed no instability at adjacent levels and much higher stresses and ROM at adjacent levels for fusion treatments [41]. In a contradicting study combining cadaveric motion and finite element results, Le Huec et al. demonstrated no difference between healthy spine motion and TDR-spine motion when the artificial disc is properly placed [44]. Although finite element studies generally agree that TDRs increase replacement level ROM and stresses, they do not show predicted outcomes of the spine-device composition over a long-period of time.

The process of pre-clinical validation is currently inadequate due to a lack of evidence of a device's long-term efficacy. Adjacent level degeneration is not simulated, and is only quantified years after device implantation [45]. No *in vitro* models currently incorporate adjacent level degeneration, which is critical to fully understanding the effects of TDR implantation over the lifetime of the device.

2.5 Previous Work and Literature

2.5.1 Determining Levels of Degeneration

Several papers have attempted to classify degeneration levels that distinguish healthy discs from more degenerated discs via characteristic disc properties [46,47]. Magnetic Resonance Imaging (MRI) techniques, as well as visual inspection, are used to identify grades of deterioration. The most common morphological grading system, and the one used in this thesis, was created by Thompson et al. [48], where five levels of degeneration that specify tissue properties of the

endplate, AF, NP, and facet joints were defined. Thompson et al. defined Grade I as being the healthiest and Grade V as being the most degenerated. Grading schemes incorporate disc dryness, bleeding, osteophytes, separation of AF lamellae, and the distinctness of the AF/NP boundary. In Figure 2.10 below, red shows vascularization of the disc, brown represents advanced decay, and the tan colors show varying degrees of dryness with darker shades showing drier disc tissue. Different levels of degeneration exhibit altered motion characteristics [15, 49, 50].

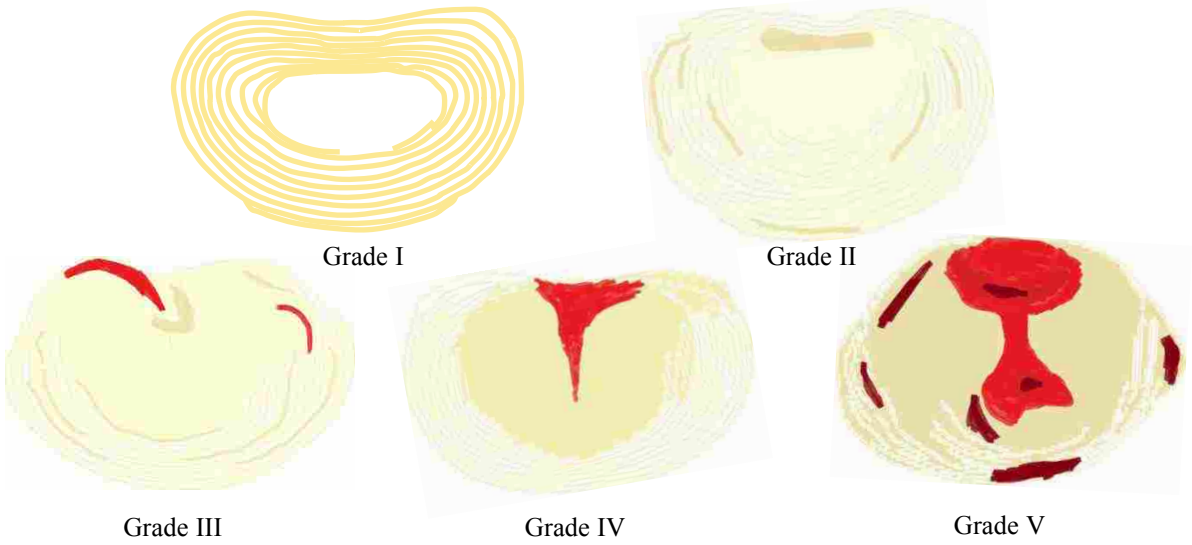

Figure 2.10: Thompson Grades for Disc Degeneration

2.5.2 Influences on Spinal Motion

Two other papers, though not directly associated with the hypothesis of this thesis, are noted here for their influence on this research. The first is by Patwardhan et al. [51]. This work centers on a "follower load", which is a compressive weight placed on a whole lumbar spine that follows the natural contour of the spine. This weight simulates the compressive upper-body weight and the muscle contraction loadings experienced in an IVD for a static loading. Such a compressive load methodology allowed *in vitro* testing to more closely match physiologic loadings.

In a second paper, by Elliott et al., the effects of needles inserted into an IVD were explored, with different diameters of needles inserted into the IVDs of several animals [52]. When the needle diameter was less than 25% of the disc height, no adverse effects of any kind were exhibited. Most

medical needle diameters used on humans do not approach this ratio in relation to the human disc. This reduces the potential influence the diameter of a needle used in human disc injections may have.

Some previous work has shown differences for individual FSUs in mechanical responses to torque. Tanaka et al. reported a general increase in ROM for LB and AR as a result of degeneration [53]. His work also noted a characteristic drop in ROM from Grade IV to Grade V (See Table 2.1). Zirbel et al. showed a general increase in ROM in AR, with a slight overall decrease in ROM in FE and a strong ROM decrease in LB (See Table 2.2) [1]. Her work also reported degeneration traits for K, HA, and HA/ROM. Stiffness generally decreased for AR, while generally increasing for higher degeneration levels in FE and LB. Hysteresis area tended to increase in AR and FE while rising sharply and then falling sharply in LB. HA/ROM saw marginal increases for degeneration in all directions. These results illustrate expected differences between degeneration grades. Zirbel et al. used the same testing hardware here at Brigham Young University, and therefore is instrumental in comparing degeneration characteristics found in this study.

2.5.3 Protease Digestion of Spinal Tissue

Human IVDs produce several proteases, or enzymes, and their matching protease inhibitors. Proteases utilize a process called "proteolysis", which is the breakdown of proteins into their core amino acids. Normally, the balance between protease activation and inhibition is regulated to create an environment of homeostasis. One sign of advanced disc degeneration is the increased presence of active proteases. An imbalance of tissue regeneration and breakdown may lead to an increase in proteolysis due to enzymes such as Matrix Metalloproteinases (MMPs), aggrecanase, and calpain [54–59]. The human body also naturally contains protease inhibitors, which essentially prevent the body from digesting itself. These proteins stop proteolysis by binding to active cleaving sites on the protease molecule, such as the zinc binding site [57]. Four tissue inhibitors of metalloproteinases (TIMPs) are known to restrict MMP and aggrecanase activity, and their decreased effectiveness during aging allows for greater protease activity [55].

Many proteases exist that have no natural connection to disc degeneration. However, some have been harvested and applied towards physically simulating degeneration. One such abundant protease commonly used in proteoglycan digestion is trypsin. Trypsin is produced in the pancreas

Table 2.1: Tanaka et al. Results [53]

	Upper		Lower	
Axial Rotation	Mean	SD	Mean	SD
Grade I	2.54	1.25	3.79	1.94
Grade II	3.15	1.47	4.23	1.68
Grade III	4.68	2.18	6.21	2.3
Grade IV	7.03	1.56	3.95	1.67
Grade V	5.21	2.24	4.42	1.66
Lateral Bending	Mean	SD	Mean	SD
Grade I	10.92	4.42	10.23	3.89
Grade II	9.27	3.04	9.78	1.82
Grade III	11.51	3.64	11.39	3.65
Grade IV	10.85	3.13	7.51	2.91
Grade V	8.36	3.38	7.27	2.63
Flexion	Mean	SD	Mean	SD
Grade I	4.07	2.93	6.52	2.69
Grade II	3.96	1.76	5.23	2.8
Grade III	4.91	2.53	6.09	2.61
Grade IV	5.52	1.5	5.57	2.85
Grade V	3.63	1.97	5.35	2.06
Extension	Mean	SD	Mean	SD
Grade I	2.78	2.01	4.21	1.42
Grade II	2.85	1.36	4.53	1.61
Grade III	3.27	1.44	3.54	2.6
Grade IV	3.9	1.75	3.62	1.47
Grade V	3.36	1.32	3.33	1.39

of humans and other mammals, and is found throughout the digestive tract. It dissolves protein peptide bonds, generally has an active pH of 7.5-8.5, and is most active at body temperature. This enzyme is commercially harvested via cattle, and is standard in biological laboratory proteolysis. Another protease is papain, which is found in unripe papaya fruit. It is commonly used in meat tenderizing and sore throat treatments.

There is medical precedence for injecting discs with a protease *in vivo*. Chemonucleolysis is the injection of a protease into the NP tissue of a herniated disc. Chymopapain, or a refined variant of papain, is the protease used due to its ability to target only NP material and leave AF tissue unharmed [60]. After administration of local anesthesia, chymopapain is injected to dissolve the extruded NP mass, thereby decreasing pressure on the compressed nerve roots. It has proven to be more effective than injection of a placebo, but less effective than performing a discectomy [61].

Table 2.2: Zirbel et al. Results [1]

	ROM			K			HA			HA/ROM		
	TG	Mean	SD	TG	Mean	SD	TG	Mean	SD	TG	Mean	SD
Axial Rotation	Grade I	2	0.58	Grade I	7.78	3.63	Grade I	2.58	1.31	Grade I	1.31	0.53
	Grade II	3.8	1.18	Grade II	4.27	1.85	Grade II	3.36	1.94	Grade II	0.87	0.35
	Grade III	3.78	2.3	Grade III	4.49	3.08	Grade III	5.23	2.46	Grade III	1.49	0.38
	Grade IV	4.98	2.53	Grade IV	2.92	1.7	Grade IV	6.33	2.62	Grade IV	1.35	0.32
	Grade V	4.4	2.15	Grade V	3.7	2.71	Grade V	6.58	2.58	Grade V	1.57	0.4
Flexion-Extension	Grade I	11.8	0.55	Grade I	0.24	0.04	Grade I	10.7	0.58	Grade I	0.91	0.01
	Grade II	9.8	1.14	Grade II	0.23	0.06	Grade II	9.5	0.36	Grade II	0.97	0.08
	Grade III	16.45	0.64	Grade III	0.1	0.05	Grade III	17.4	2.54	Grade III	1.06	0.14
	Grade IV	10.83	1.79	Grade IV	0.58	0.48	Grade IV	15.1	3.43	Grade IV	1.4	0.26
	Grade V	9.34	3.98	Grade V	0.98	1.06	Grade V	17.52	8.66	Grade V	1.85	0.32
Lateral Bending	Grade I	11.53	6.91	Grade I	1.11	0.67	Grade I	19.09	5.26	Grade I	1.95	0.66
	Grade II	16.3	4.71	Grade II	0.35	0.32	Grade II	29.17	9.75	Grade II	1.8	0.37
	Grade III	11.8	6.07	Grade III	1.03	1.03	Grade III	19.07	10.68	Grade III	1.59	0.26
	Grade IV	9.17	4.03	Grade IV	1.47	0.91	Grade IV	19.11	8.72	Grade IV	2.15	0.38
	Grade V	4.73	3.51	Grade V	4.48	2.82	Grade V	10.06	6.36	Grade V	2.24	0.3

This practice was discontinued in the U.S. in January 2003, due to concerns of life-threatening allergic reactions to papain [62]. Chrondoitinase ABC (CABC), a less-aggressive protease secreted from the bacteria *Proteus vulgaris* (commonly found in the digestive tracts of humans and animals), has become a prime candidate in replacing chymopapin [63, 64].

Many previous studies have focused on the effects of introducing proteases into a healthy mammalian disc environment. Some used CABC, while others utilized trypsin, papain, or MMPs. Experiments included bovine (cow), ovine (sheep), caprine (goat), canine, rat, rabbit, and even primate subjects. These studies found that injecting animal discs with protease solutions caused an acceleration of tissue breakdown. Notably, major disc alterations centered around a decrease in stiffness and loss of disc height, which corresponded to a drop in proteoglycan and water content in the NP [64–68]. Detiger et al. also found stiffness in caprine discs decreased in LB and AR, while ROM increased in AR and LB via CABC injection [69]. CABC and chymopapain injections also increased NZ measurements in all bending directions in canine discs [63], while loss of NP cells and increased hysteresis in rats was also exhibited [70]. Decreased intradiscal pressure in ovine discs from CABC injections was also demonstrated [71].

The goal of advancing mechanical degeneration in human IVDs via trypsin injections is a natural extension of three similar projects. Mwale et al. subjected bovine tail segments to trypsin treatment and compressive loading for 16 hours to determine the effect on MRI parameters, as well as to determine changes in mechanical and biochemical properties [72]. Trypsin caused greater alterations to mechanical properties than the applied loadings. A second study completed by Roberts et al. subjected bovine tail discs to different enzyme solutions for up to three weeks. In comparison to disc samples in saline-buffered solutions, trypsin- and papain-treated discs showed extensive damage after testing, with most changes taking place in the NP [73]. Papain caused more extensive damage in less time in comparison to trypsin. Roberts et al. aimed to introduce the possibility of a gene therapy or injectable synthetic gel for restoring NP function [74].

Another investigation was performed by Bishop et al. [75]. After trypsin injection, intact bovine coccygeal FSUs were subjected to compression/tension, AR, or FE testing. Significant decreases in ROM were discovered in all modes of loading for one hour after injection. The same decreases were found for three hours after injection. ROM decreases were found at the 30 minute mark for compression and flexion-extension, though ROM increases were reported for

axial rotation. These three studies concluded that trypsin injections into bovine coccygeal segments accelerated mechanical degeneration. Since bovine discs are one of the more similar animal models to human lumbar IVDs, trypsin injections will likely have the same degenerative effect in cadaveric specimens.

2.6 Animal Models and Cadaveric Testing

Ideally, treatments of disc degeneration would first be validated through animal models. However, this proves to be far more difficult in reality due to fundamental differences between human and animal IVDs [76]. Most mammals are quadrupeds, which puts their spine perpendicular to gravitational forces rather than parallel like humans. This leads to differences in the force and moment loadings experienced in the discs. Anatomical differences exist as well, with variations in process shape and function, ligament amount and location, and sizes of spinal components. Not only are most mammal spines smaller, which requires scaling to equate results to human scenarios, they also have different relative sizes between sections compared to humans. In other words, the difference between a cervical FSU and a lumbar FSU in size and shape is generally smaller in animals, whereas humans see a greater contrast between cervical, thoracic, and lumbar regions.

Another critical area of difference is in biochemical and cellular make-up of an IVD. Collagen fiber content is not the same. Also, animal discs contain notochordal cells throughout their life, whereas humans lose notochordal cells completely by young adulthood [77–79]. Though animal models are useful in exploring disc degeneration problems, care must be taken in extrapolating the results of animal studies to humans.

Human cadaver models certainly provide a much higher degree of fidelity in predicting *in vivo* effects in people. However, cadaver models also have shortcomings. Cadaver models lack what animal models can offer in abundance and cost-friendliness of test specimens. For ethical reasons, human subjects must consent to tissue donation, which significantly reduces the pool of available discs. This is coupled with the fact that most cadaveric spinal tissues come from donors over 50 years old, meaning most test tissue is already somewhat degenerated. Finally, most human spinal tissues cost well over 1,000 dollars (US), making acquisition of cadaver spines relatively cost-prohibitive.

One important note in human testing is the significant chance for large variability between subjects. No two individuals have identical structure and composition in their bodies. Differences in lifestyles, health, injury history, and other such factors can greatly complicate biological testing results by introducing large amounts of variance. However, until successful minimally-invasive *in vivo* testing can be ethically accomplished, cadaveric tissue testing provides the most accurate model.

2.7 Proposed Solution

Building off the previous research, the present work progressed *in vitro* testing from using animal specimens as degeneration models to using cadaveric lumbar IVDs. Trypsin was utilized as the primary enzyme used to simulate accelerated disc degeneration. Differences found in the Thompson Grade (TG) of each disc due to testing were compared to that found in previous work. Such differences were also utilized to approximate a repeatable correlation between time and nature of testing, specifics of protease injection, and change in TG. This correlation could be extended for use in pre-clinical testing of spinal implants to simulate the mechanical effects of such devices on the adjacent spinal levels where degeneration due to aging is mimicked.

3. PREDICTING THE EFFECTS OF DEGENERATION ON SPINAL MOTION

3.1 Creation of a Degeneration Baseline

In creating an *in vitro* degeneration model based on trypsin injections, the natural changes in biomechanics of an FSU from healthy to diseased states must first be established. Several studies reported such changes in spinal motion, but all lacked important test methodologies that impacted specimen performance [15,49,50,53]. No FSU mobility study (other than Zirbel et al. [1]) reported the use of a compressive follower load during testing. Studies from relevant literature did not incorporate body temperature settings, instead testing at room temperature [15,49,50,53]. Weights and pulleys, rather than a stepper motor, were used to create a torque on the FSU [15, 49, 50, 53]. Since this method of applying torque was discrete and quasi-static, quality of motion parameters like stiffness, hysteresis, and neutral zone exhibited a lack of resolution in observed results [80].

By combining relevant data from Zirbel et al. [1] with pre-injection flexibility results from this needle injection study, a new natural degeneration model was created. This model predicts the mechanical behavior of a single FSU in any normal bending mode (i.e., AR, FE, LB) for any degeneration state using seven major motion parameters (i.e., ROM, K, NZ, etc.). This model defines clear mechanical changes between degeneration levels to mimic in the potential use of an *in vitro* protease injection model.

3.2 Specimen Preparation

Sixteen cadaveric lumbar spines were dissected of all musculature and adipose tissue, leaving vertebral bodies, IVDs and spinal ligaments intact. Eight were tested by Zirbel et al. [1], and eight were used for trypsin injection studies in this thesis. Spines were hydrated throughout dissection by frequent spritzing of tissue with phosphate-buffered saline (PBS) solution [1, 81]. After

dissection, 41 FSUs were segmented from the spines, deemed eligible for testing, and stored at a temperature of -20°C until the commencement of testing.

Prior to flexibility testing, the FSU was allowed to thaw overnight. Each vertebral body was potted by using a two-part epoxy resin (Bondo, 3M, St. Paul, MN). These potting structures were trimmed to size in order to secure them in metal potting fixtures that attached to a custom-built spine simulator. Once secured in the environmental chamber of the spine tester, four high-contrast marker plates were attached to two sides of the superior endplate fixture. The FSU was then left in the environmental chamber for a half-hour to bring the disc up to body temperature [1].

3.3 Mechanical Simuation of Spinal Motion

3.3.1 Mechanical Testing Hardware

The spine tester, dubbed MASSUCE (Multi-Axial Spine Simulator Under a Controlled Environment), utilized a rotational load cell, or torque cell, to collect the resistive torque of the motion segment. The MASSUCE was modeled after a similar spine tester detailed by Oxland et al. [80], but has been modified to include a compressive follower load, as well as an integrated environmental chamber capable of supporting the testing specimen at body temperature (37°C) and near 100% humidity. A stepper motor with an attached rotary encoder created a continuous torque on the shaft that moved the FSU. A universal joint attached the main motor shaft to a steel elbow which carried the pure moment to the test specimen. This set-up was used for FE and LB, where switching these two directions was done by rotating the FSU 90°. Moments in the AR direction were applied by removing the motor and shaft from the table-top position and attaching it to an overhead platform directly above the FSU (See Figure 3.1). In the AR configuration, the universal joint attached directly to the FSU superior fixture. This whole procedure allowed the specimen to always be tested with a pure moment.

A 440 N compressive follower load was applied to each segment during testing to simulate the *in vivo* forces caused by upper body weight and muscle action [51, 82]. Placement of follower load cables on the superior potting fixture was optimized to minimize static moments in both lateral bending and flexion-extension axes. The cables were fixed so as to cause the FSU's initial axis of rotation to be as close to the neutral position as possible (starting location was calibrated

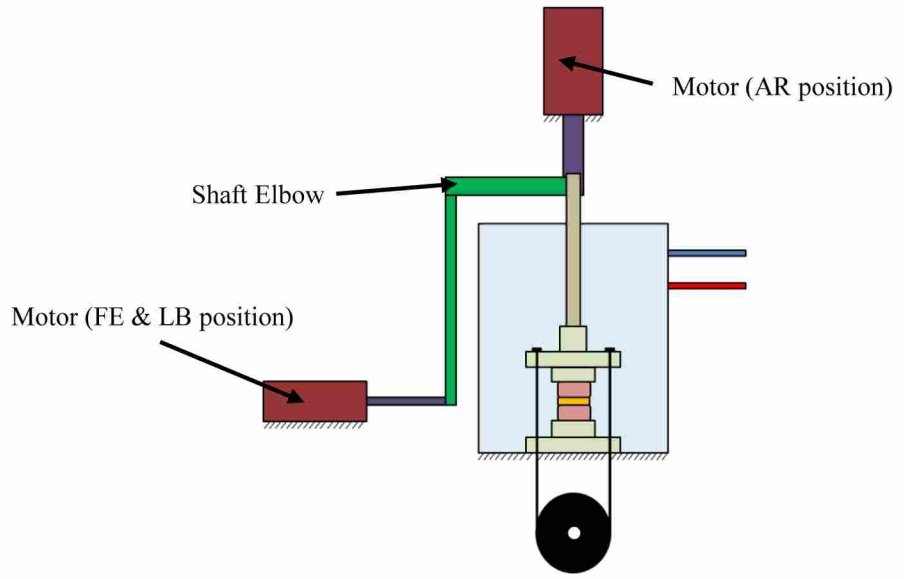

Figure 3.1: Simplified Front View of MASSUCE with Motor Arrangements

to $\pm$0.3 Nm, with 0.0 Nm defined as the neutral position). High-resolution 3D motion tracking of the FSU was achieved using calibrated cameras mounted outside the environmental chamber (See Figure 3.2).

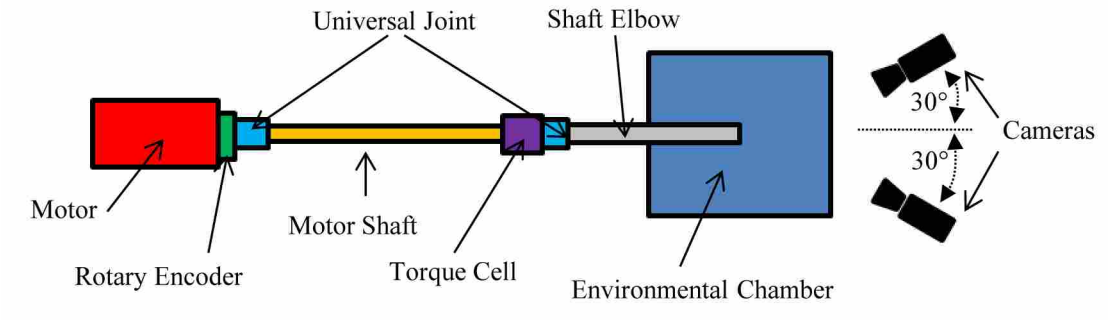

Figure 3.2: Simplified Top View of MASSUCE

The torque cell collected approximately 1,000 data points between each frame saved from the cameras. This torque data was averaged over the time between frames, then assigned to the corresponding camera frame to allow for plotting a synchronized moment-rotation response from the spinal test specimen.

3.3.2 Testing Procedure

Each FSU underwent a series of ten pre-conditioning motion cycles for each mode of loading (AR, FE, and LB), ensuring consistent characteristic motion. The order of bending directions between FSUs was randomized to minimize bias. Each test cycle started at zero torque, with the torque load increased to 7.5 Nm before reversing rotation and eventually reaching -7.5 Nm of torque, all while rotating at a rate of 1° per second [83]. A testing cycle was completed once the initial zero-torque reading was reached following the movement through the maximum and minimum desired torques. On the final cycle of each test series in each direction of loading, torque cell readings and camera images were recorded.

After the final flexibility test was conducted, the FSU was removed from the environmental chamber and transected mid-disc. Preliminary degeneration levels were characterized using the Thompson Scale [48]. One FSU tested by Zirbel et al. was discarded due to tearing of disc tissue part-way through testing.

3.4 Motion Data Processing

3.4.1 Data Analysis

All images captured by the spine simulator cameras were subjected to custom-made motion analysis software to determine the FSU rotations using direct-linear transformation techniques [84]. Moment-rotation plots were fit using a Boltzmann dual-inflection point (DIP) curve [1], which was used to find all motion parameters (i.e., ROM, K, H, etc.). Average curve fits held R^2 values of 0.9972.

The Boltzmann DIP curve fit is a modification of the Boltzmann equation, with a second inflection point added to the exponential function [1]. This equation (Equation 3.1) relates bending moment to angular displacement and includes six parameters for each curve.

$$\theta = \frac{A}{1+e^{\alpha_1(m-m_1)}} - \frac{B}{1+e^{\alpha_2(m-m_2)}} + B \tag{3.1}$$

Two of the parameters, “A” and “B”, determine the maximum and minimum ending points of the curve, and are found by dividing the ROM of the curve in half (See Figure 3.3). “m_1” is the location

(on the applied-torque axis) of the left-most inflection point, and "m_2" is the site of the right-most inflection point. "α_1" and "α_2" are the slopes of the curve fit at "m_1"and "m_2", respectively. These four curve-fit parameters are calculated using a general linear solver that finds the minimum sum of the squared differences between the collected data and the curve fit.

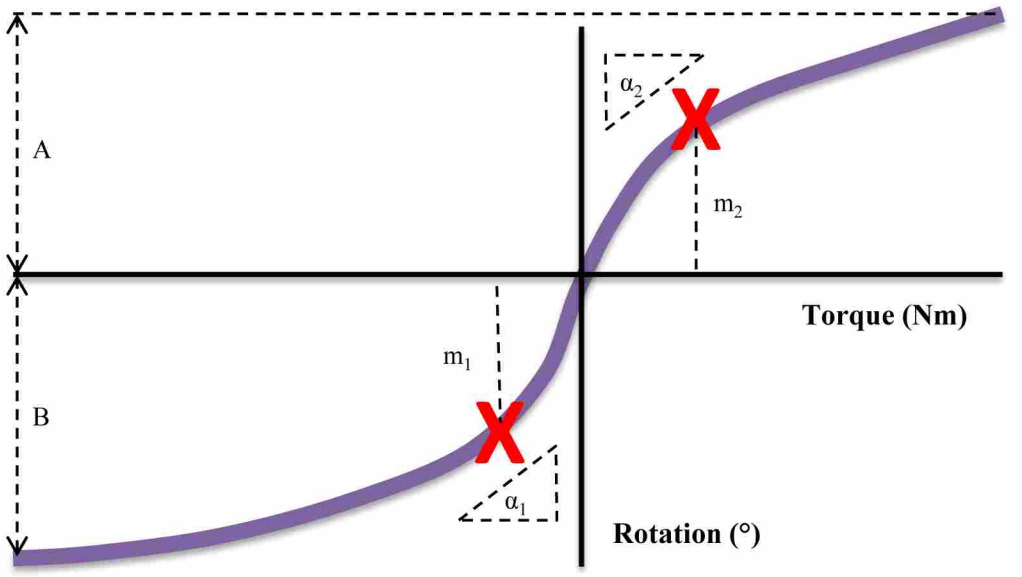

Figure 3.3: DIP-Boltzmann Curve Parameters

The complete data set of an FSU motion test is divided into two curves, an upper and a lower curve (See Figure 3.4). These six parameters are found for both curves, giving each individual test run twelve curve-fit parameters. However, "A" and "B" for the upper and lower curves are the same, giving each test ten independent parameters. These ten curve-fit parameters are used to calculate all of the major motion parameters that describe FSU flexibility.

Since the Boltzmann DIP curve-fit is an exponential equation, no standardized filtering was applied. However, there were a handful of instances where the torque cell output an irregular spike. These outliers in torque data could slightly alter the curve-fit parameters, especially since the sum of squared-differences solver gives greater attention to these abnormalities than to other data points. Motion tracking results also occasionally output irregular results that created spikes in the data. This occurred when the motion tracking program that followed the high-contrast marker plates suddenly lost those plates for reasons unrelated to spinal motion. Streaks of water or larger amounts of condensation on the inner glass surface, poor lighting placement that created glare,

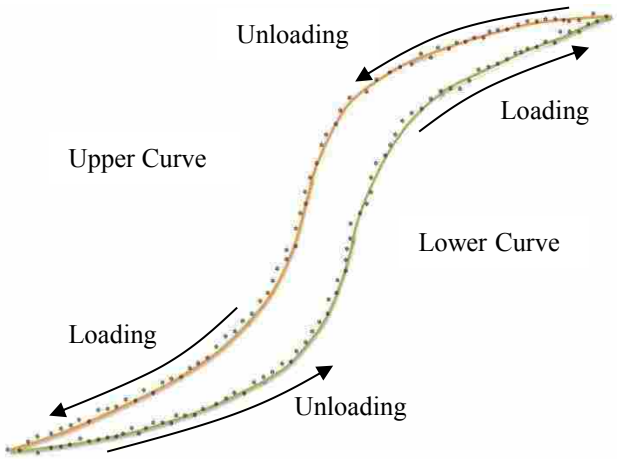

Figure 3.4: Upper and Lower Boltzmann DIP Curve-Fits with Data

or dim lighting caused most motion tracking disturbances. A simple band-pass filter using three standard deviations as the cutoff was applied to the data, effectively eliminating these sources of systemic noise. This filtering of data spikes generally caused curve-fit parameter alterations of 10% or lower. As this was only performed on about 2% of test runs, this filtering had little effect on overall curve behavior.

3.4.2 Statistical Modeling and Analysis

Most statistic analytical models fall under the umbrella term of "General Linear Models". Such models include t-tests, linear regression, and analysis of variance (ANOVA). ANOVA can look at variance between all treatments (e.g., injection A, injection B, injection C, etc.) using one-way between-subjects testing [85]. ANOVA can also look at variation due to time through one-way within-subjects testing. T-tests, which are frequently used in statistical analysis of experimental results, are intended to discern differences between only two groups (e.g., injection A and injection B) of one independent variable (ex. injection treatment). The combination of both within-subjects (i.e., effect of time on same specimen) and between-subjects (i.e., effect of different treatments) analysis for multiple treatments and times of data collection called for the use of mixed-models ANOVA for this trypsin-model study.

ANOVA is based on three major assumptions: the errors in the data are independent of each other, the independent errors are normally distributed, and the variances within or between

groups of independent variables (i.e., time and injection treatment) are equal. Efforts were taken to ensure these assumptions were met. The first assumption was met by the testing methodology. Since separate FSUs had no interaction with each other after dissection, the eight spines came from random donors with no related history, and the same general methodology was used for each FSU, the flexibility of a single FSU had no effect on the flexibility of any other specimen. This fulfilled the first assumption. The second assumption was tested by running Shapiro-Wilk and Kolmogorov-Smirnov tests with an alpha value of $p<0.001$ [85]. Results showed that the majority of parameters (89%) from the collected data did not violate this assumption. Since violations of this assumption occurred where outliers had not been eliminated, they were ignored. Finally, homogeneity analysis using Levene, Brown-Forsythe, Bartlett, and Welch tests with an alpha level of $p<0.05$ was used to test the third assumption. Results from homogeneity analysis showed that the third assumption was met. With these three assumptions adequately addressed, ANOVA use was considered appropriate.

A one-way ANOVA using SAS 9.3© was calculated to determine statistically significant trends in degeneration results. Degeneration levels were classified as the independent variable. P-values of <0.05 were deemed statistically significant. Any individual test results showing procedure abnormalities were discarded from further examination.

3.5 Results

ROM results in AR were very similar for Grades I and II, then increased several degrees for Grade III where it stayed constant for more degenerated grades (See Figure 3.5). Stiffness results followed the same trend, where Grades I and II were similar to each other and different from Grades III through V, though the change was a decrease instead. Changes from Grades II to IV and from Grades II to V were considered significant ($p<0.05$). Hysteresis area gradually increased as greater degeneration was experienced, though a sharp decrease at Grade II interrupted this trend (See Figure 3.8). H, HA/ROM and NZ/ROM all decreased through Grade III, then increased through Grade V (See Figures 3.8 and 3.11, and 3.12). Neutral zone decreased to Grade II, then increased from thereon (See Figure 3.12).

Flexion-Extension ROM stayed very constant through all grades, with the exception of a large spike at Grade III (See Figure 3.6). Stiffness, however, fell sharply through Grade III, then

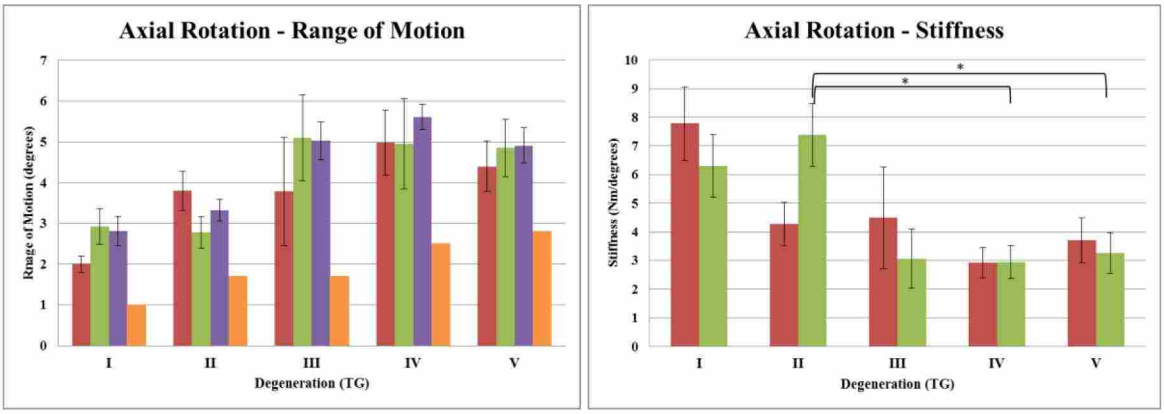

Figure 3.5: Degeneration Effects on AR ROM and K (Red represents findings by Zirbel et al., Green shows combined results from this study and Zirbel et al., Orange shows medians reported by Krismer et al., and Violet represents findings from Tanaka et al.; * - $p<0.05$)

increased at Grade IV before falling again. H and HA/ROM similarly declined through Grade III, followed by an increase through Grade V (See Figures 3.9 and 3.11). Interestingly, HA and the neutral zone parameters started with a slight decrease, only to alternate increasing and decreasing from grade to grade afterwards (See Figures 3.9 and 3.13).

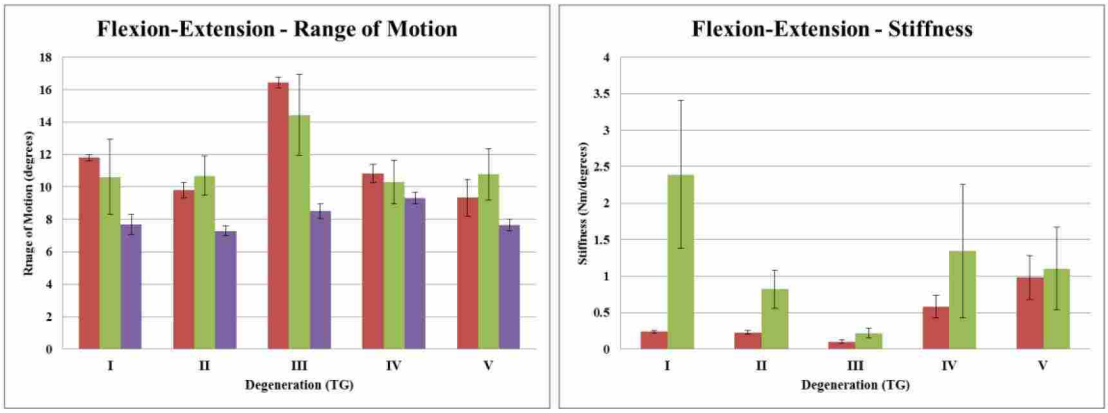

Figure 3.6: Degeneration Effects on FE ROM and K (Red represents findings by Zirbel et al., Green shows combined results from this study and Zirbel et al., and Violet represents findings from Tanaka et al.)

Lateral Bending ROM decreased with the advancement of degeneration, with the loss of ROM becoming more substantial after each grade (See Figure 3.7). Changes from Grades II to IV and from Grades II to V were considered significant ($p<0.05$). K dropped slightly from Grade I

to Grade II, followed by an exponential increase through each grade (See Figure 3.7). Grades I, II, and III were all considered significantly different from Grade V ($p<0.05$). HA and the neutral zone parameters stayed relatively constant between Grades I and II and between Grades III and IV, with substantial drops from Grades II to III and from Grades IV to V (See Figures 3.10 and 3.14). Hysteresis and HA/ROM declined slightly through Grade III, followed by a jump at Grade IV (See Figures 3.10 and 3.11). (For raw means and standard deviations, please see Table B.1 in Appendix B.)

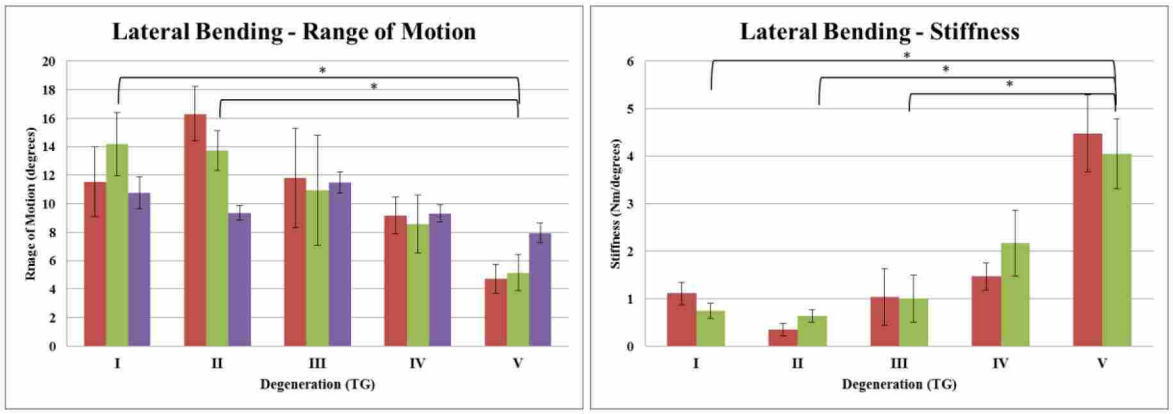

Figure 3.7: Degeneration Effects on LB ROM and K (Red represents findings by Zirbel et al., Green shows combined results from this study and Zirbel et al., and Violet represents findings from Tanaka et al.; * - $p<0.05$)

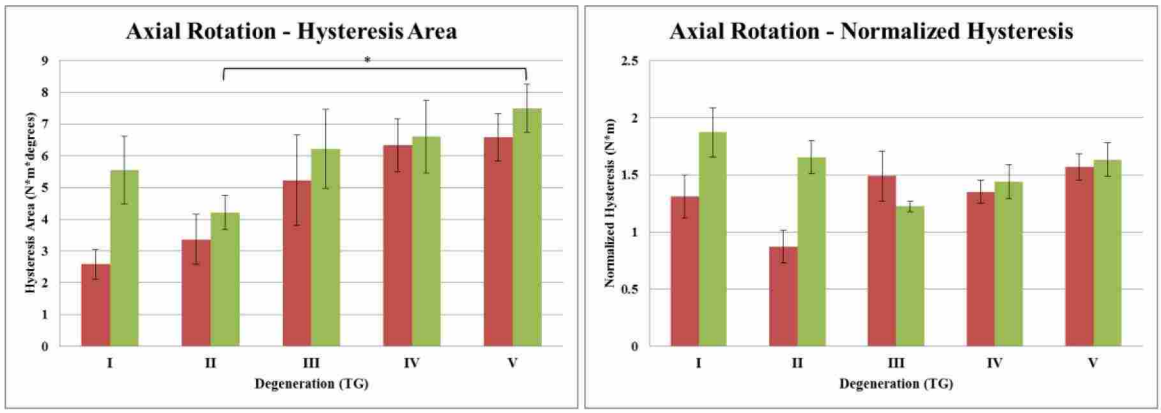

Figure 3.8: Degeneration Effects on AR HA and HA/ROM (Red represents findings by Zirbel et al., Green shows combined results from this study and Zirbel et al.; * - $p<0.05$)

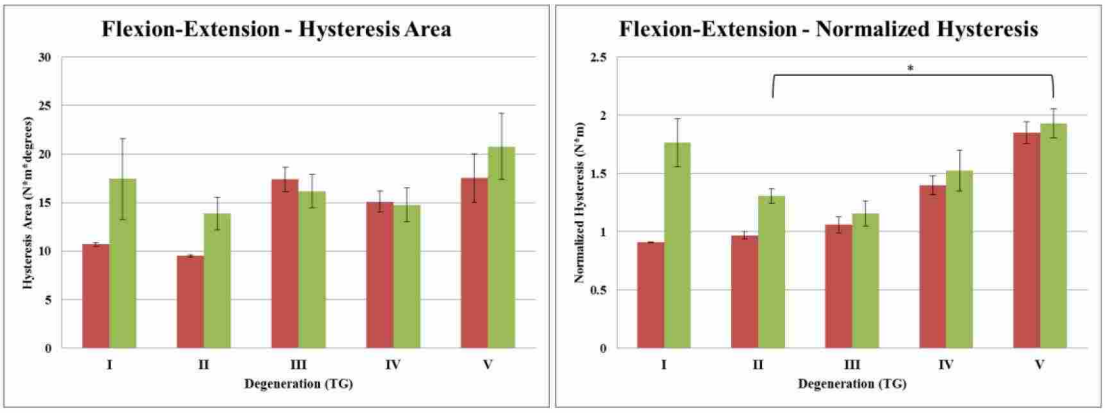

Figure 3.9: Degeneration Effects on FE HA and HA/ROM (Red represents findings by Zirbel et al., Green shows combined results from this study and Zirbel et al.; * - $p<0.05$)

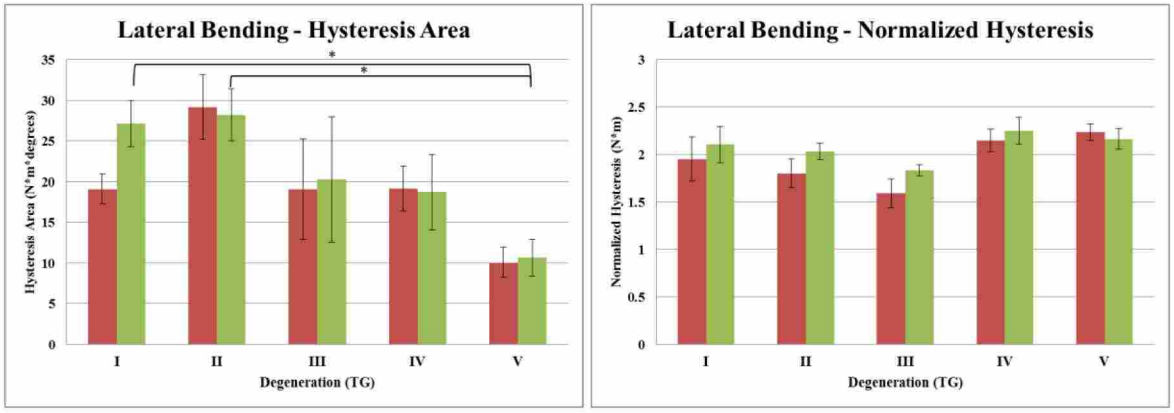

Figure 3.10: Degeneration Effects on LB HA and HA/ROM (Red represents findings by Zirbel et al., Green shows combined results from this study and Zirbel et al.; * - $p<0.05$)

3.6 Discussion

This combined study with Zirbel et al. [1] added greater clarity to the expected mechanical outcomes of natural disc degeneration. In several instances, such as FE ROM, LB ROM, LB K, and LB HA/ROM, the combined findings closely matched those from Zirbel et al. In other instances, such as FE K and AR HA/ROM, distinct differences were observed. Generally, differences that did exist between the combined study and Zirbel et al. were observed at Grades I and II while greater similarities were seen at higher grades of degeneration. These differences were caused by two factors. First, Zirbel et al. combined body temperature and room temperature testing results in their final outcomes. In this combined degeneration study, only body temperature findings

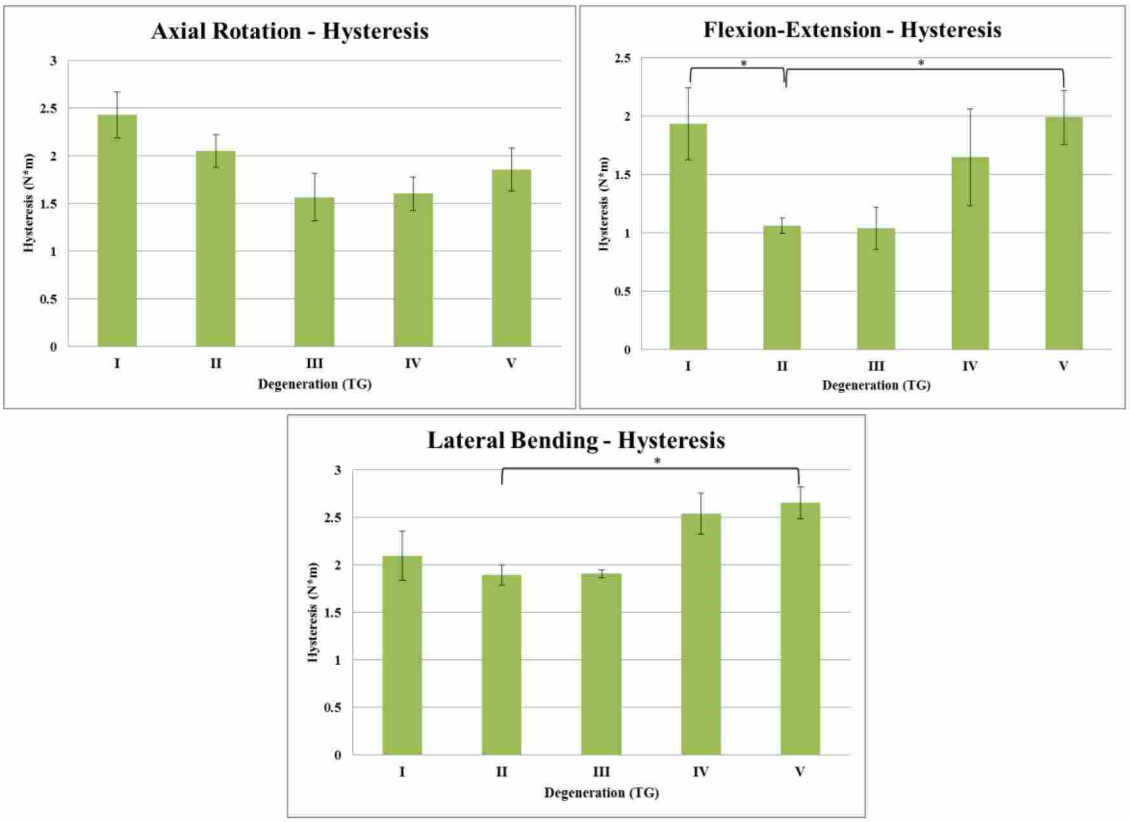

Figure 3.11: Degeneration Effects on Hysteresis for the Combined Study in All Directions (* - $p<0.05$)

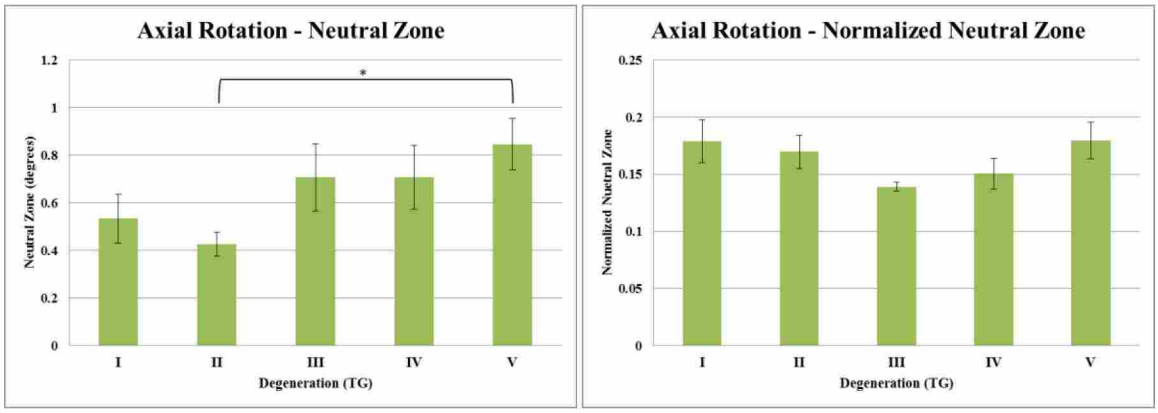

Figure 3.12: Degeneration Effects on AR NZ and NZ/ROM for the Combined Study (* - $p<0.05$)

were incorporated. Second, the addition of flexibility characteristics from 20 FSUs (16 of which were Grade I, II, or III) greatly enhanced those findings already reported by Zirbel et al. Another

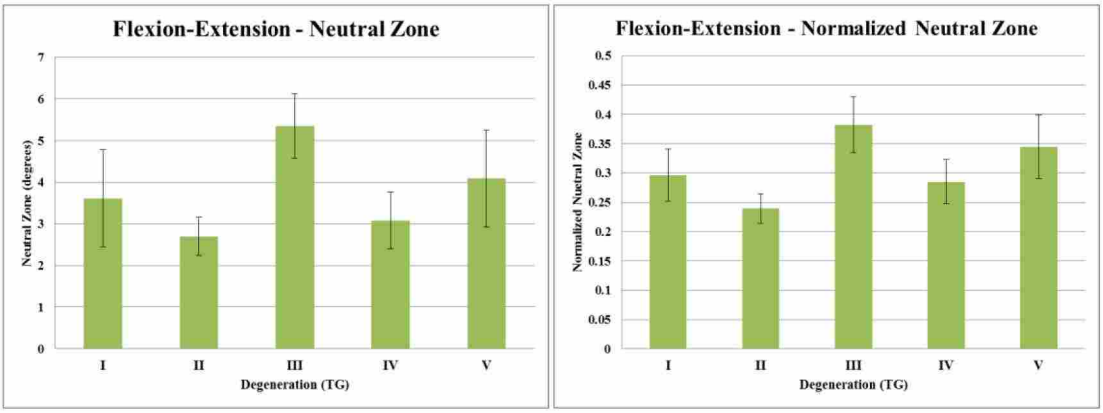

Figure 3.13: Degeneration Effects on FE NZ and NZ/ROM for the Combined Study

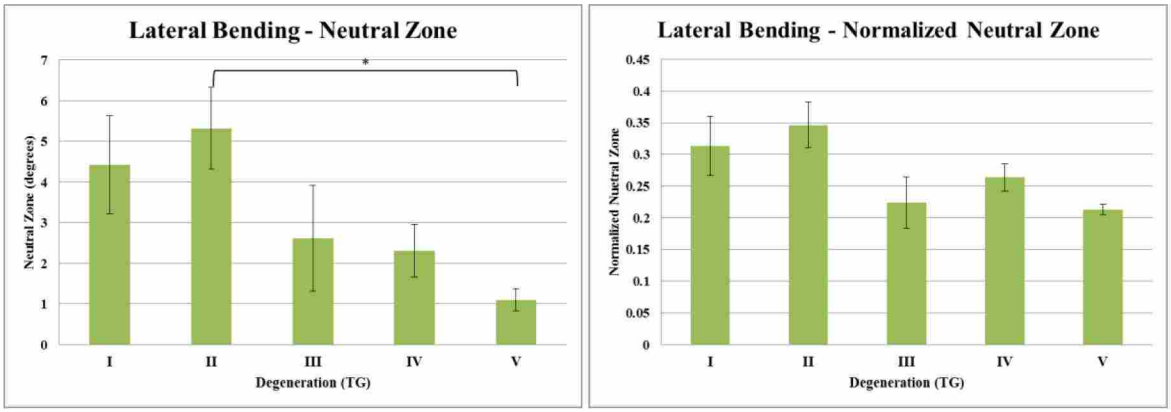

Figure 3.14: Degeneration Effects on LB NZ and NZ/ROM for the Combined Study (* - $p<0.05$)

outcome unique to this combined study was the reporting of NZ, NZ/ROM, and H results, which were not reported by Zirbel et al.

For AR ROM results, these findings were a close match to the findings of Tanaka et al. [53], which may mean a follower load and body temperature settings are not required to test ROM in AR. However, this was not the case in FE or in LB for ROM, where significant changes existed between the two studies. Therefore, introducing the follower load and the environmental chamber may introduce substantial alterations to FSU mechanics when testing in FE or LB. These alterations are likely exaggerated at higher levels of degeneration (i.e., Grades IV and V) where there is a significant change in disc height due to fluid loss. Thus, geometric effects such as facet contact may play a significant role.

Generally, healthier disc mechanics were significantly different from more degenerated discs. Establishment of statistical significance between healthier disc grades using this testing methodology likely requires a larger sample size (26 discs graded I-III were utilized in the combined study). Although few statistically-significant differences were found between healthier discs (i.e., Grades I, II, and III), healthier grades frequently exhibited distinct alterations in mechanics. Such was the case in all bending directions for NZ, H and HA/ROM for AR and FE, HA for AR and LB, and ROM and K in all directions. Several of these parameters, like ROM, K, and NZ, exhibited distinct patterns of modified mechanics.

The combination of the results from these two studies yielded two outcomes that benefit this research of mimicked degenerative spine mechanics. First, the overall sample size of the Zirbel study was doubled, thus giving greater statistical power due to an increased sample size. This is especially true of healthier grades of degeneration. Such an increase allowed for a refinement of expected motion alterations due to degeneration. Such was the case for stiffness in LB, where the updated plots are in greater agreement with accepted degenerative biomechanics of the spine. The other outcome is that additional neutral zone parameters and hysteresis measurements were reported, thus giving additional motion parameters to distinguish patterns in changes to quality of motion. These patterns of change in healthier disc mechanics provide a solid framework for creation of a protease-injection degeneration model.

4. MIMICKING THE EFFECTS OF DEGENERATION ON SPINAL MOTION[1]

4.1 Introduction

Chronic low-back pain (LBP) is a debilitating condition that affects millions every day, and which has no known cure. LBP has several potential sources, such as osteoarthritis, muscle strains, dysfunctional ligaments, and degenerated intervertebral discs (IVD) [10]. Disc degeneration occurs naturally in adults during the advancement of aging, and is hypothesized to be a leading pain generator. As the disc degrades, annulus fibrosis (AF) and nucleus pulposis (NP) tissues alter their cellular and biochemical characteristics [18]. Such changes cause a shift in mechanical behavior of the disc, which in turn affects the clinical stability of the spine [15, 50, 53].

In severe cases of chronic LBP, surgical operations can be performed on the IVD. Orthopedic spinal procedures may temporarily reduce pain by removing problematic discs, but do so at the expense of normal functional biomechanics. This trade-off makes even the "gold standard" of IVD surgeries, spinal fusion, exhibit mixed results in alleviating pain [33]. Such inconsistent success of treatment has led to the development of various motion-restoration devices such as total disc replacements (TDR). Motion-restoration devices show promise in providing mechanical performance consistent with that seen in healthy spinal motion segments. Because of these devices' relatively recent development (less than 10 years in the U.S.), their long-term performance in patients is currently unknown. With no reliable validation of device lifetime performance and durability, the overall mechanical effects of these surgically-implanted devices on the spine are difficult to predict [37]. Pre-clinical methods of modeling the behavior of an implanted spinal device can address this inadequacy. One potential method is *in vitro* testing that simulates advanced degeneration with a TDR implanted in a cadaveric spine. Currently, no *in vitro* methodology considers the advancement of adjacent disc level degeneration, and its potential effect on TDR performance.

[1] This chapter is a copy of an article to be submitted to a peer-reviewed journal.

Previous research has shown that injection of a protease solution into the IVD of bovine coccygeal segments induces disc degeneration [67, 72, 73, 75]. The literature contains no reported findings of the injection of a protease into cadaveric disc specimens. Though several studies have reported the effect of degeneration on spinal quality of motion, an attempt to artificially mimic the acceleration of disc degeneration *in vitro* has not been published. A novel approach to mechanically simulating disc degeneration via protease injections could potentially provide a protocol to pre-clinically validate the effect of TDRs and related motion restoration devices on adjacent spinal level biomechanics.

4.2 Methods and Materials

4.2.1 Specimen Preparation

Eight cadaveric lumbar spines (4 male and 4 female, aged 16-79 with an average age of 47.6 years) were dissected of all musculature and adipose tissue, leaving vertebral bodies, IVDs and spinal ligaments intact. Functional spinal units (FSUs) with damaged anterior longitudinal ligaments, supraspinous ligaments, and interspinous ligaments were excluded. During dissection, the cadaveric spine was spritzed with a phosphate-buffered saline (PBS) solution [86] every five-to-ten minutes to maintain full hydration [1, 16, 81]. Conditions of the spines and the separate FSUs were recorded in a lab notebook and documented visually with a digital camera. After dissection, eighteen FSUs were segmented from the spines, deemed eligible for testing, and stored at a temperature of -20°C until the commencement of testing.

Prior to flexibility testing, the FSU was thawed overnight at room temperature. Afterwards, the FSU was potted to form a rigid gripping surface on each vertebral endplate by using a two-part epoxy resin (Bondo, 3M, St. Paul, MN). These potting structures were secured in metal potting fixtures that attached to a custom-built spine simulator (See Figure 4.1). This spine motion simulator was capable of applying pure moment loads via a stepper motor attached to an adjustable motor shaft [80]. The orientation of the potted FSU, as well as the location of the motor, could be altered to test for axial rotation (AR), flexion-extension (FE), and lateral bending (LB). The spine simulator had an integrated environmental chamber, which maintained internal conditions of body temperature (37°C) and near 100% humidity [1]. Once the FSU was secured in the environmental

chamber, four high-contrast marker plates were attached to two sides of the superior endplate fixture. A compressive follower load of 440 N (meant to simulate upper body weight and muscle activation forces) was attached to the superior potting fixture through a cable-and-pulley system. The placement of the follower load cables was optimized to minimize static moments in both lateral bending and flexion-extension axes. The FSU was then left in the environmental chamber for a half-hour to warm the disc up to body temperature.

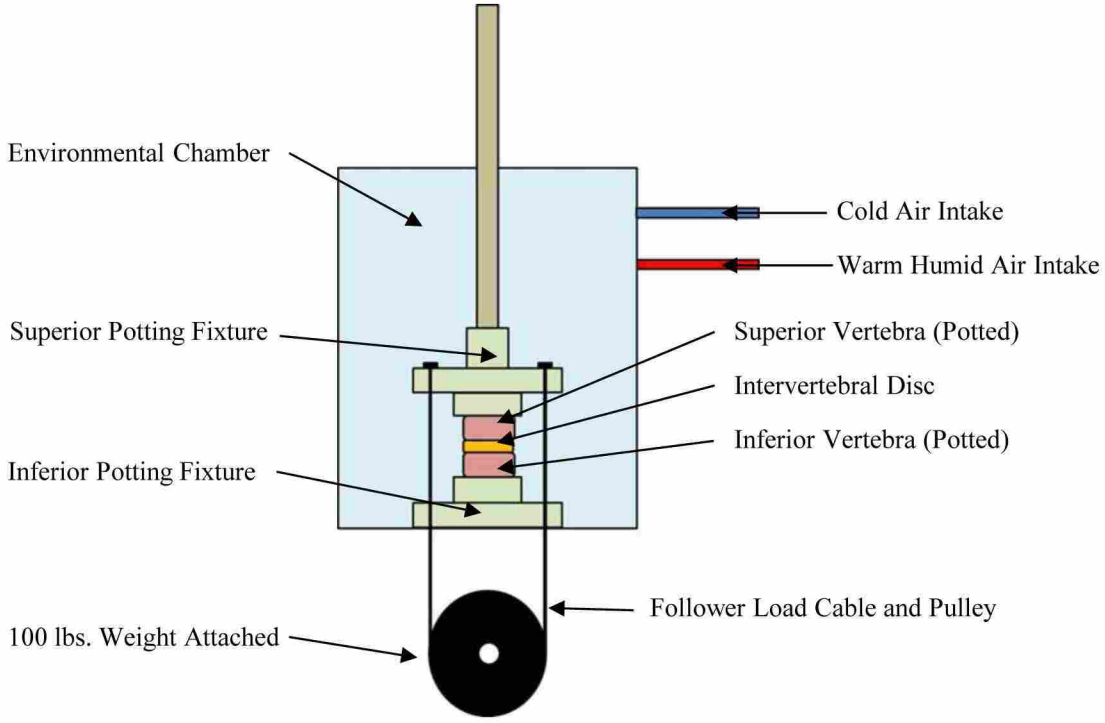

Figure 4.1: Environmental Chamber Set-up

4.2.2 Testing Procedure

Each FSU underwent a series of ten pre-conditioning motion cycles for each mode of loading (i.e., AR, FE, LB) to ensure greater repeatability in FSU motion. Each test cycle started at the FSU's neutral position (i.e., zero torque), with the torque load increased to 7.5 Nm at a rate of 1° per second. Once the maximum torque was reached, the motor instantaneously switched directions and eventually reached -7.5 Nm of torque while rotating at the same rate [83]. A testing cycle was completed once the neutral position was reached following the movement through the desired

maximum and minimum torques. On the final cycle of each pre-conditioning test series, segmental flexibility data was recorded to serve as a pre-injection baseline. Collected data included torque sensor readings from the torque cell and 3D positional data acquired from two cameras positioned outside the environmental chamber angled at 60° from each other. Transparency of the glass separating the cameras and FSU-marker plate system was ensured by using a heat gun to keep the glass warmer than the environmental chamber's internal temperature.

Following pre-conditioning data collection, 600 μL of trypsin-solution (HyClone 2.5% 10x, Thermo Scientific, Waltham, MA) was injected at six equally-spaced intervals (D) along the circumference of the disc into the AF of 12 discs at a constant depth of approximately 1 cm (See Figure 4.2). Prior to injection, the trypsin solution was mixed with a Brilliant Blue FCF food dye (Assorted Food Color & Egg Dye, McCormick & Co., Inc., Hunt Valley, MD), which aided post-test inspection of protease diffusion throughout the disc. During injection, the needle was inserted to the depth of the attached cork spacer and then pulled out approximately 2 mm to allow greater space for solution diffusion. This also minimized trypsin leakage out the injection point by reducing the effect of internal swelling pressure. 27 gauge (0.4128 mm outer diameter) needles were used to minimize AF tissue damage [52].

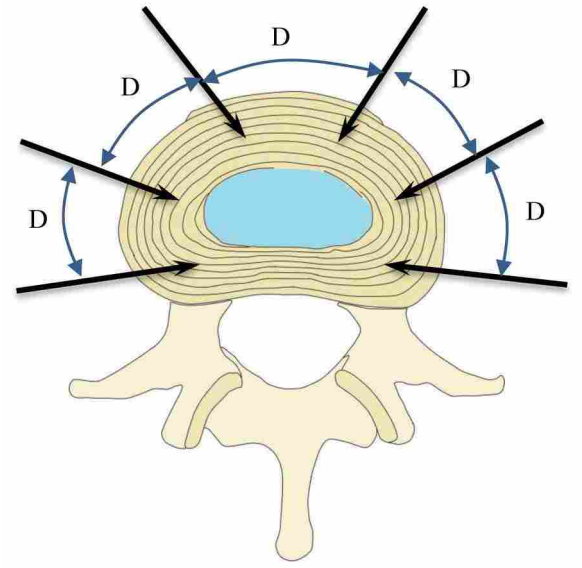

Figure 4.2: Disc Injection Sites

The FSU was immediately tested after injection (Time 0) for three cycles in all three directions of loading (i.e., AR, FE, LB), with torque-rotation data recorded on the final cycle for each bending direction. This testing was repeated every 30 minutes for three hours (See Figure 4.3). The order of testing directions (i.e., AR, FE, LB) was kept consistent between each flexibility test run, but randomized between each FSU. Once the final flexibility test was conducted, the FSU was removed from the environmental chamber and transected along the injection points (See Figure 4.4). Preliminary degeneration levels were then visually characterized using the Thompson Scale [48].

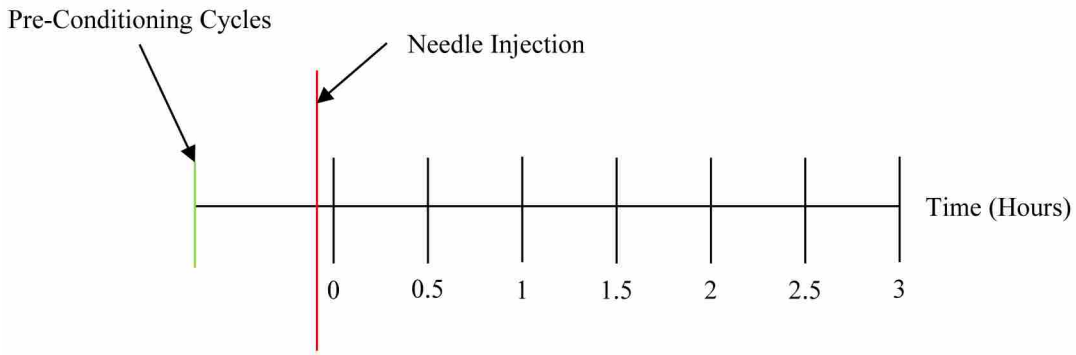

Figure 4.3: Flexibility Testing Timeline

Figure 4.4: Diffusion of Trypsin/Blue Dye Solution

This same procedure was followed for the injection of a PBS solution into three FSUs (from two cadavers), which was targeted as a control group. A second control group of three FSUs (from two cadavers) was subjected to needle penetration at the same six locations, but with no fluid injection, and was also subjected to flexibility testing at the same time points using the same procedure (See Table 4.1 for treatment summary). Previous testing by Stolworthy and Zirbel provided a control scenario for comparison, where FSUs were tested multiple times over an extended period using the same test set-up (including the same follower-load and environmental conditions). Their results showed that no differences in segmental flexibility in the flexion-extension mode of loading occurred throughout the duration of their testing [83].

Table 4.1: Disc Injection Treatments

Name	# of FSUs	Treatment
Control	3	Needle punctures with no volume of fluid injected
Fluid	15	Any non-control test with fluid injected (i.e., saline and trypsin)
Saline	3	PBS injections (600 μL)
Trypsin	12	Trypsin injections (600 μL)

4.2.3 Data Analysis

All images captured by the spine simulator cameras (See Figure 4.5) were subjected to custom-made motion analysis software to determine the FSU rotations through direct-linear transformation techniques [84]. Rotations were sequenced with corresponding torque measurements and plotted. The resulting plots were then fit using a Boltzmann dual-inflection point (DIP) curve [1] which was used to find range of motion (ROM), stiffness (K), hysteresis (H), and neutral zone (NZ) characteristics. The average R^2 value of the curve fits was 0.9972.

A mixed-models analysis of variance (ANOVA) using SAS 9.3© was applied to determine statistically significant trends in test results. Time after injection was the independent within-subjects variable, and injection treatment (i.e., trypsin, saline, control) was the independent between-subjects variable. Variance was decreased by normalizing data in two fashions: percentage changes from the injection baseline time, and raw differences from the injection baseline time. P-values of <0.05 were deemed statistically significant. A previous mixed-models ANOVA determined that

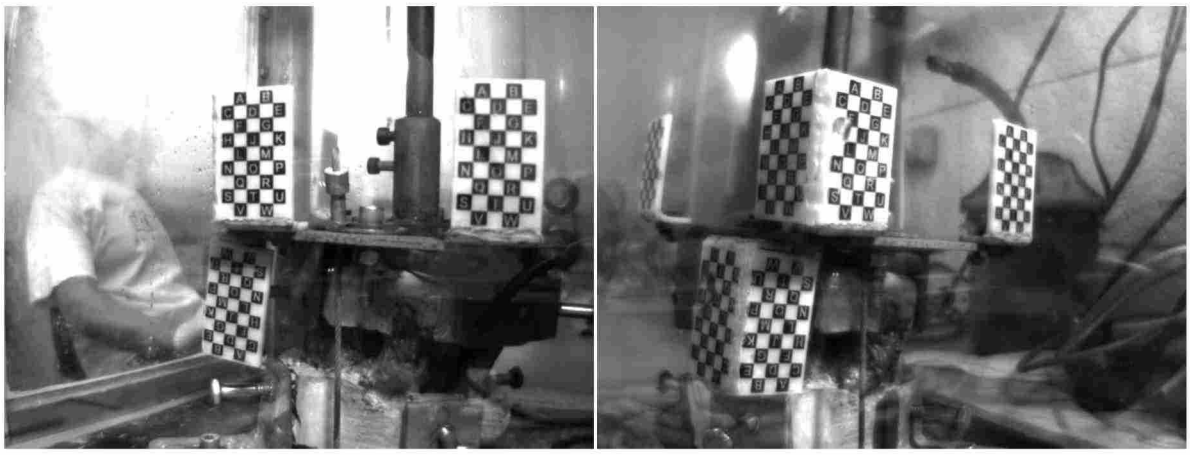

Figure 4.5: Sample Images Used in Processing Rotation Data

FSUs initially showing advanced degeneration (i.e., Thompson Grades IV and V) were significantly different from all other tests, and were therefore excluded from final analysis. A separate mixed-models ANOVA combined saline and trypsin effects into a single test variable titled "Fluid". This was done to consider the potential of non-protease solutions for use in changing FSU flexibility characteristics. Any individual test showing procedure abnormalities was discarded from further examination.

4.3 Results

4.3.1 Trypsin

Lateral Bending appeared to experience the most significant changes after injection. ROM decreased immediately post-injection for LB ($p<0.001$), then slowly increased (See Figure 4.6). The reverse was true for LB stiffness, with a large jump post-injection ($p<0.0001$) followed by a steady decline. Time "0" stiffness was different from the control group in LB, but was not significantly different. NZ, Normalized Neutral Zone (NZ/ROM), and Hysteresis Area (HA) had similar results, with trypsin significantly different from control at Time "0" due to a large decrease post-injection ($p<0.005$), but then steadily returning to baseline thereafter. Normalized Hysteresis (HA/ROM) also immediately dropped post-injection ($p<0.005$), but did not increase as much

afterwards. (For charts showing changes over time and treatment for NZ, NZ/ROM, H, HA, and HA/ROM, please see Appendix C.)

Flexion-Extension appeared to experience the smallest post-injection changes. ROM increased marginally over time after the initial drop post-injection (See Figure 4.8). Stiffness increased greatly at Time "0" ($p<0.0005$), then steadily dropped (See Figure 4.9). NZ, NZ/ROM, and HA dropped post-injection, then increased over time. Hysteresis increased slightly post-injection, then returned to baseline.

Axial Rotation, unlike FE and LB, did not experience a significant ROM difference at Time "0" (See Figure 4.10). Instead, it slowly increased, becoming statistically different at 1.5 hours ($p<0.05$). An increase in stiffness took place immediately post-injection then dropped below baseline (See Figure 4.11). HA and NZ both slowly increased after injection, with other parameters experiencing little to no change.

4.3.2 Saline

Lateral Bending ROM showed a more pronounced decrease immediately post-injection than trypsin treatments did (See Figure 4.6), followed by a similar increase ($p<0.005$). Stiffness increased substantially immediately after time "0", then steadily returned to baseline (See Figure 4.7). All hysteresis and neutral zone metrics decreased immediately post-injection, followed by a gradual increase towards baseline.

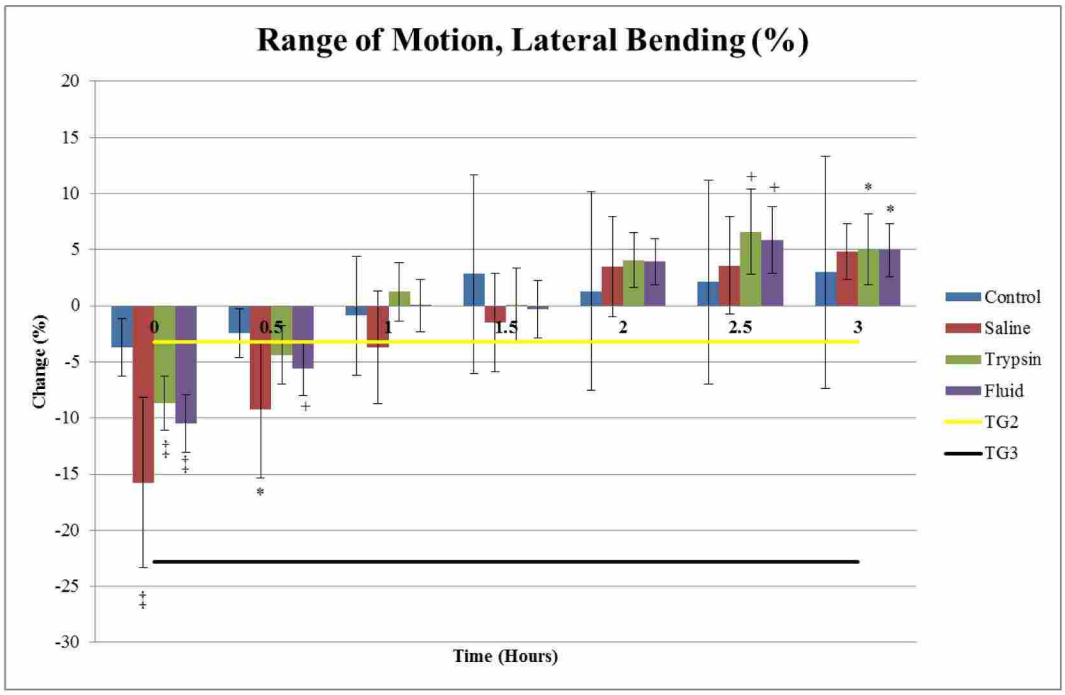

Figure 4.6: Lateral Bending ROM (TG2 and TG3 show changes from TG1 found in Chap. 3; * - $p<0.05$, + - $p<0.01$, ‡ - $p<0.005$)

Flexion-Extension ROM had a slight increase over time (See Figure 4.8), while stiffness experienced no significant change (See Figure 4.9). Neutral zone parameters exhibited an increase over time, while hysteresis parameters showed a marginal increase.

Axial Rotation ROM and stiffness saw a marginal increase and decrease, respectfully (See Figures 4.10 and 4.11). Similarly to trypsin, saline injections did not cause immediate alterations. All hysteresis and neutral zone parameters saw a slight downward trend.

ANOVA results showed not only statistical differences between different treatments and times individually, but also a group. Type 3 tests for fixed effects were performed for time, treatment, and the combined effect of time and treatment. Results showed that only time had a significant impact on motion changes, with LB experiencing the greatest change (See Table 4.2). No significant changes were found for treatment or the combination of time and treatment.

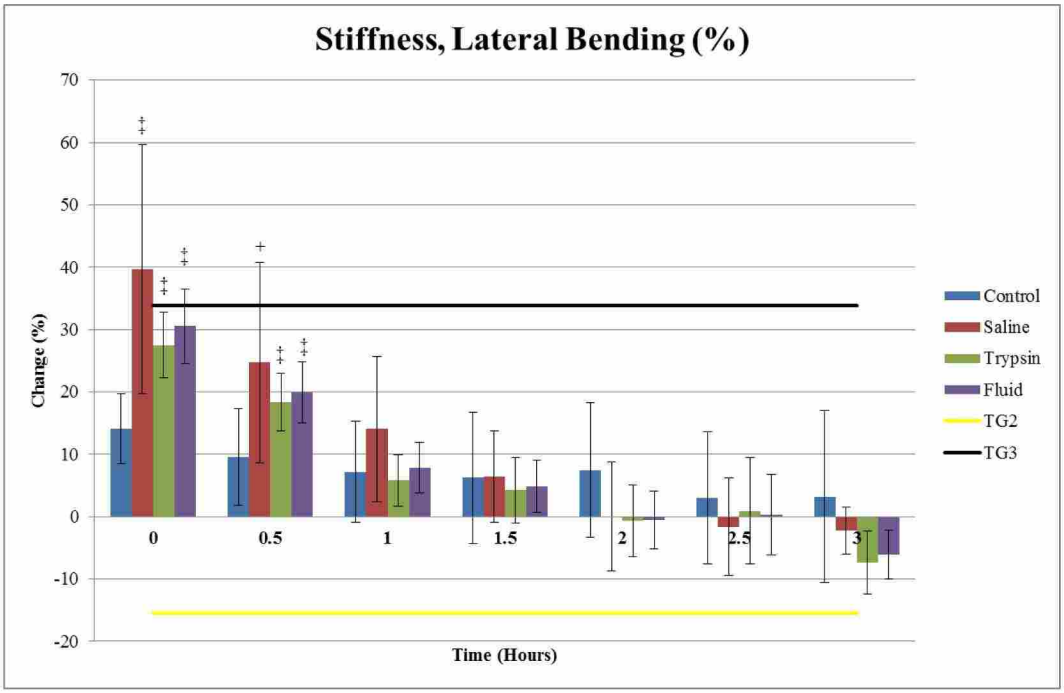

Figure 4.7: Lateral Bending K (TG2 and TG3 show changes from TG1 found in Chap. 3; + - $p<0.01$, ‡ - $p<0.005$)

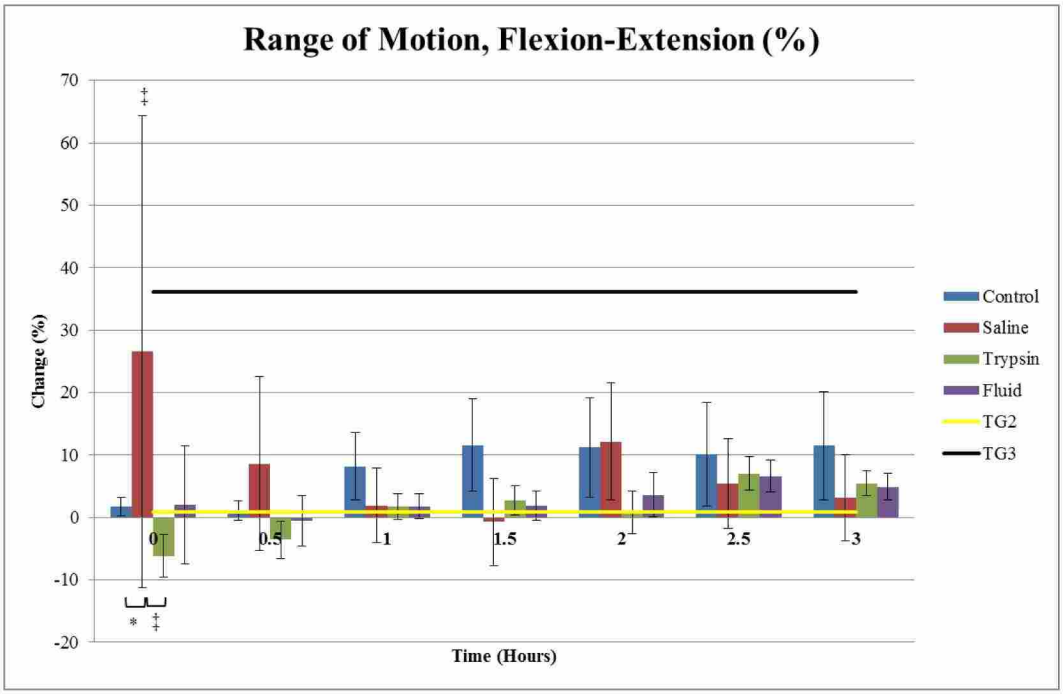

Figure 4.8: Flexion-Extension ROM (TG2 and TG3 show changes from TG1 found in Chap. 3; * - $p<0.05$, ‡ - $p<0.005$)

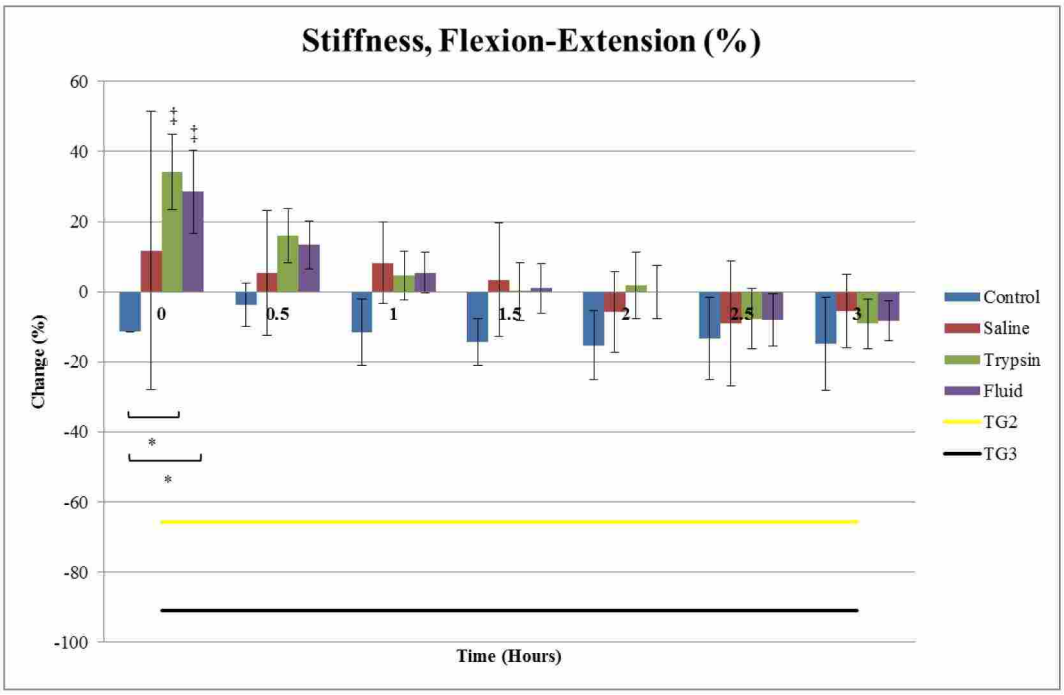

Figure 4.9: Flexion-Extension K (TG2 and TG3 show changes from TG1 found in Chap. 3; * - $p<0.05$, ‡ - $p<0.005$)

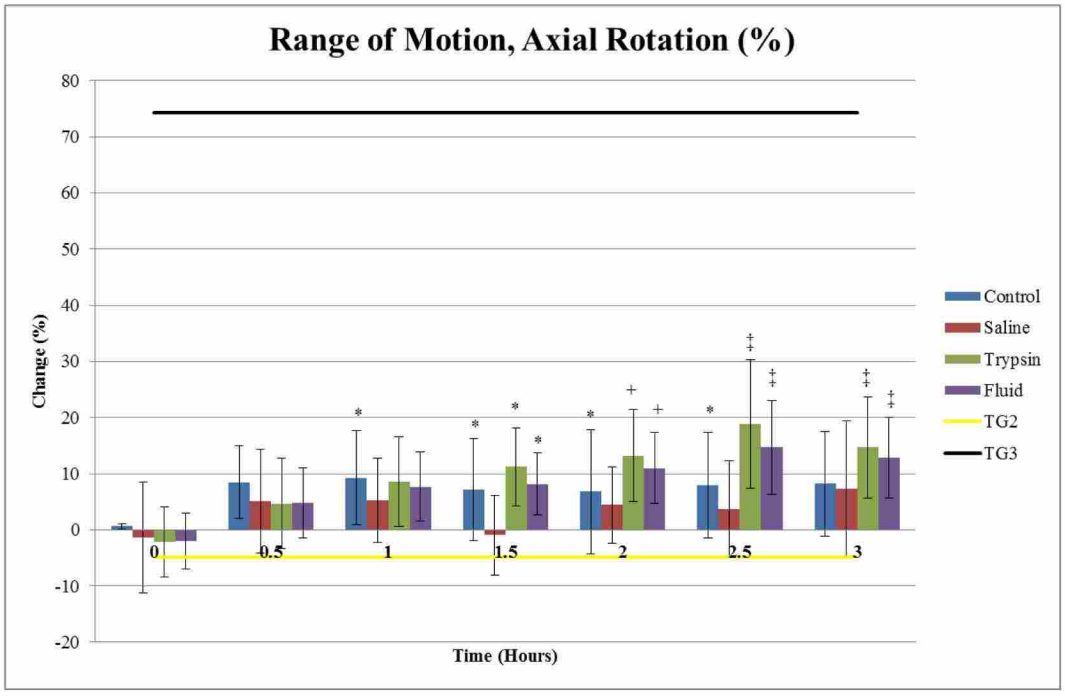

Figure 4.10: Axial Rotation ROM (TG2 and TG3 show changes from TG1 found in Chap. 3; * - $p<0.05$, + - $p<0.01$, ‡ - $p<0.005$)

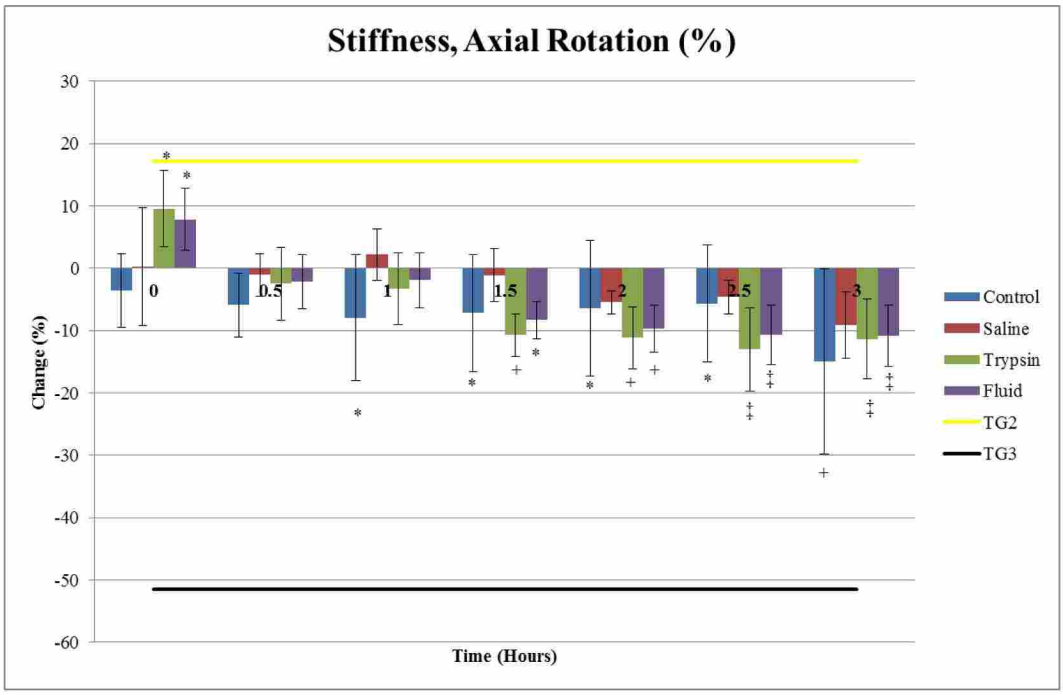

Figure 4.11: Axial Rotation K (TG2 and TG3 show changes from TG1 found in Chap. 3; * - $p<0.05$, + - $p<0.01$, ‡ - $p<0.005$)

Table 4.2: Parameters with Statistically Significant Changes Due to Time

ANOVA Type 3 Tests for Fixed Effect of Time	
Axial Rotation	
Motion Parameter	*P-Value*
Range of Motion	0.0074
Stiffness	0.0002
Normalized Neutral Zone	0.0457
Normalized Hysteresis Area	0.0435
Flexion-Extension	
Motion Parameter	*P-Value*
Neutral Zone	0.0105
Normalized Neutral Zone	0.0127
Lateral Bending	
Motion Parameter	*P-Value*
Range of Motion	<0.0001
Stiffness	<0.0001
Neutral Zone	<0.0001
Normalized Neutral Zone	<0.0001
Hysteresis Area	<0.0001
Normalized Hysteresis Area	0.0340

4.4 Discussion

While the hypothesis of this study proved to be valid (shown in signs of greater degeneration via trypsin injections), several interesting phenomena were observed unrelated to trypsin. Saline injections also proved to influence FSU mechanics, even though no proteolysis took place. Effects were quite different in most neutral zone and hysteresis-based parameters, with trends either opposite that of trypsin or more pronounced in the same direction. Interestingly, the control group showed similar results to the saline group in these parameters. This suggests trypsin had a unique effect on the viscoelasticity of the AF. Concurrently, even sticking a small needle into the AF of an FSU may cause a decrease in its viscoelasticity. This observation seems odd, especially when mechanics after injection of a small needle into human disc tissue were expected to be unchanged [52]. However, reported findings from the literature did not include hysteresis and neutral zone measurements of any subjects experiencing the same bending rotations seen in this study (i.e., AR, FE, LB) [52]. Though control tests did not show any significant changes for ROM and K (anticipated from findings from the literature), other parameters were susceptible to change. ANOVA tests confirmed that treatment group may not play the largest role in mimicking the advancement of degeneration, but rather time after injection.

Generally, a large increase in K and a large decrease in ROM took place immediately post-injection. This large alteration in mechanics was significant for the fluid injections, which means the injection of an adequate volume of any fluid could cause immediate change in ROM and K. Over time, this steep change dissipated as test subjects reverted towards baseline measurements. Even with proteolysis present in the disc, alterations to FSU mechanics ceased within two hours of injection. Alterations to disc mechanics via protease or saline injections, therefore, can be obtained in a short amount of time.

Of all results presented, findings in the AR and LB directions showed the greatest potential for use as a degeneration model. Lateral Bending ROM and K was the most linear in nature for changes due to natural degeneration, and most Grade III changes by injection treatments took place in AR (See Table 4.3). Trypsin and Saline injections caused healthy discs to act like a Grade II rather than a Grade I IVD in LB ROM. Trypsin and Saline injections also caused healthy discs to mimic the LB stiffness of a Grade III IVD rather than Grade I. These affects only lasted

immediately post-injection, and were weaker once a half-hour was reached. Therefore, using these results as a degeneration model would require great care and speed in implementation.

Table 4.3: Natural Degeneration Mechanics Matched by Injection Treatments

Control		
Axial Rotation NZ/ROM at 3 Hours (TG3) HA/ROM from 0.5 - 3 Hours (TG2) H at 3 Hours (TG2)	*Flexion-Extension* HA/ROM at 0 Hours (TG3)	*Lateral Bending* ROM at 0 Hours (TG2)
Fluid		
Axial Rotation HA at 1 Hour (TG3)	*Flexion-Extension*	*Lateral Bending* ROM at 0 and 0.5 Hours (TG2)
Saline		
Axial Rotation NZ/ROM at 3 Hours (TG3) HA/ROM at 0 and 2 - 3 Hours (TG2) HA at 0.5 and 1 Hours (TG3) H at 3 Hours (TG2)	*Flexion-Extension* NZ/ROM at 2 and 2.5 Hours (TG3) HA/ROM at 0 and 0.5 Hours (TG3)	*Lateral Bending* ROM from 0 - 1 Hours (TG2) K at 0 Hours (TG3) HA at 0 Hours (TG3) H at 0, 0.5, 1.5 and 2 Hours (TG3)
Trypsin		
Axial Rotation HA at 1 and 2 - 3 Hours (TG3)	*Flexion-Extension*	*Lateral Bending* ROM at 0 and 0.5 Hours (TG2)

There were several other instances where a treatment caused an FSU to act like a more degenerated disc. NZ/ROM in AR reached Grade III mechanics through saline injection or needle-stick only, and Grade II in HA/ROM and H for the same treatments. Trypsin, though, caused HA for AR to act at Grade III levels. Saline also caused all hysteresis parameters in LB to act like a Grade III disc. However, since the changes between Grades I and V in such parameters did not naturally follow a predictable pattern, caution should be used in relying on these results for mimicking degeneration.

Flexion-Extension experienced the least change in all parameters. This is most likely due to needle-injection site location. Of the six injection sites, four would be considered lateral while the other two are more anterior. With greater concentrations of trypsin and saline in the lateral AF, and with no injections made posteriorly, LB and AR movements experienced a greater injected-fluid influence.

The ramifications of altering the amount of fluid injected into the disc are not fully known. It is likely that decreasing the amount of trypsin and saline injected may diminish the impact on

disc mechanics, while increasing the volume injected could increase the mechanical impact. Also, the use of papain (a more aggressive protease) or any other solution is unknown.

In summary, saline injections caused a significant change in FSU mechanics and showed potential for use as a cadaveric degeneration model. Saline injections were the most effective method of causing Grade III mechanics in the disc, with most of these changes occurring within the first half-hour post-injection. Immediately post-injection test results showed Grade III changes in the LB parameters of H, HA, and K and the FE parameter of HA/ROM. The half-hour mark exhibited Grade III changes in LB H, FE HA/ROM, and AR HA. Although all treatments mimicked some form of mechanical disc degeneration, saline proved the most effective in the establishment of an *in vitro* model.

5. OBSERVATIONS AND DISCUSSION

5.1 Testing Limitations

5.1.1 Compressive Follower Load

Even though the testing methodology proved successful in revealing how to accelerate the mechanics of disc degeneration, there were limitations that must be detailed. One such limitation was the compressive follower load applied to each spine segment. In each individual test, the 440 N bilateral pulley-weight system hung from the superior potting fixture attached to the FSU. This set-up is a modification of the original follower load detailed by Patwardhan et al., which was applied to a full lumbrosacral spine using a bilateral guidance system that followed the spine's natural curvature [51, 82]. No attempt was made to follow the FSU's curvature at the inferior potting fixture in this study, which may have slightly altered biomechanical behavior in the FE and LB directions near their maximum rotations.

A peculiar development in the interaction between the follower load and the FSU's neutral position was observed. The cables securing the dead weights for the follower load were initially placed as close to the FSU's neutral position (0.0 Nm) as possible. Recordings of moments applied by the follower load showed variation over time in the FSU axis of rotation, with no discernible patterns of the magnitude of moment applied or the direction of application (i.e., positive or negative). Although this movement of the axis of rotation around the neutral position did not seem to influence FSU biomechanics, its effect is not fully understood.

5.1.2 Temperature Maintenance

A second testing limitation was environmental control in the spine tester. In order to keep the environmental chamber at body temperature, a humidifier was used to provide hot, moist air. If the chamber's temperature was too low, more water was added to create steam. If the temperature

was too hot, cool air was added via pressurized air. This system, though adequate for keeping temperatures close to 37°C, left room for deviation from the targeted temperature. Small errors in intended temperatures may have slightly affected test performance. This did not include the numerous instances where the chamber door needed to be opened for adjusting the specimen's testing direction or was opened to aid in cooling the chamber down.

A related limitation that may have played a role in introducing variation into the tests was the preparation of the FSU. Each specimen was stored in a -20°C freezer for a minimum of several weeks before testing. Some specimens were stored for much longer than others, which potentially played a small role in affecting a disc's tissue properties. In addition, the vertebrae were fixed in a cured polyester resin that was used for attachment to the potting fixtures [1, 15]. This epoxy reached temperatures well over that seen in the body while hardening (approaching 50°C). This exothermal reaction lasted for approximately 15 minutes, and was repeated for both the superior and inferior vertebrae. Such extremes in temperature, though separated by several hours (usually 8-12 hours), may adversely affect the disc tissue.

Ideally, fresh cadaveric samples would be available to dissect and immediately test. Such testing would theoretically include a fast-curing potting material with lower exothermal setting temperatures (e.g., fiberglass used in casts for bone fractures). Due to the time demands of dissection and each flexibility test, however, testing of fresh tissue was not possible. The process of storing and thawing frozen spinal tissue is considered standard protocol in flexibility testing [1,16,19,29,49,50,81], and has been reported to induce little to no effect on disc water content or motion behavior [16, 87]. Also, methodologies from the literature commonly use Polymethyl Methacrylate (PMMA, or acrylic glass) for setting vertebrae into potting fixtures [49,50,53], which also undergoes an exothermal reaction while hardening. Although the current procedure of freezing spinal tissue for storage and potting vertebrae in polyester resin is not ideal, it does follow common practice for *in vitro* spine tissue testing. Disc biomechanics appear to experience little to no adverse impact from these procedures [16].

5.1.3 Health Background of Donors

In this study, requests to tissue banks were made for non-smoker cadaveric tissue for testing. This was because tobacco use introduces toxins that prevent TIMPs from working, thus al-

lowing higher levels of proteolysis activity to digest disc tissue [23]. (This is a major reason why smokers experience LBP more frequently than non-smokers.) However, this request limited the field of potential tissue donors, and was not always possible to fulfill. In fact, over half of the eight spines used in the injection study (75%) came from donors with a long smoking history. Although discs from non-smokers most likely would have been healthier, this factor was accounted for by characterizing the degeneration level of each spinal segment that was tested.

5.2 Lessons Learned

5.2.1 Needle Placement

Another portion of the methodology that may have introduced variation was the insertion location of the needle into the disc. For each test, the needle was injected manually. Although visual guides were employed to aid the manual placement process, inadvertent variations in needle placement could potentially have introduced variability into the results. The relative magnitude of such variation is considered to be low.

5.2.2 Volume Injection Protocol

In addition to location variability, differences in needle injection depths did exist. The needle was always pulled out approximately 2 mm from maximum entry depth right before fluid injection. This allowed for a prepared space for some of the liquid to disperse into. This procedure came about due to high internal disc pressures causing substantial fluid to flow back out of the injection site. (This protocol was practiced and developed prior to recorded testing, making all test runs as consistent as possible.) Although this injection procedure was successfully followed for all test runs, it had an inherit variability in maximum needle puncture depth and injection depth. A slice of cork (2 mm thick) was applied on the needle to reduce the maximum entry depth of the needle. However, the cork thickness was not sliced using an automated method, thereby causing thickness to have some variability. The entry depth of 1 cm was chosen to keep the injected fluid out of the NP. Inner AF tissue was targeted for degradation, since trypsin interaction with the NP was hypothesized to have unpredictable side-effects on FSU motion. Finally, the syringes used for fluid

injection have 10 μL markings as the most precise for volume, suggesting potential variation of several microliters worth of fluid for each needle insertion. In future related projects, an automated technique for controlling injection depths, injected volume amounts, and needle angles could be developed to potentially reduce variation in test results.

A large factor in mimicking disc degeneration mechanics is the injection volume of the protease and saline solutions. The chosen volume of 600 μL was selected for injection procedure convenience rather than relative disc volume. Bishop et al. utilized 240 μL trypsin injections [75]. Based on that work, the first two test runs (unreported) of this research used that same fluid volume. However, no noteworthy changes took place, suggesting a lack of proteolytic activity. These test runs were disregarded, and following tests used the increased volume. Effects of using different volumes of trypsin, as well as other solutions such as CABC or papain, should be considered in producing a tighter calibration of this *in vitro* degeneration model.

Finally, the molecular weights (MW) of the trypsin, saline and food dyes may impact diffusivity through AF tissue. Trypsin molecules (MW: 23.3 kg/mol) are much larger than the blue food dye molecules (MW: 0.793 kg/mol) and substantially larger than saline molecules (MW: 0.0955 kg/mol). This may have kept the trypsin solution much more localized in its effect than the diffused blue dye would suggest.

5.2.3 Effect of Needle Puncture

Based on the findings of Elliott et al. [52], it was assumed that inserting a needle with a diameter of less than 25% disc height would have no adverse effects on FSU biomechanics. Using 10.9 mm as the average disc height in human IVDs [52], the 27 gauge needles used for fluid injection in this study would have an outer diameter of about 4% disc height. However, some differences were noted in the fluid-less control injections, which seemingly contradicts the study by Elliott et al. Several factors should be considered in addressing this conflict in results.

Elliott et al. tested rat IVDs in axial compression/tension and ovine (sheep) IVDs in axial compression/tension and axial rotation. Since Instron© axial testers were used, no FE or LB testing was performed. Ovine IVDs had a needle diameter to disc height ratio of 10% (compared to 4% in humans), well short of the reported 25% threshold for influencing FSU biomechanics. However, ovine specimens showed a 15% decrease in axial compressive stiffness, a 12% drop in

axial rotation stiffness (reported with torque-rotation axes inverted), and a 15% drop in axial torque range (p=0.05) after needle injection. These results were considered small in magnitude.

With no testing in FE and LB directions performed by Elliott et al., no direct comparisons in these bending modes can be made with this study. When adjusting the torque-rotation axes for the fluid-less control results from this study, a 8% increase in AR stiffness is seen through 1 hour post-injection and a 17% increase at the 3 hour mark, similar magnitudes (though positive rather than negative) reported by Elliott et al. Also, a maximum drop of 8% in AR torque range (adjusted torque-rotation axes) is observed post-injection, which is smaller than the 15% reported by Elliott et al. These comparisons suggest that the findings of this study are in close agreement with the findings of Elliott et al., where applicable comparisons can be made. Thus, although a needle puncture did cause changes in FSU biomechanics, these alterations were minor. Interestingly, the more notable changes in the fluid-less control group occurred in neutral zone and hysteresis-based parameters. As results for these parameters were not reported by Elliott et al., no related inferences can be made from their findings.

5.2.4 Effect of Environmental Chamber over Time

Another assumption going into this research was that the integrated environmental chamber had no effect on spinal biomechanics over time. This was established through the findings of Stolworthy et al. [83], which looked at rate dependency of FSU mechanics. No control tests that excluded needle punctures were attempted for this thesis. However, the rate testing done by Stolworthy et al. was performed in FE only using the same testing conditions, follower load, and environmental conditions. Their results demonstrated that segmental flexibility was unaltered by time of exposure to the environmental conditions (up to 45 minutes following segmental preconditioning). It is possible, that at extended periods, and/or in other modes of loading (i.e., AR, LB), there may be time-dependent changes due to degradation of tissue over time in the environmental chamber. We consider this to be unlikely, but do not have sufficient data to exclude this possibility.

6. CONCLUSION

6.1 Summary

This thesis has presented a promising *in vitro* method for pre-clinically validating a spinal device through mimicking the mechanics of a degenerating IVD. Although injection of trypsin was the targeted method for inducing mechanical degeneration, injection of PBS proved to be more effective in altering FSU biomechanics. This suggests that injection of any fluid can be utilized in mimicking the advancement of degeneration [75]. Even a fluid-less needle puncture can cause mild alterations to biomechanics, especially in neutral zone and hysteresis measurements.

The findings in this model can be compared against the predicted changes in mechanics as a disc naturally deteriorates, which was also detailed in this thesis. Further work may determine whether other proteases or other solutions are more effective, and precisely what role volume of the injected fluid plays. Combined with the flexibility characteristics of natural degeneration detailed in this study, a predictable fluid-based degeneration model may soon be found proving the efficacy of next-generation spinal devices.

6.2 Future Work

The results presented in this thesis provide a successful proof-of-concept for the use of protease injections for an *in vitro* degeneration model. This testing method provides a promising path to further validating TDR effects on overall spine biomechanics, especially over the full lifetime of the device. Although the methodology worked, several steps should be taken to optimize the procedure.

Further calibration of volume injection needs to be explored. In this study, only 600 μL of fluid was injected. Several different injection volumes should be compared to determine optimal fluid volume for predicting mechanical degeneration. Different proteases, such as CABC and

papain, could be used to further calibrate the methodology. More importantly, with only three full tests reported with saline injected, additional testing with PBS injections should be performed to provide lower variance in predicting effects on biomechanics. Once the methodology is better calibrated, several tests on multi-segment spines, with and without implanted TDRs, should be performed. Several iterations of this final step will provide a suitable protocol for pre-clinically validating motion restoration devices *in vitro*.

REFERENCES

[1] Zirbel, S. A., Stolworthy, D. K., Bowden, A. E., and Howell, L. L., 2013. "Intervertebral disc degeneration alters lumbar spine segmental stiffness in all modes of loading under a compressive follower load." *The Spine Journal*. 1, 16, 18, 22, 23, 25, 31, 36, 40, 51

[2] http://www.aans.org/patient 3

[3] http://www.ninds.nih.gov/disorders/backpain/detail_backpain.htm. 3

[4] de Schepper, E. I., Damen, J., van Meurs, J. B., Ginai, A. Z., Popham, M., Hofman, A., Koes, B. W., and Bierma-Zeinstra, S. M., 2010. "The association between lumbar disc degeneration and low back pain: the influence of age, gender, and individual radiographic features." *Spine,* **35**(5), p. 531. 3

[5] Chou, R., Atlas, S. J., Stanos, S. P., and Rosenquist, R. W., 2009. "Nonsurgical interventional therapies for low back pain: a review of the evidence for an american pain society clinical practice guideline." *Spine,* **34**(10), pp. 1078–1093. 3

[6] Kuo, P., and Loh, Z., 1987. "Treatment of lumbar intervertebral disc protrusions by manipulation." *Clin Orthop,* **215**, pp. 47–55. 3

[7] BenEliyahu, D. J., et al., 1996. "Magnetic resonance imaging and clinical follow-up: study of 27 patients receiving chiropractic care for cervical and lumbar disc herniations." *Journal of manipulative and physiological therapeutics,* **19**(9), p. 597. 3

[8] Netter, F. H., 2010. *Atlas of human anatomy*. Saunders. 4

[9] http://design.ae.utexas.edu/spine/final.html. 5

[10] Adams, M. A., and Roughley, P. J., 2006. "What is intervertebral disc degeneration, and what causes it?." *Spine,* **31**(18), pp. 2151–2161. 6, 9, 11, 35

[11] Urban, J. P., Smith, S., and Fairbank, J. C., 2004. "Nutrition of the intervertebral disc." *Spine,* **29**(23), pp. 2700–2709. 6

[12] http://www.med.upenn.edu/orl/research/bioengineering/disc.htm. 6

[13] http://emedicine.medscape.com/article/1145703-overview. 6

[14] http://www.spineuniverse.com/anatomy/ligaments. 7

[15] Mimura, M., Panjabi, M., Oxland, T., Crisco, J., Yamamoto, I., Vasavada, A., et al., 1994. "Disc degeneration affects the multidirectional flexibility of the lumbar spine.." *Spine,* **19**(12), p. 1371. 8, 15, 22, 35, 51

[16] Wilke, H.-J., Wenger, K., and Claes, L., 1998. "Testing criteria for spinal implants: recommendations for the standardization of in vitro stability testing of spinal implants." *European Spine Journal,* **7**(2), pp. 148–154. 8, 36, 51

[17] CALLISTER, W. D., 2007. "Fundamentals of materials science & engineering: an integrated approach.". 8

[18] Buckwalter, J. A., et al., 1995. "Aging and degeneration of the human intervertebral disc.." *Spine,* **20**(11), p. 1307. 9, 35

[19] Adams, M. A., Freeman, B. J., Morrison, H. P., Nelson, I. W., and Dolan, P., 2000. "Mechanical initiation of intervertebral disc degeneration." *Spine,* **25**(13), pp. 1625–1636. 9, 51

[20] Panjabi, M. M., Krag, M. H., Chung, T., et al., 1984. "Effects of disc injury on mechanical behavior of the human spine.." *Spine,* **9**(7), p. 707. 9

[21] Stokes, I. A., and Iatridis, J. C., 2004. "Mechanical conditions that accelerate intervertebral disc degeneration: overload versus immobilization." *Spine,* **29**(23), pp. 2724–2732. 9

[22] Hangai, M., Kaneoka, K., Hinotsu, S., Shimizu, K., Okubo, Y., Miyakawa, S., Mukai, N., Sakane, M., and Ochiai, N., 2009. "Lumbar intervertebral disk degeneration in athletes." *The American Journal of Sports Medicine,* **37**(1), pp. 149–155. 9

[23] Fogelholm, R., and Alho, A., 2001. "Smoking and intervertebral disc degeneration." *Medical hypotheses,* **56**(4), pp. 537–539. 9, 52

[24] Videman, T., Leppävuori, J., Kaprio, J., Battie, M. C., Gibbons, L. E., Peltonen, L., Koskenvuo, M., et al., 1998. "Intragenic polymorphisms of the vitamin d receptor gene associated with intervertebral disc degeneration.." *Spine,* **23**(23), p. 2477. 9

[25] Sambrook, P., MacGregor, A., and Spector, T., 1999. "Genetic influences on cervical and lumbar disc degeneration." *Arthritis Rheum,* **42**(2), p. 336. 9

[26] http://www.tbilawyers.com/herniated-disc.html. 10

[27] Setton, L. A., and Chen, J., 2006. "Mechanobiology of the intervertebral disc and relevance to disc degeneration." *The Journal of Bone & Joint Surgery,* **88**(suppl_2), pp. 52–57. 11

[28] Urban, J., Roberts, S., and Ralphs, J., 2000. "The nucleus of the intervertebral disc from development to degeneration." *American Zoologist,* **40**(1), pp. 53–061. 11

[29] Antoniou, J., Steffen, T., Nelson, F., Winterbottom, N., Hollander, A. P., Poole, R. A., Aebi, M., and Alini, M., 1996. "The human lumbar intervertebral disc: evidence for changes in the biosynthesis and denaturation of the extracellular matrix with growth, maturation, ageing, and degeneration.." *Journal of Clinical Investigation,* **98**(4), p. 996. 11, 51

[30] Ishihara, H., McNally, D. S., Urban, J., and Hall, A. C., 1996. "Effects of hydrostatic pressure on matrix synthesis in different regions of the intervertebral disk." *Journal of Applied Physiology,* **80**(3), pp. 839–846. 11

[31] Gibson, J., and Waddell, G., 2008. "Surgical interventions for lumbar disc prolapse." *The Cochrane Library*. 12

[32] Deyo, R. A., Nachemson, A., and Mirza, S. K., 2004. "Spinal-fusion surgerythe case for restraint." *New England Journal of Medicine,* **350**(7), pp. 722–726. 12

[33] Blumenthal, S., McAfee, P. C., Guyer, R. D., Hochschuler, S. H., Geisler, F. H., Holt, R. T., Garcia Jr, R., Regan, J. J., and Ohnmeiss, D. D., 2005. "A prospective, randomized, multicenter food and drug administration investigational device exemptions study of lumbar total disc replacement with the charite artificial disc versus lumbar fusion: Part i: evaluation of clinical outcomes." *Spine,* **30**(14), pp. 1565–1575. 12, 35

[34] http://commons.wikimedia.org/wiki/file:wiki_postop.jpg#file. 12

[35] Zander, T., Rohlmann, A., and Bergmann, G., 2009. "Influence of different artificial disc kinematics on spine biomechanics." *Clinical biomechanics,* **24**(2), pp. 135–142. 13

[36] Jacobs, W. C., Van der Gaag, N. A., Kruyt, M. C., Tuschel, A., de Kleuver, M., Peul, W. C., Verbout, A. J., and Oner, F. C., 2012. "Total disc replacement for chronic discogenic low-back pain: A cochrane review." *Spine*. 13

[37] Goel, V. K., Panjabi, M. M., Patwardhan, A. G., Dooris, A. P., and Serhan, H., 2006. "Test protocols for evaluation of spinal implants." *The Journal of Bone & Joint Surgery,* **88**(suppl_2), pp. 103–109. 13, 35

[38] Hitchon, P. W., Eichholz, K., Barry, C., Rubenbauer, P., Ingalhalikar, A., Nakamura, S., Follett, K., Lim, T. H., and Torner, J., 2005. "Biomechanical studies of an artificial disc implant in the human cadaveric spine." *Journal of Neurosurgery: Spine,* **2**(3), pp. 339–343. 13

[39] Cakir, B., Richter, M., Käfer, W., Puhl, W., and Schmidt, R., 2005. "The impact of total lumbar disc replacement on segmental and total lumbar lordosis." *Clinical Biomechanics,* **20**(4), pp. 357–364. 14

[40] Chung, S. K., Kim, Y. E., and Wang, K.-C., 2009. "Biomechanical effect of constraint in lumbar total disc replacement: a study with finite element analysis." *Spine,* **34**(12), pp. 1281–1286. 14

[41] Chen, S.-H., Zhong, Z.-C., Chen, C.-S., Chen, W.-J., Hung, C., et al., 2009. "Biomechanical comparison between lumbar disc arthroplasty and fusion.." *Medical engineering & physics,* **31**(2), p. 244. 14

[42] Denozière, G., Ku, D. N., et al., 2006. "Biomechanical comparison between fusion of two vertebrae and implantation of an artificial intervertebral disc.." *Journal of biomechanics,* **39**(4), p. 766. 14

[43] Kim, K.-T., Lee, S.-H., Suk, K.-S., Lee, J.-H., and Jeong, B.-O., 2010. "Biomechanical changes of the lumbar segment after total disc replacement: Charite®, prodisc® and maverick® using finite element model study." *Journal of Korean Neurosurgical Society,* **47**(6), pp. 446–453. 14

[44] Le Huec, J.-C., Lafage, V., Bonnet, X., Lavaste, F., Josse, L., Liu, M., and Skalli, W., 2010. "Validated finite element analysis of the maverick total disc prosthesis." *Journal of spinal disorders & techniques,* **23**(4), pp. 249–257. 14

[45] Huang, R. C., Tropiano, P., Marnay, T., Girardi, F. P., Lim, M. R., and Cammisa, F. P., 2006. "Range of motion and adjacent level degeneration after lumbar total disc replacement." *The Spine Journal,* **6**(3), pp. 242–247. 14

[46] Nachemson, A., et al., 1960. "Lumbar intradiscal pressure. experimental studies on post-mortem material.." *Acta orthopaedica Scandinavica. Supplementum,* **43**, p. 1. 14

[47] Pfirrmann, C. W., Metzdorf, A., Zanetti, M., Hodler, J., Boos, N., et al., 2001. "Magnetic resonance classification of lumbar intervertebral disc degeneration." *SPINE-PHILADELPHIA-HARPER AND ROW PUBLISHERS THEN JB LIPPINCOTT COMPANY-,* **26**(17), pp. 1873–1878. 14

[48] Thompson, J., Pearce, R., Schechter, M., Adams, M., Tsang, I., Bishop, P., et al., 1990. "Preliminary evaluation of a scheme for grading the gross morphology of the human intervertebral disc.." *Spine,* **15**(5), p. 411. 14, 25, 39

[49] Krismer, M., Haid, C., Behensky, H., Kapfinger, P., Landauer, F., and Rachbauer, F., 2000. "Motion in lumbar functional spine units during side bending and axial rotation moments depending on the degree of degeneration." *Spine,* **25**(16), p. 2020. 15, 22, 51

[50] Fujiwara, A., Lim, T., An, H., Tanaka, N., Jeon, C., Andersson, G., and Haughton, V., 2000. "The effect of disc degeneration and facet joint osteoarthritis on the segmental flexibility of the lumbar spine." *Spine,* **25**(23), p. 3036. 15, 22, 35, 51

[51] Patwardhan, A., Havey, R., Meade, K., Lee, B., and Dunlap, B., 1999. "A follower load increases the load-carrying capacity of the lumbar spine in compression." *Spine,* **24**(10), p. 1003. 15, 23, 50

[52] Elliott, D., Yerramalli, C., Beckstein, J., Boxberger, J., Johannessen, W., and Vresilovic, E., 2008. "The effect of relative needle diameter in puncture and sham injection animal models of degeneration." *Spine,* **33**(6), pp. 588–596. 15, 38, 47, 53

[53] Tanaka, N., An, H., Lim, T., Fujiwara, A., Jeon, C., and Haughton, V., 2001. "The relationship between disc degeneration and flexibility of the lumbar spine." *The spine journal,* **1**(1), pp. 47–56. 16, 17, 22, 33, 35, 51

[54] Fukuta, S., Miyamoto, K., Suzuki, K., Maehara, H., Inoue, T., Kikuike, K., and Shimizu, K., 2011. "Abundance of calpain and aggrecan-cleavage products of calpain in degenerated human intervertebral discs." *Osteoarthritis and Cartilage,* **19**(10), pp. 1254–1262. 16

[55] Le Maitre, C. L., Freemont, A. J., and Hoyland, J. A., 2004. "Localization of degradative enzymes and their inhibitors in the degenerate human intervertebral disc." *The Journal of pathology,* **204**(1), pp. 47–54. 16

[56] Le Maitre, C., Freemont, A., and Hoyland, J., 2006. "Human disc degeneration is associated with increased mmp 7 expression." *Biotechnic & Histochemistry,* **81**(4-6), pp. 125–131. 16

[57] Pasternak, B., and Aspenberg, P., 2009. "Metalloproteinases and their inhibitors-diagnostic and therapeutic opportunities in orthopedics." *Acta orthopaedica,* **80**(6), pp. 693–703. 16

[58] Patel, K. P., Sandy, J. D., Akeda, K., Miyamoto, K., Chujo, T., An, H. S., and Masuda, K., 2007. "Aggrecanases and aggrecanase-generated fragments in the human intervertebral disc at early and advanced stages of disc degeneration." *Spine,* **32**(23), pp. 2596–2603. 16

[59] Roberts, S., Caterson, B., Menage, J., Evans, E. H., Jaffray, D. C., and Eisenstein, S. M., 2000. "Matrix metalloproteinases and aggrecanase: their role in disorders of the human intervertebral disc." *Spine,* **25**(23), pp. 3005–3013. 16

[60] Garvin, P., Jennings, R., and Stern, I., 1977. "Enzymatic digestion of the nucleus pulposus: a review of experimental studies with chymopapain.." *The Orthopedic clinics of North America,* **8**(1), p. 27. 17

[61] Simmons, J. W., Nordby, E. J., and Hadjipavlou, A. G., 2001. "Chemonucleolysis: the state of the art." *European Spine Journal,* **10**(3), pp. 192–202. 17

[62] Mitra, R., Wedemeyer, M., and Cheng, I., 2008. "Chymopapain: A shot from the past." *Pain Practice,* **8**(4), pp. 331–332. 19

[63] Lü, D.-S., Shono, Y., Oda, I., Abumi, K., and Kaneda, K., 1997. "Effects of chondroitinase abc and chymopapain on spinal motion segment biomechanics: an in vivo biomechanical, radiologic, and histologic canine study." *Spine,* **22**(16), p. 1828. 19

[64] Sugimura, T., Kato, F., Mimatsu, K., Takenaka, O., and Iwata, H., 1996. "Experimental chemonucleolysis with chondroitinase abc in monkeys." *Spine,* **21**(2), pp. 161–165. 19

[65] Barbir, A., Michalek, A. J., Abbott, R. D., and Iatridis, J. C., 2010. "Effects of enzymatic digestion on compressive properties of rat intervertebral discs." *Journal of biomechanics,* **43**(6), pp. 1067–1073. 19

[66] Boxberger, J. I., Orlansky, A. S., Sen, S., and Elliott, D. M., 2009. "Reduced nucleus pulposus glycosaminoglycan content alters intervertebral disc dynamic viscoelastic mechanics." *Journal of biomechanics,* **42**(12), pp. 1941–1946. 19

[67] Chan, S. C., Bürki, A., Bonél, H. M., Benneker, L. M., and Gantenbein-Ritter, B., 2013. "Papain-induced in vitro disc degeneration model for the study of injectable nucleus pulposus therapy." *The Spine Journal*. 19, 36

[68] Takahashi, T., Kurihara, H., Nakajima, S.-i., Kato, T., Matsuzaka, S., Sekiguchi, T., Onaya, M., Miyauchi, S., Mizuno, S., Horie, K., et al., 1996. "Chemonucleolytic effects of chondroitinase abc on normal rabbit intervertebral discs: course of action up to 10 days postinjection and minimum effective dose." *Spine,* **21**(21), pp. 2405–2411. 19

[69] Detiger, S. E., Hoogendoorn, R. J., van der Veen, A. J., van Royen, B. J., Helder, M. N., Koenderink, G. H., and Smit, T. H., 2012. "Biomechanical and rheological characterization of mild intervertebral disc degeneration in a large animal model." *Journal of Orthopaedic Research*. 19

[70] Norcross, J. P., Lester, G. E., Weinhold, P., and Dahners, L. E., 2003. "An in vivo model of degenerative disc disease." *Journal of orthopaedic research,* **21**(1), pp. 183–188. 19

[71] Sasaki, M., Takahashi, T., Miyahara, K., Hirose, T., et al., 2001. "Effects of chondroitinase abc on intradiscal pressure in sheep: an in vivo study." *Spine,* **26**(5), pp. 463–468. 19

[72] Mwale, F., Demers, C., Michalek, A., Beaudoin, G., Goswami, T., Beckman, L., Iatridis, J., and Antoniou, J., 2008. "Evaluation of quantitative magnetic resonance imaging, biochemical and mechanical properties of trypsin-treated intervertebral discs under physiological compression loading." *Journal of Magnetic Resonance Imaging,* **27**(3), pp. 563–573. 19, 36

[73] Roberts, S., Menage, J., Sivan, S., and Urban, J., 2008. "Bovine explant model of degeneration of the intervertebral disc." *BMC musculoskeletal disorders,* **9**(1), p. 24. 19, 36

[74] Chadderdon, R. C., Shimer, A. L., Gilbertson, L. G., and Kang, J. D., 2004. "Advances in gene therapy for intervertebral disc degeneration." *The Spine Journal,* **4**(6), pp. S341–S347. 19

[75] Sessions, J., Bishop, T., Sessions, A., and Bowden, A. E., 2009. "Mechanical characterization of a bovine tail analog for enzymatic disc degeneration." Orthopedic Research Society. 19, 36, 53, 55

[76] Alini, M., Eisenstein, S. M., Ito, K., Little, C., Kettler, A. A., Masuda, K., Melrose, J., Ralphs, J., Stokes, I., and Wilke, H. J., 2008. "Are animal models useful for studying human disc disorders/degeneration?." *European Spine Journal,* **17**(1), pp. 2–19. 20

[77] Aguiar, D. J., Johnson, S. L., Oegema, T. R., et al., 1999. "Notochordal cells interact with nucleus pulposus cells: regulation of proteoglycan synthesis.." *Experimental cell research,* **246**(1), p. 129. 20

[78] Erwin, W. M., and Inman, R. D., 2006. "Notochord cells regulate intervertebral disc chondrocyte proteoglycan production and cell proliferation." *Spine,* **31**(10), p. 1094. 20

[79] Pazzaglia, U., Salisbury, J., and Byers, P., 1989. "Development and involution of the notochord in the human spine.." *Journal of the Royal Society of Medicine,* **82**(7), p. 413. 20

[80] Goertzen, D. J., Lane, C., and Oxland, T. R., 2004. "Neutral zone and range of motion in the spine are greater with stepwise loading than with a continuous loading protocol. an in vitro porcine investigation." *Journal of biomechanics,* **37**(2), pp. 257–261. 22, 23, 36

[81] Costi, J. J., Hearn, T. C., and Fazzalari, N. L., 2002. "The effect of hydration on the stiffness of intervertebral discs in an ovine model." *Clinical Biomechanics,* **17**(6), pp. 446–455. 22, 36, 51

[82] Patwardhan, A., Havey, R., Carandang, G., Simonds, J., Voronov, L., Ghanayem, A., Meade, K., Gavin, T., and Paxinos, O., 2003. "Effect of compressive follower preload on the flexion–extension response of the human lumbar spine." *Journal of orthopaedic research,* **21**(3), pp. 540–546. 23, 50

[83] Stolworthy, D. K., Zirbel, S. A., Howell, L. L., Samuels, M., and Bowden, A. E., 2013. "Characterization and prediction of rate-dependent flexibility in lumbar spine biomechanics at room and body temperature." *The Spine Journal* in review, submitted 3 May 2012. 25, 37, 40, 54

[84] Nigg, B. M., and Herzog, W., 2007. *Biomechanics of the musculo-skeletal system*. John Wiley & Son Ltd. 25, 40

[85] Gamst, G., Meyers, L. S., and Guarino, A., 2008. *Analysis of variance designs: A conceptual and computational approach with SPSS and SAS*. Cambridge University Press. 27, 28

[86] Dulbecco, R., and Vogt, M., 1954. "Plaque formation and isolation of pure lines with poliomyelitis viruses." *The Journal of experimental medicine,* **99**(2), pp. 167–182. 36

[87] Pflaster, D. S., Krag, M. H., Johnson, C. C., Haugh, L. D., and Pope, M. H., 1997. "Effect of test environment on intervertebral disc hydration." *Spine,* **22**(2), p. 133. 51

APPENDIX A. ANATOMICAL DIRECTIONS AND SPINAL MOVEMENT

Features within the spine are referenced relative to anatomical directions (See Figure A.1). Spinal tissue above another tissue is referred to as “superior”, while tissue below another tissue is titled “inferior”. Tissue facing towards the front of the body is “anterior”, while rearward-facing tissue is “posterior”. Tissue closer to the center of the body is “medial”, whereas tissue farther out from center is “lateral”.

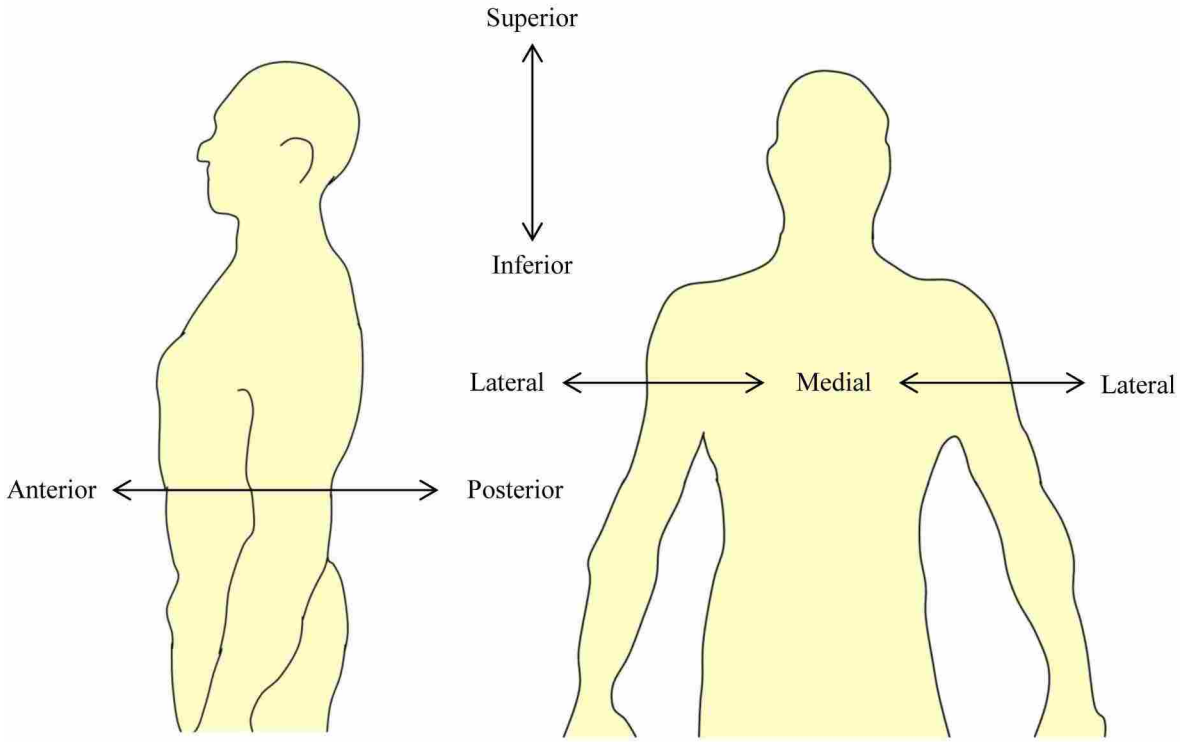

Figure A.1: Anatomical Directions

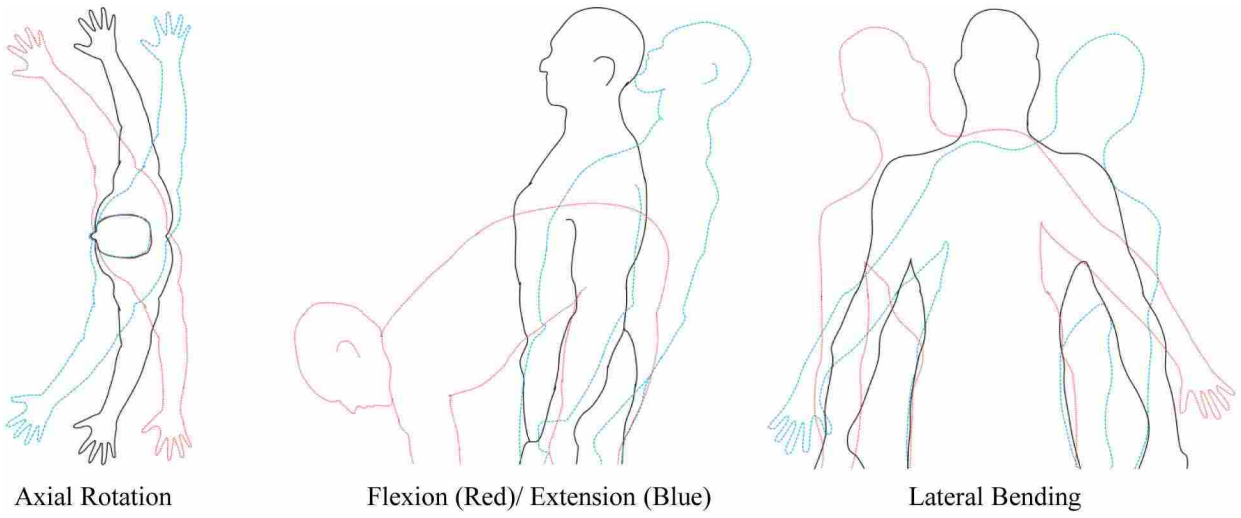

Figure A.2: Spinal Bending Motions

APPENDIX B. NATURAL DEGENERATION MODEL RAW VALUES

Table B.1: Means and Standard Deviations of Degeneration Results

	Axial Rotation			**Flexion-Extension**			**Lateral Bending**		
	TG	Mean	SD	TG	Mean	SD	TG	Mean	SD
Range of Motion	I	2.9268	1.2323	I	10.6077	6.9380	I	14.1879	6.6506
	II	2.7834	1.4106	II	10.6960	4.5494	II	13.7324	5.1480
	III	5.1025	1.8150	III	14.4462	4.3342	III	10.9504	5.4724
	IV	4.9495	2.7161	IV	10.2942	3.2651	IV	8.5558	4.9644
	V	4.8501	2.0045	V	10.7745	4.5211	V	5.1537	3.5828
Stiffness	I	6.3013	3.0890	I	2.3923	3.0264	I	0.7488	0.4759
	II	7.3864	3.9277	II	0.8223	0.9797	II	0.6332	0.4898
	III	3.0620	1.7873	III	0.2188	0.1152	III	1.0029	0.7013
	IV	2.9401	1.4293	IV	1.3451	2.2418	IV	2.1689	1.7039
	V	3.2564	1.9973	V	1.1033	1.5971	V	4.0522	2.0798
Neutral Zone	I	0.5336	0.2915	I	3.6135	3.5052	I	4.4262	3.6214
	II	0.4265	0.1822	II	2.6987	1.6938	II	5.3245	3.7847
	III	0.7066	0.2448	III	5.3486	1.3457	III	2.6071	1.8458
	IV	0.7063	0.3283	IV	3.0828	1.6711	IV	2.3139	1.5884
	V	0.8464	0.3091	V	4.0877	3.2953	V	1.0968	0.7691
Normalized Neutral Zone	I	0.1790	0.0530	I	0.2963	0.1340	I	0.3134	0.1397
	II	0.1697	0.0529	II	0.2392	0.0930	II	0.3463	0.1355
	III	0.1392	0.0064	III	0.3823	0.0830	III	0.2240	0.0566
	IV	0.1505	0.0334	IV	0.2852	0.0919	IV	0.2637	0.0533
	V	0.1794	0.0451	V	0.3447	0.1532	V	0.2130	0.0232
Hysteresis Area	I	5.5472	2.9873	I	17.4744	12.4820	I	27.1442	8.6317
	II	4.2159	1.9355	II	13.8924	6.2826	II	28.2178	12.0033
	III	6.2099	2.1640	III	16.1833	2.9601	III	20.2970	10.9177
	IV	6.6114	2.8095	IV	14.7763	4.2596	IV	18.7052	11.3278
	V	7.4995	2.1622	V	20.7917	9.6830	V	10.6501	6.3678
Normalized Hysteresis Area	I	1.8714	0.6006	I	1.7670	0.6166	I	2.1048	0.5731
	II	1.6559	0.5204	II	1.3070	0.2327	II	2.0319	0.3224
	III	1.2243	0.0776	III	1.1565	0.1876	III	1.8334	0.0808
	IV	1.4387	0.3622	IV	1.5238	0.4312	IV	2.2530	0.3415
	V	1.6332	0.4093	V	1.9326	0.3502	V	2.1644	0.3141
Hysteresis	I	2.4313	0.6795	I	1.9362	0.9193	I	2.0960	0.7754
	II	2.0520	0.6279	II	1.0636	0.2489	II	1.8946	0.4051
	III	1.5673	0.4304	III	1.0433	0.3145	III	1.9060	0.0594
	IV	1.6040	0.4303	IV	1.6507	1.0184	IV	2.5403	0.5255
	V	1.8580	0.6386	V	1.9933	0.6550	V	2.6558	0.4667

APPENDIX C. EFFECTS OF INJECTION TREATMENTS

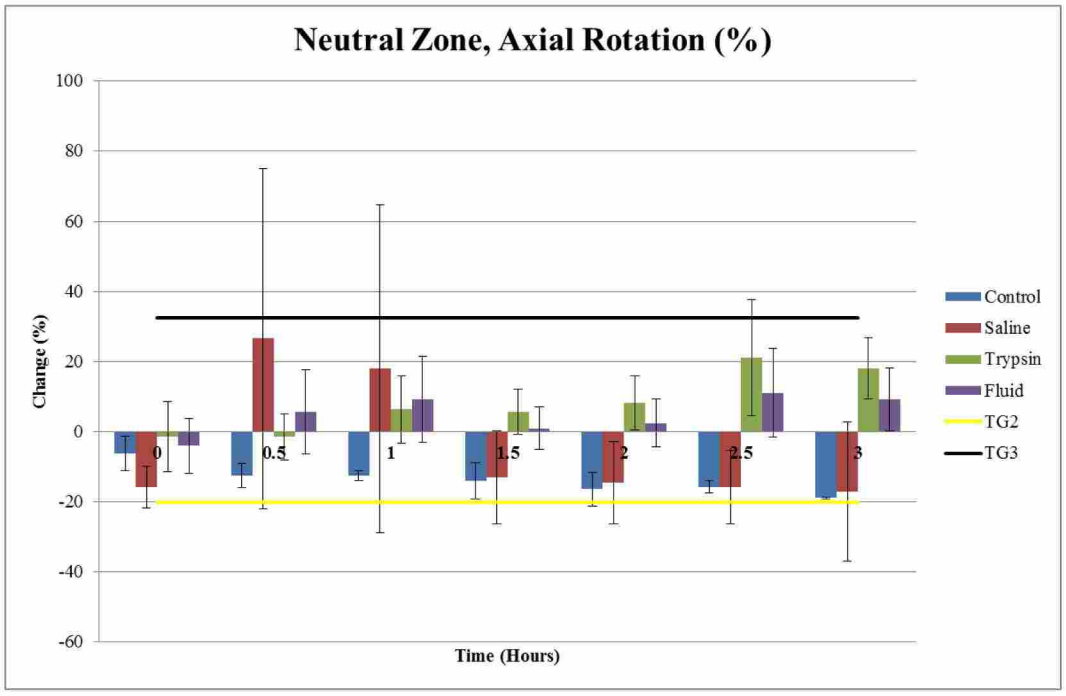

Figure C.1: Axial Rotation NZ (TG2 and TG3 show changes from TG1 found in Chap. 3)

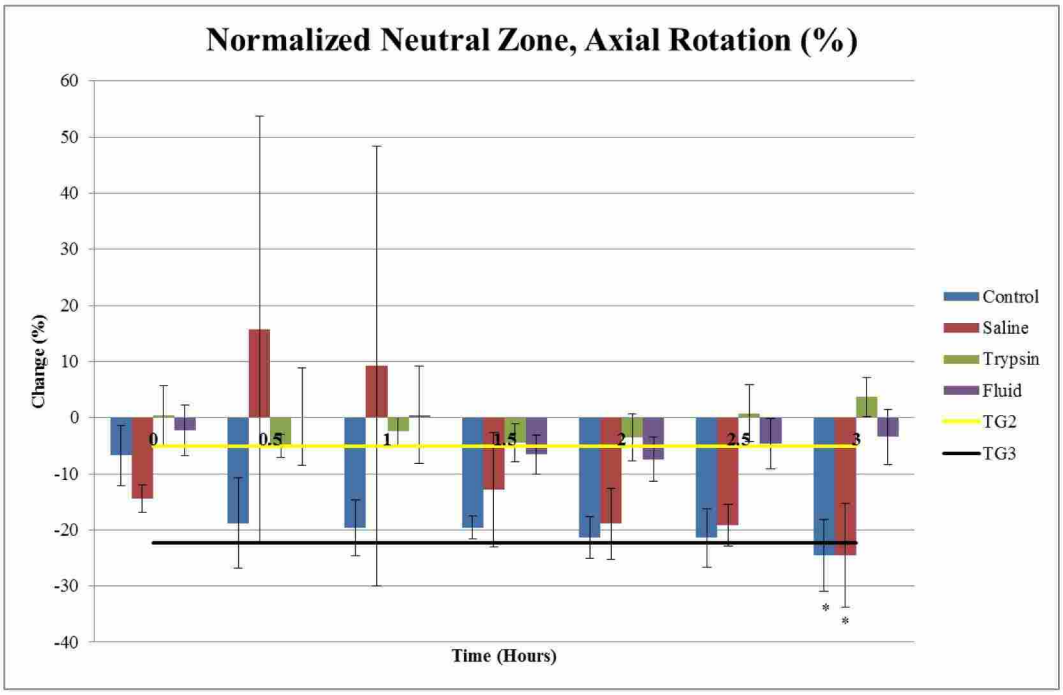

Figure C.2: Axial Rotation NZ/ROM (TG2 and TG3 show changes from TG1 found in Chap. 3; * - $p<0.05$)

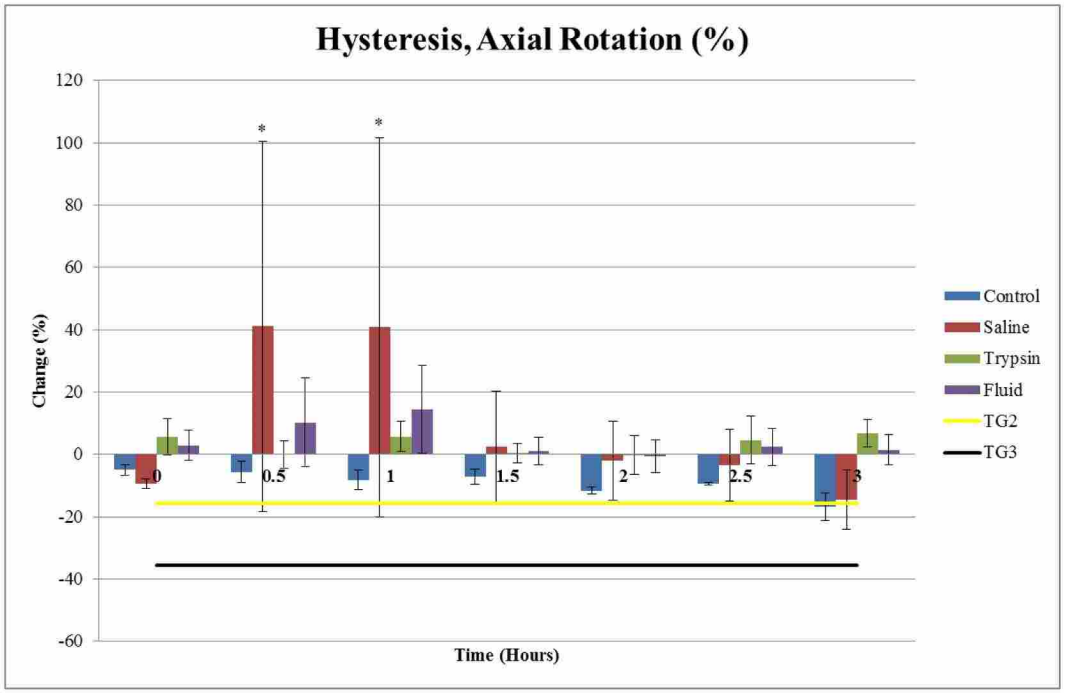

Figure C.3: Axial Rotation H (TG2 and TG3 show changes from TG1 found in Chap. 3; * - $p<0.05$)

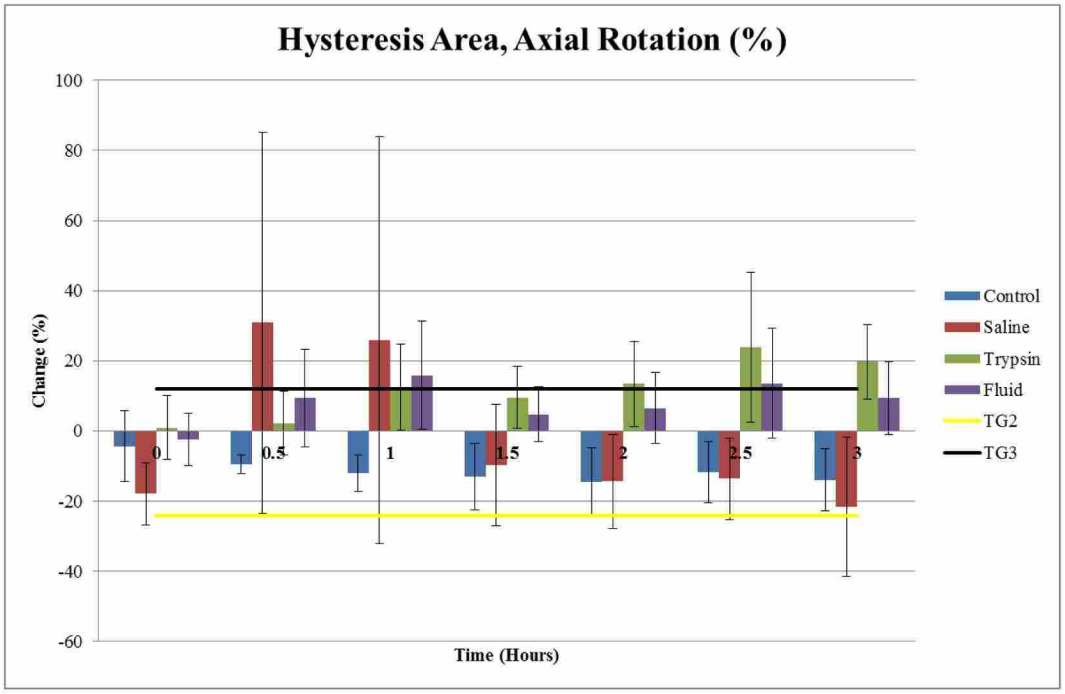

Figure C.4: Axial Rotation HA (TG2 and TG3 show changes from TG1 found in Chap. 3)

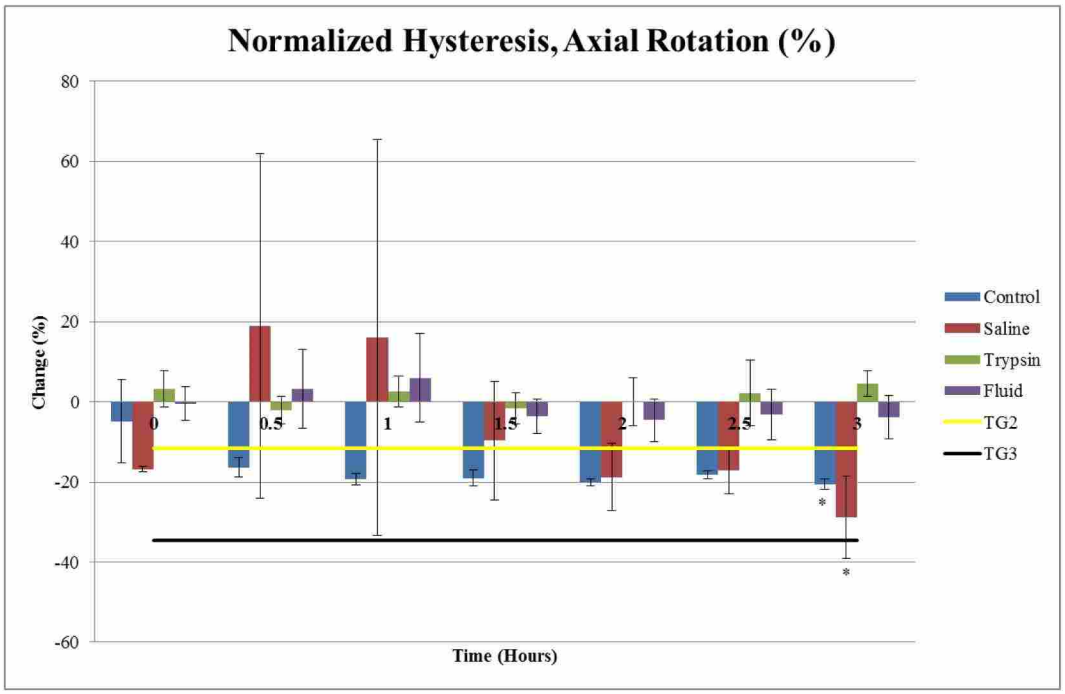

Figure C.5: Axial Rotation HA/ROM (TG2 and TG3 show changes from TG1 found in Chap. 3; * - $p<0.05$)

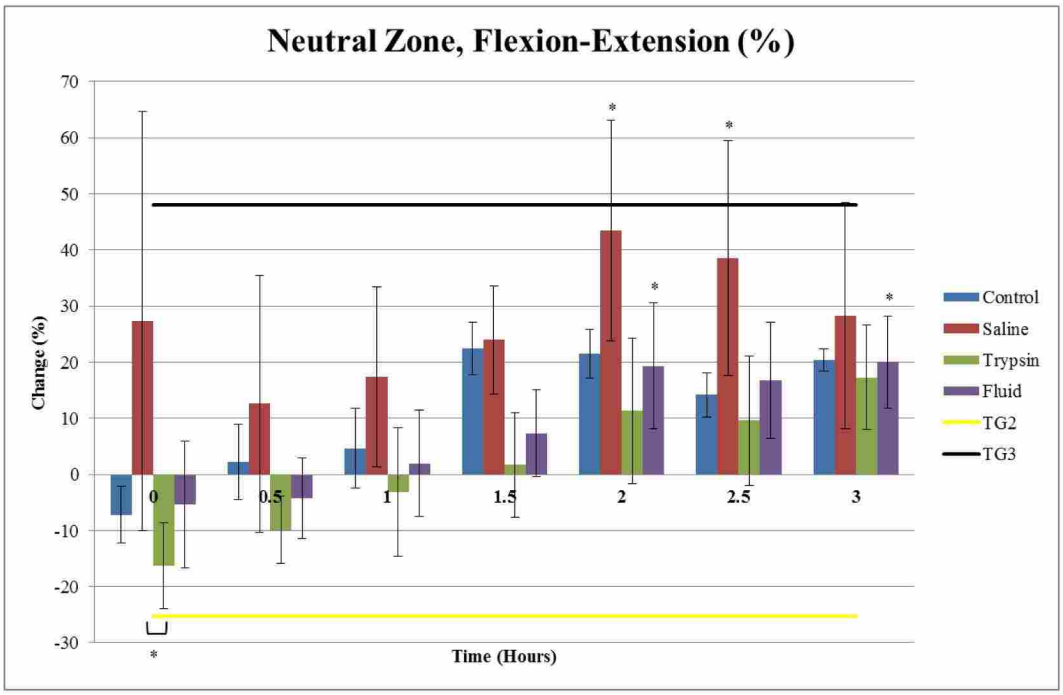

Figure C.6: Flexion-Extension NZ (TG2 and TG3 show changes from TG1 found in Chap. 3; * - $p<0.05$)

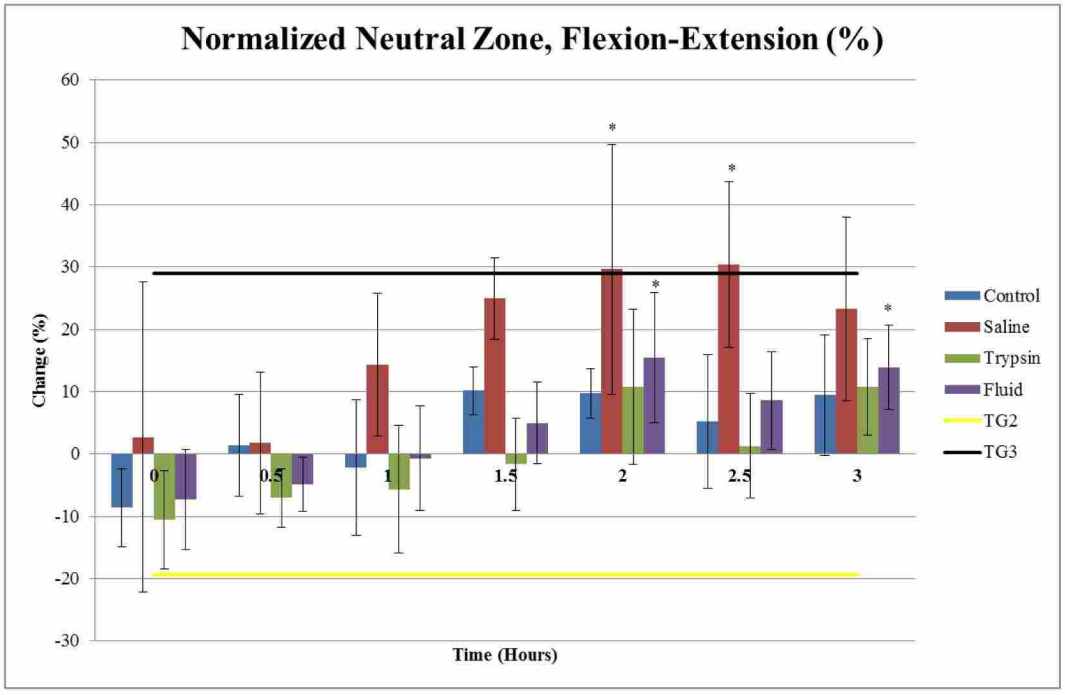

Figure C.7: Flexion-Extension NZ/ROM (TG2 and TG3 show changes from TG1 found in Chap. 3; * - $p<0.05$)

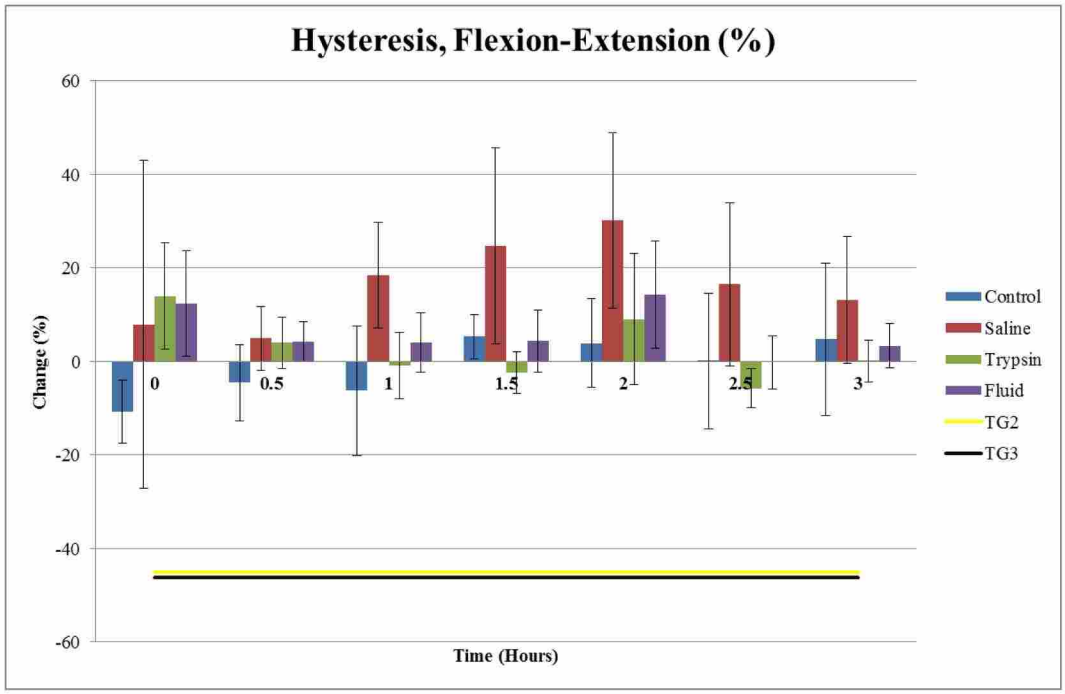

Figure C.8: Flexion-Extension H (TG2 and TG3 show changes from TG1 found in Chap. 3)

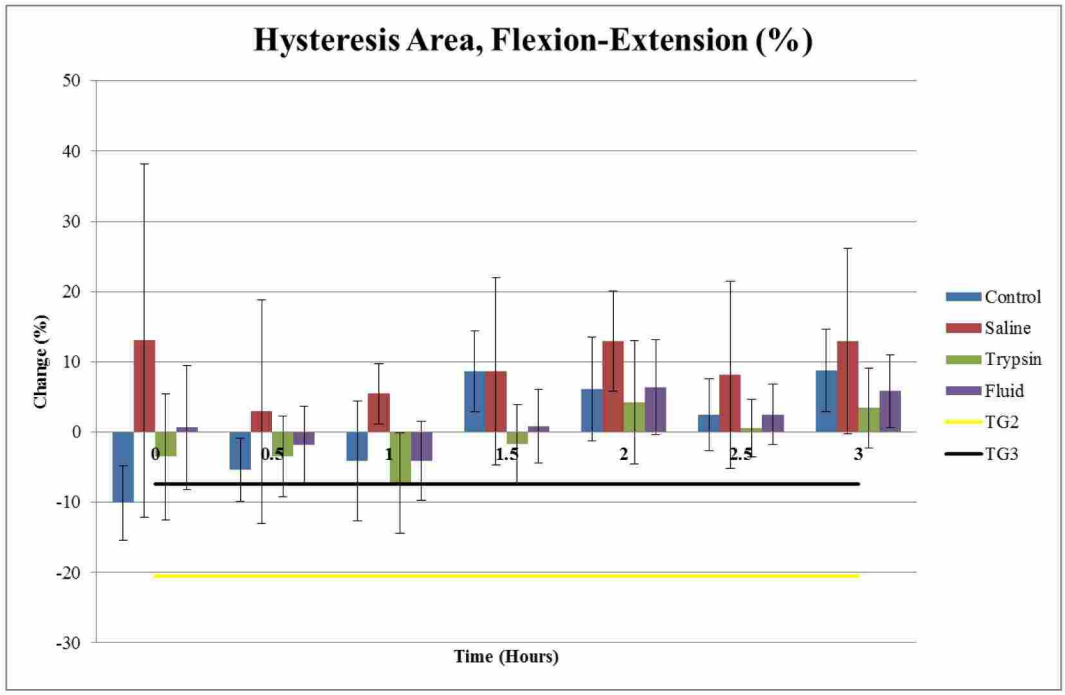

Figure C.9: Flexion-Extension HA (TG2 and TG3 show changes from TG1 found in Chap. 3)

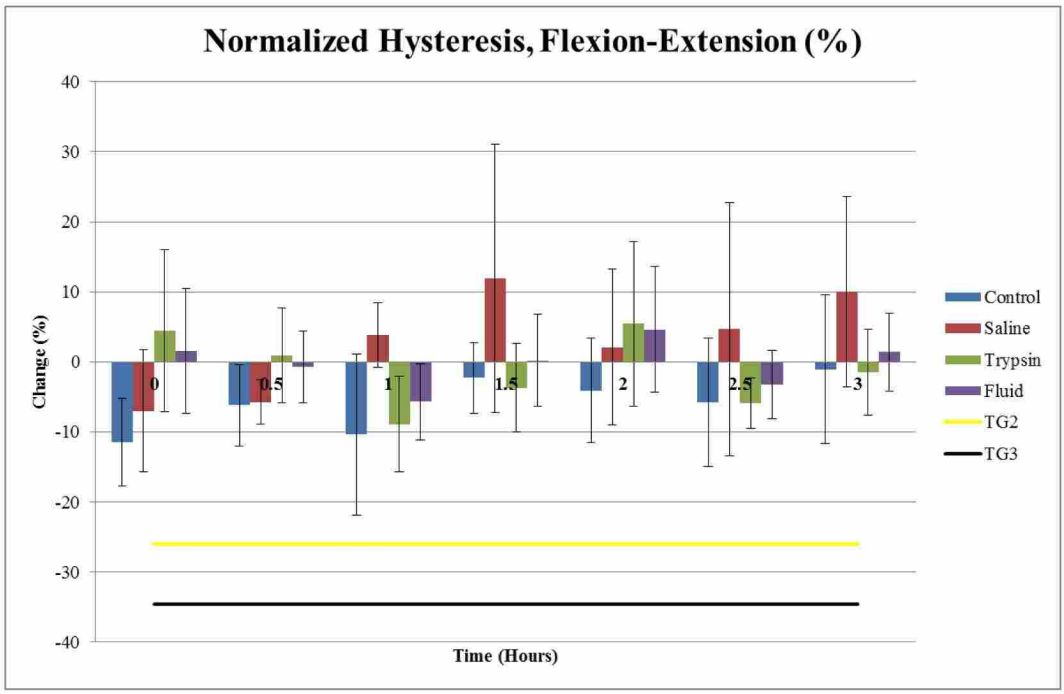

Figure C.10: Flexion-Extension HA/ROM (TG2 and TG3 show changes from TG1 found in Chap. 3)

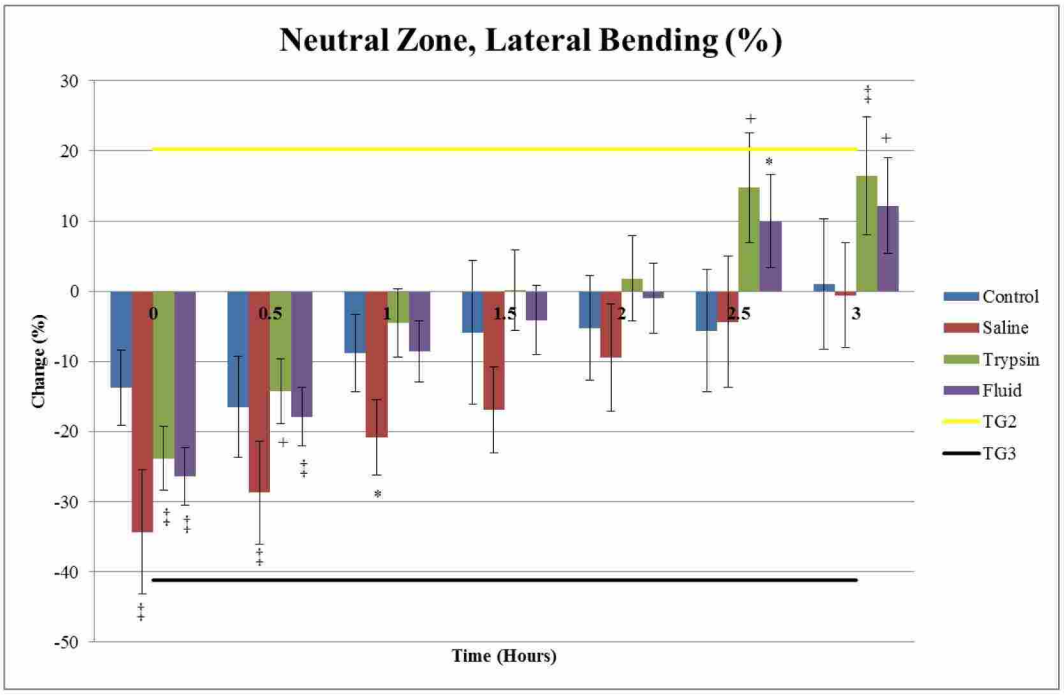

Figure C.11: Lateral Bending NZ (TG2 and TG3 show changes from TG1 found in Chap. 3; + - $p<0.01$, ‡ - $p<0.005$)

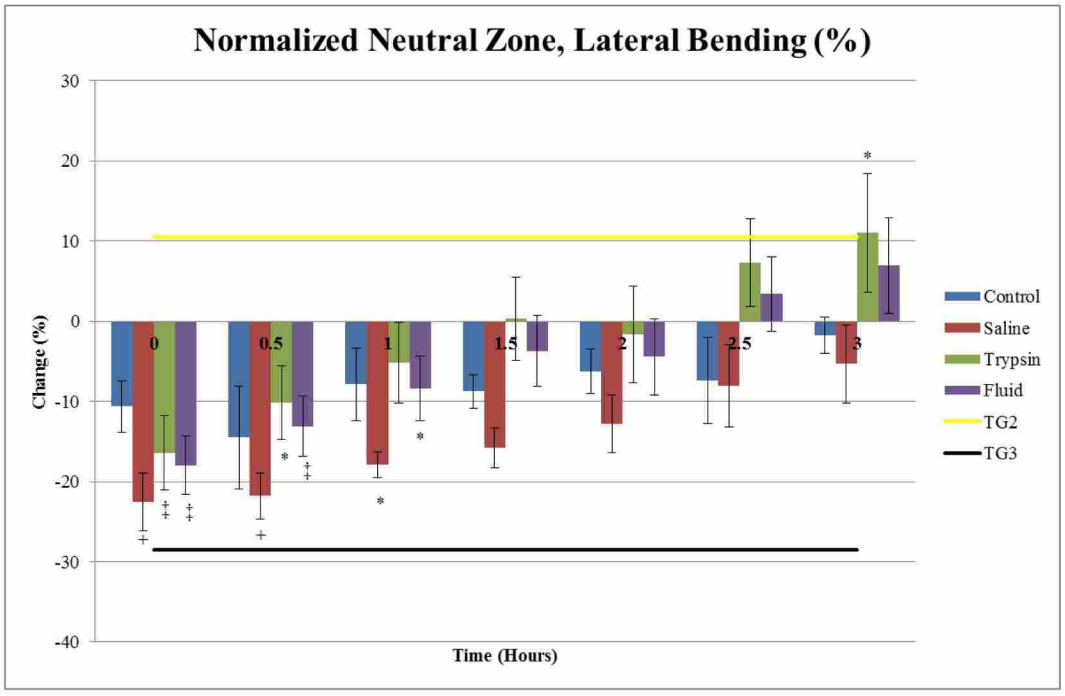

Figure C.12: Lateral Bending NZ/ROM (TG2 and TG3 show changes from TG1 found in Chap. 3; * - $p<0.05$, + - $p<0.01$, ‡ - $p<0.005$)

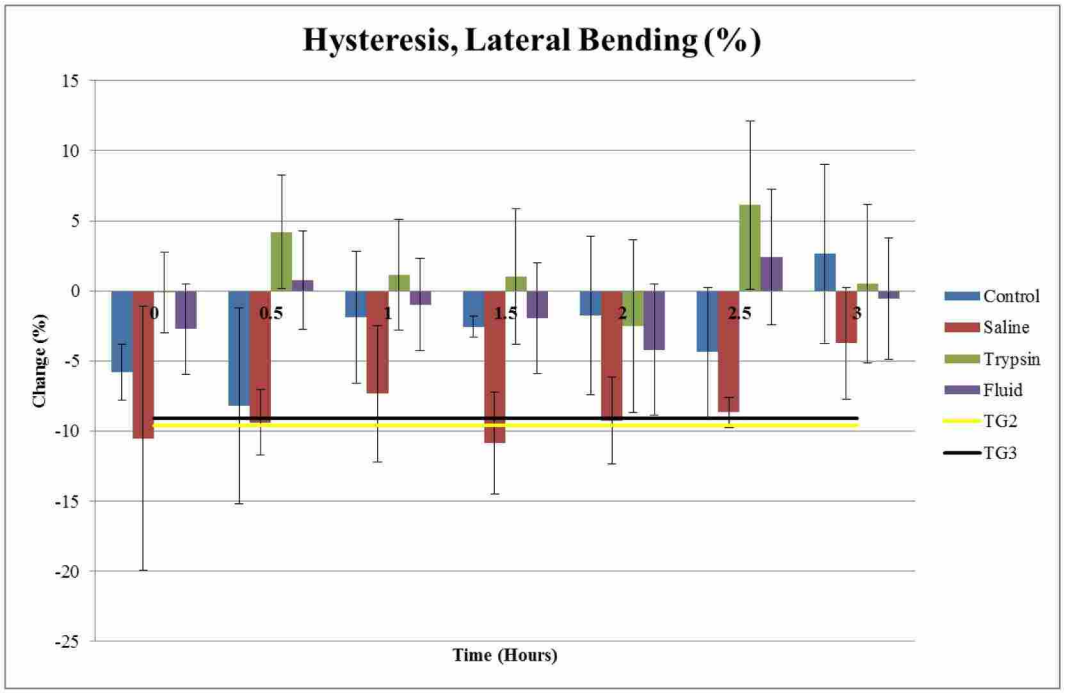

Figure C.13: Lateral Bending H (TG2 and TG3 show changes from TG1 found in Chap. 3; * - $p<0.05$)

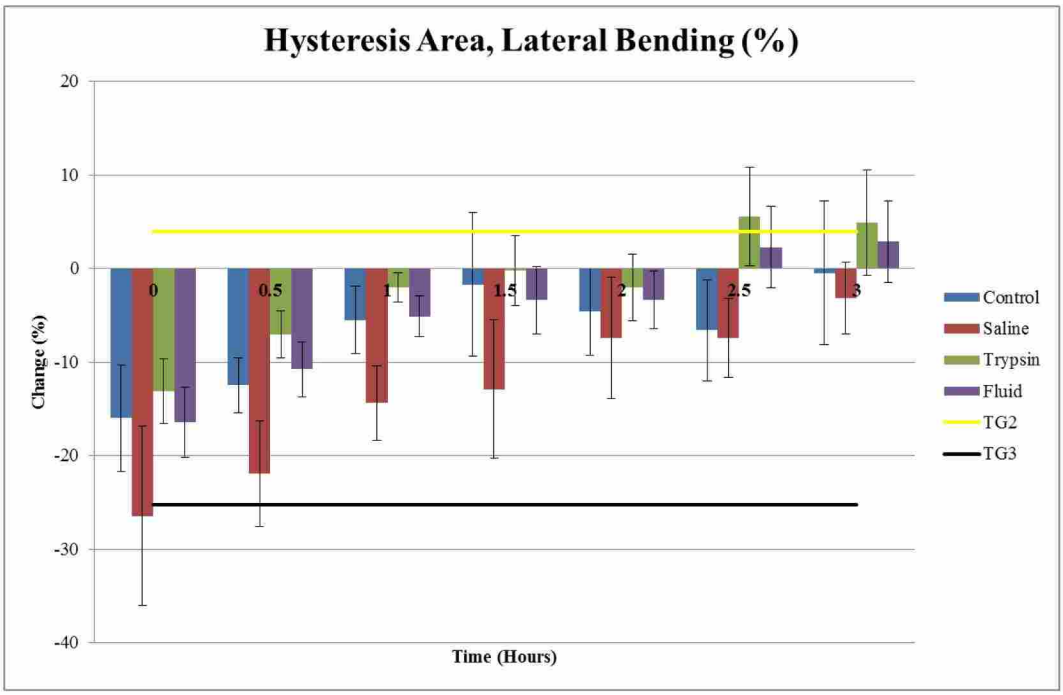

Figure C.14: Lateral Bending HA (TG2 and TG3 show changes from TG1 found in Chap. 3; * - $p<0.05$, + - $p<0.01$, ‡ - $p<0.005$)

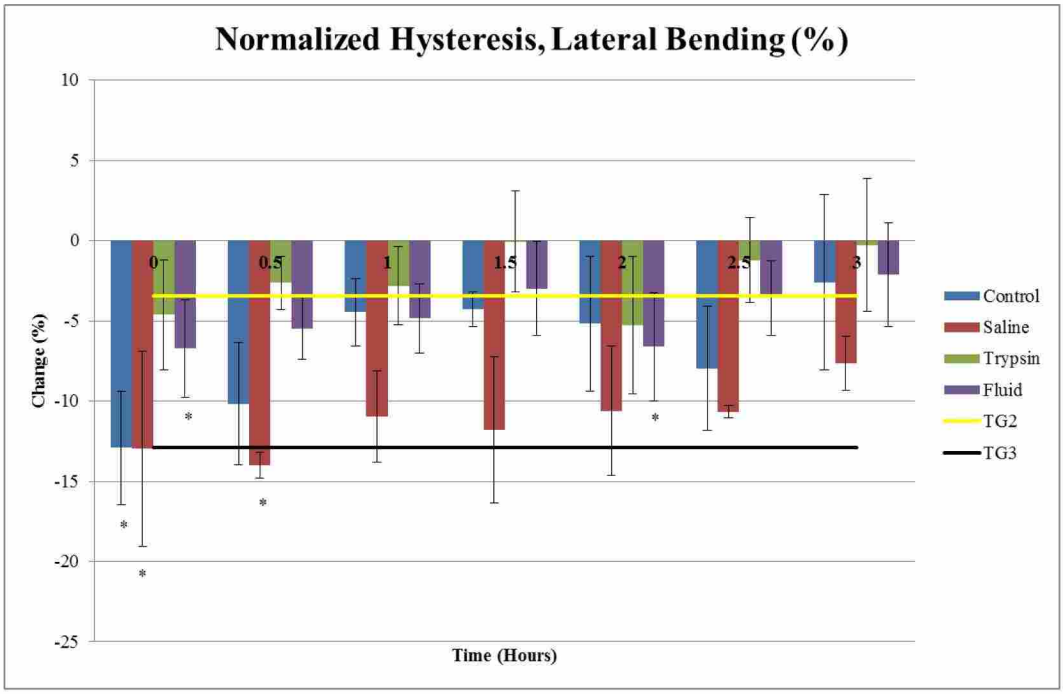

Figure C.15: Lateral Bending HA/ROM (TG2 and TG3 show changes from TG1 found in Chap. 3)

Table C.1: Statistically Significant Results for Control Treatments (P.I. - Pre-Injection)

Control						
Axial Rotation	*Range of Motion*			*Stiffness*		
	Time 1	Time 2	p-value	Time 1	Time 2	p-value
	P.I.	1	0.0473	P.I.	1.5	0.0234
	P.I.	1.5	0.0205	P.I.	2	0.0456
	P.I.	2	0.0379	P.I.	2.5	0.0195
	P.I.	2.5	0.0266	P.I.	3	0.0066
				0	3	0.0393
	Neutral Zone			*Normalized Neutral Zone*		
	Time 1	Time 2	p-value	Time 1	Time 2	p-value
				P.I.	3	0.0190
	Hysteresis Area			*Normalized Hystersis Area*		
	Time 1	Time 2	p-value	Time 1	Time 2	p-value
				P.I.	3	0.0374
	Hysteresis					
	Time 1	Time 2	p-value	Time 1	Time 2	p-value
Flexion-Extension	*Range of Motion*			*Stiffness*		
	Time 1	Time 2	p-value	Time 1	Time 2	p-value
	Neutral Zone			*Normalized Neutral Zone*		
	Time 1	Time 2	p-value	Time 1	Time 2	p-value
	Hysteresis Area			*Normalized Hystersis Area*		
	Time 1	Time 2	p-value	Time 1	Time 2	p-value
	Hysteresis					
	Time 1	Time 2	p-value	Time 1	Time 2	p-value
Lateral Bending	*Range of Motion*			*Stiffness*		
	Time 1	Time 2	p-value	Time 1	Time 2	p-value
	Neutral Zone			*Normalized Neutral Zone*		
	Time 1	Time 2	p-value	Time 1	Time 2	p-value
	Hysteresis Area			*Normalized Hystersis Area*		
	Time 1	Time 2	p-value	Time 1	Time 2	p-value
	P.I.	0	0.0347	P.I.	0	0.0397
	0	3	0.0401			
	Hysteresis					
	Time 1	Time 2	p-value	Time 1	Time 2	p-value

Table C.2: Statistically Significant Results for Saline Treatments in AR (P.I. - Pre-Injection)

Saline: Axial Rotation					
Range of Motion			*Stiffness*		
Time 1	Time 2	p-value	Time 1	Time 2	p-value
Neutral Zone			*Normalized Neutral Zone*		
Time 1	Time 2	p-value	Time 1	Time 2	p-value
0.5	1.5	0.0225	P.I.	3	0.0415
0.5	2	0.0179	0.5	1.5	0.0180
0.5	2.5	0.0150	0.5	2	0.0045
0.5	3	0.0124	0.5	2.5	0.0042
1	3	0.0435	0.5	3	0.0010
			1	2	0.0199
			1	2.5	0.0188
			1	3	0.0055
Hysteresis Area			*Normalized Hystersis Area*		
Time 1	Time 2	p-value	Time 1	Time 2	p-value
0.5	1.5	0.0392	P.I.	3	0.0307
0.5	2	0.0221	0.5	1.5	0.0318
0.5	2.5	0.0241	0.5	2	0.0051
0.5	3	0.0082	0.5	2.5	0.0072
1	2	0.0407	0.5	3	0.0005
1	2.5	0.0440	1	2	0.0096
1	3	0.0161	1	2.5	0.0132
			1	3	0.0010
Hysteresis					
Time 1	Time 2	p-value	Time 1	Time 2	p-value
P.I.	0.5	0.0101	0.5	3	0.0006
P.I.	1	0.0108	1	1.5	0.0166
0.5	1.5	0.0156	1	2	0.0076
0.5	2	0.0071	1	2.5	0.0058
0.5	2.5	0.0054	1	3	0.0007

Table C.3: Statistically Significant Results for Saline Treatments in FE (P.I. - Pre-Injection)

Saline: Flexion-Extension					
Range of Motion			*Stiffness*		
Time 1	Time 2	p-value	Time 1	Time 2	p-value
P.I.	0	0.0042			
0	1	0.0077			
0	1.5	0.0033			
0	2.5	0.0216			
0	3	0.0111			
Neutral Zone			*Normalized Neutral Zone*		
Time 1	Time 2	p-value	Time 1	Time 2	p-value
P.I.	2	0.0139	P.I.	2	0.0371
P.I.	2.5	0.0285	P.I.	2.5	0.0328
			0.5	2	0.0498
			0.5	2.5	0.0443
Hysteresis Area			*Normalized Hystersis Area*		
Time 1	Time 2	p-value	Time 1	Time 2	p-value
Hysteresis					
Time 1	Time 2	p-value	Time 1	Time 2	p-value

Table C.4: Statistically Significant Results for Saline Treatments in LB (P.I. - Pre-Injection)

Saline: Lateral Bending					
Range of Motion			*Stiffness*		
Time 1	Time 2	p-value	Time 1	Time 2	p-value
P.I.	0	0.0004	P.I.	0	<0.0001
P.I.	0.5	0.0338	P.I.	0.5	0.0099
0	1	0.0060	0	1	0.0075
0	1.5	0.0013	0	1.5	0.0006
0	2	<0.0001	0	2	<0.0001
0	2.5	<0.0001	0	2.5	<0.0001
0	3	<0.0001	0	3	<0.0001
0.5	2	0.0039	0.5	2	0.0098
0.5	2.5	0.0036	0.5	2.5	0.0060
0.5	3	0.0015	0.5	3	0.0051
Neutral Zone			*Normalized Neutral Zone*		
Time 1	Time 2	p-value	Time 1	Time 2	p-value
P.I.	0	0.0004	P.I.	0	0.0066
P.I.	0.5	0.0027	P.I.	0.5	0.0084
P.I.	1	0.0277	P.I.	1	0.0297
0	2	0.0091	0	3	0.0363
0	2.5	0.0018	0.5	3	0.0447
0	3	0.0005			
0.5	2	0.0414			
0.5	2.5	0.0104			
0.5	3	0.0032			
1	3	0.0319			
Hysteresis Area			*Normalized Hystersis Area*		
Time 1	Time 2	p-value	Time 1	Time 2	p-value
P.I.	0	0.0006	P.I.	0	0.0388
P.I.	0.5	0.0042	P.I.	0.5	0.0261
0	2	0.0125			
0	2.5	0.0125			
0	3	0.0024			
0.5	3	0.0135			
Hysteresis					
Time 1	Time 2	p-value	Time 1	Time 2	p-value

Table C.5: Statistically Significant Results for Trypsin Treatments in AR (P.I. - Pre-Injection)

Trypsin: Axial Rotation					
Range of Motion			*Stiffness*		
Time 1	Time 2	p-value	Time 1	Time 2	p-value
P.I.	1.5	0.0184	P.I.	0	0.0172
P.I.	2	0.0058	P.I.	1.5	0.0076
P.I.	2.5	0.0004	P.I.	2	0.0057
P.I.	3	0.0023	P.I.	2.5	0.0033
0	1	0.0243	P.I.	3	0.0049
0	1.5	0.0052	0	0.5	0.0029
0	2	0.0014	0	1	0.0016
0	2.5	<0.0001	0	1.5	<0.0001
0	3	0.0005	0	2	<0.0001
0.5	2.5	0.0077	0	2.5	<0.0001
0.5	3	0.0352	0	3	<0.0001
			0.5	1.5	0.0387
			0.5	2	0.0304
			0.5	2.5	0.0179
			0.5	3	0.0266
			1	2	0.0491
			1	2.5	0.0293
			1	3	0.0433
Neutral Zone			*Normalized Neutral Zone*		
Time 1	Time 2	p-value	Time 1	Time 2	p-value
0	2.5	0.0444			
0.5	2.5	0.0440			
Hysteresis Area			*Normalized Hystersis Area*		
Time 1	Time 2	p-value	Time 1	Time 2	p-value
Hysteresis					
Time 1	Time 2	p-value	Time 1	Time 2	p-value

Table C.6: Statistically Significant Results for Trypsin Treatments in FE (P.I. - Pre-Injection)

Trypsin: Flexion-Extension					
Range of Motion			*Stiffness*		
Time 1	Time 2	p-value	Time 1	Time 2	p-value
0	2.5	0.0132	P.I.	0	0.0001
0	3	0.0279	0	0.5	0.0342
0.5	2.5	0.0458	0	1	0.0007
			0	1.5	0.0001
			0	2	0.0002
			0	2.5	$<$0.0001
			0	3	$<$0.0001
			0.5	2.5	0.0062
			0.5	3	0.0038
Neutral Zone			*Normalized Neutral Zone*		
Time 1	Time 2	p-value	Time 1	Time 2	p-value
0	2	0.0071	0	2	0.0100
0	2.5	0.0114	0	3	0.0099
0	3	0.0012	0.5	2	0.0302
0.5	2	0.0365	0.5	3	0.0300
0.5	3	0.0079	1	2	0.0452
1	3	0.0439	1	3	0.0450
Hysteresis Area			*Normalized Hystersis Area*		
Time 1	Time 2	p-value	Time 1	Time 2	p-value
Hysteresis					
Time 1	Time 2	p-value	Time 1	Time 2	p-value

Table C.7: Statistically Significant Results for Trypsin Treatments in LB (P.I. - Pre-Injection)

Trypsin: Lateral Bending

Range of Motion

Time 1	Time 2	p-value
P.I.	0	0.0007
P.I.	2.5	0.0093
P.I.	3	0.0459
0	1	0.0001
0	1.5	0.0006
0	2	<0.0001
0	2.5	<0.0001
0	3	<0.0001
0.5	1	0.0246
0.5	2	0.0009
0.5	2.5	<0.0001
0.5	3	0.0003
1	2.5	0.0341
1.5	2.5	0.0103
1.5	3	0.0496

Stiffness

Time 1	Time 2	p-value
P.I.	0	<0.0001
P.I.	0.5	0.0011
0	1	0.0001
0	1.5	<0.0001
0	2	<0.0001
0	2.5	<0.0001
0	3	<0.0001
0.5	1	0.0229
0.5	1.5	0.0109
0.5	2	0.0007
0.5	2.5	0.0018
0.5	3	<0.0001
1	3	0.0167
1.5	3	0.0339

Neutral Zone

Time 1	Time 2	p-value
P.I.	0	<0.0001
P.I.	0.5	0.0094
P.I.	2.5	0.0071
P.I.	3	0.0029
0	1	0.0005
0	1.5	<0.0001
0	2	<0.0001
0	2.5	<0.0001
0	3	<0.0001
0.5	1.5	0.0087
0.5	2	0.0036
0.5	2.5	<0.0001
0.5	3	<0.0001
1	2.5	0.0005
1	3	0.0002
1.5	2.5	0.0077
1.5	3	0.0032
2	2.5	0.0175
2	3	0.0077

Hysteresis Area

Time 1	Time 2	p-value
P.I.	0	0.0031
0	1	0.0118
0	1.5	0.0036
0	2	0.0118
0	2.5	<0.0001
0	3	<0.0001
0.5	2.5	0.0044
0.5	3	0.0067

Normalized Hystersis Area

Time 1	Time 2	p-value

Normalized Neutral Zone

Time 1	Time 2	p-value
P.I.	0	0.0007
P.I.	0.5	0.0318
P.I.	3	0.0206
0	1	0.0185
0	1.5	0.0006
0	2	0.0021
0	2.5	<0.0001
0	3	<0.0001
0.5	1.5	0.0270
0.5	2.5	0.0003
0.5	3	<0.0001
1	2.5	0.0089
1	3	0.0008
1.5	3	0.0244
2	3	0.0080

Hysteresis

Time 1	Time 2	p-value

Table C.8: Statistically Significant Results for Fluid Treatments in AR (P.I. - Pre-Injection)

Fluid: Axial Rotation					
Range of Motion			*Stiffness*		
Time 1	Time 2	p-value	Time 1	Time 2	p-value
P.I.	1.5	0.0439	P.I.	0	0.0210
P.I.	2	0.0072	P.I.	1.5	0.0158
P.I.	2.5	0.0009	P.I.	2	0.0051
P.I.	3	0.0019	P.I.	2.5	0.0040
0	1	0.0146	P.I.	3	0.0020
0	1.5	0.0107	0	0.5	0.0039
0	2	0.0014	0	1	0.0047
0	2.5	0.0002	0	1.5	$<$0.0001
0	3	0.0003	0	2	$<$0.0001
0.5	2.5	0.0258	0	2.5	$<$0.0001
0.5	3	0.0473	0	3	$<$0.0001
			0.5	2	0.0276
			0.5	2.5	0.0214
			0.5	3	0.0122
			1	2	0.0236
			1	2.5	0.0183
			1	3	0.0103
Neutral Zone			*Normalized Neutral Zone*		
Time 1	Time 2	p-value	Time 1	Time 2	p-value
Hysteresis Area			*Normalized Hystersis Area*		
Time 1	Time 2	p-value	Time 1	Time 2	p-value
Hysteresis					
Time 1	Time 2	p-value	Time 1	Time 2	p-value

Table C.9: Statistically Significant Results for Fluid Treatments in FE (P.I. - Pre-Injection)

Fluid: Flexion-Extension					
Range of Motion			*Stiffness*		
Time 1	Time 2	p-value	Time 1	Time 2	p-value
			P.I.	0	0.0001
			0	0.5	0.0370
			0	1	0.0018
			0	1.5	0.0002
			0	2	0.0001
			0	2.5	$<$0.0001
			0	3	$<$0.0001
			0.5	2.5	0.0037
			0.5	3	0.0034
Neutral Zone			*Normalized Neutral Zone*		
Time 1	Time 2	p-value	Time 1	Time 2	p-value
P.I.	2	0.0270	P.I.	2	0.0275
P.I.	3	0.0222	P.I.	3	0.0469
0	2	0.0051	0	2	0.0015
0	2.5	0.0116	0	2.5	0.0245
0	3	0.0040	0	3	0.0029
0.5	2	0.0073	0.5	2	0.0042
0.5	2.5	0.0161	0.5	3	0.0080
0.5	3	0.0058	1	2	0.0217
1	2	0.0464	1	3	0.0376
1	3	0.0387			
Hysteresis Area			*Normalized Hystersis Area*		
Time 1	Time 2	p-value	Time 1	Time 2	p-value
Hysteresis					
Time 1	Time 2	p-value	Time 1	Time 2	p-value

Table C.10: Statistically Significant Results for Fluid Treatments in LB (P.I. - Pre-Injection)

Fluid: Lateral Bending								
Range of Motion			*Stiffness*			*Neutral Zone*		
Time 1	Time 2	p-value	Time 1	Time 2	p-value	Time 1	Time 2	p-value
P.I.	0	<0.0001	P.I.	0	<0.0001	P.I.	0	<0.0001
P.I.	0.5	0.0090	P.I.	0.5	<0.0001	P.I.	0.5	0.0002
P.I.	2.5	0.0068	0	0.5	0.0224	P.I.	2.5	0.0312
P.I.	3	0.0205	0	1	<0.0001	P.I.	3	0.0091
0	0.5	0.0234	0	1.5	<0.0001	0	1	0.0002
0	1	<0.0001	0	2	<0.0001	0	1.5	<0.0001
0	1.5	<0.0001	0	2.5	<0.0001	0	2	<0.0001
0	2	<0.0001	0	3	<0.0001	0	2.5	<0.0001
0	2.5	<0.0001	0.5	1	0.0098	0	3	<0.0001
0	3	<0.0001	0.5	1.5	0.0014	0.5	1	0.0454
0.5	1	0.0089	0.5	2	<0.0001	0.5	1.5	0.0034
0.5	1.5	0.0135	0.5	2.5	<0.0001	0.5	2	0.0004
0.5	2	<0.0001	0.5	3	<0.0001	0.5	2.5	<0.0001
0.5	2.5	<0.0001	1	3	0.0030	0.5	3	<0.0001
0.5	3	<0.0001	1.5	3	0.0192	1	2.5	0.0001
1	2.5	0.0069				1	3	<0.0001
1	3	0.0209				1.5	2.5	0.0027
1.5	2	0.0474				1.5	3	0.0006
1.5	2.5	0.0044				2	2.5	0.0181
1.5	3	0.0140				2	3	0.0049
Hysteresis Area			*Normalized Hystersis Area*			*Normalized Neutral Zone*		
Time 1	Time 2	p-value	Time 1	Time 2	p-value	Time 1	Time 2	p-value
P.I.	0	<0.0001	P.I.	0	0.0295	P.I.	0	<0.0001
P.I.	0.5	0.0044	P.I.	2	0.0320	P.I.	0.5	0.0015
0	1	0.0028				P.I.	1	0.0388
0	1.5	0.0006				0	1	0.0188
0	2	0.0006				0	1.5	0.0006
0	2.5	<0.0001				0	2	0.0011
0	3	<0.0001				0	2.5	<0.0001
0.5	1.5	0.0473				0	3	<0.0001
0.5	2	0.0474				0.5	1.5	0.0211
0.5	2.5	0.0006				0.5	2	0.0332
0.5	3	0.0004				0.5	2.5	<0.0001
1	2.5	0.0472				0.5	3	<0.0001
1	3	0.0320				1	2.5	0.0040
						1	3	0.0002
						1.5	3	0.0092
						2	3	0.0055
Hysteresis								
Time 1	Time 2	p-value						

Table C.11: Cross-Treatment Comparisons for Axial Rotation

Axial Rotation			
Normalized Neutral Zone			
Time	Treatment 1	Treatment 2	p-value
0.5	Saline	Control	0.0235
1	Saline	Control	0.0284
3	Saline	Trypsin	0.0154
2.5	Trypsin	Control	0.0497
3	Trypsin	Control	0.0062
3	Fluid	Control	0.0321
Normalized Hystersis Area			
Time	Treatment 1	Treatment 2	p-value
0.5	Saline	Control	0.0407
1	Saline	Control	0.0256
3	Saline	Trypsin	0.0190
3	Trypsin	Control	0.0232
1	Fluid	Control	0.0409
Hysteresis			
Time	Treatment 1	Treatment 2	p-value
0.5	Saline	Trypsin	0.0198
0.5	Saline	Control	0.0285
1	Saline	Trypsin	0.0460
1	Saline	Control	0.0168

Table C.12: Cross-Treatment Comparisons for Flexion-Extension and Lateral Bending

Flexion-Extension			
Range of Motion			
Time	Treatment 1	Treatment 2	p-value
0	Saline	Trypsin	0.0004
0	Saline	Control	0.0246
Stiffness			
Time	Treatment 1	Treatment 2	p-value
0	Trypsin	Control	0.0062
0	Fluid	Control	0.0105
Neutral Zone			
Time	Treatment 1	Treatment 2	p-value
0	Saline	Trypsin	0.0196
Lateral Bending			
Hysteresis Area			
Time	Treatment 1	Treatment 2	p-value
0.5	Saline	Trypsin	0.0367